Summer 1988

A Finite Element Formulation for the Large Deflection Random Response of Thermally Buckled Structures

James Eugene Locke
Old Dominion University

A FINITE ELEMENT FORMULATION FOR THE LARGE DEFLECTION RANDOM RESPONSE OF THERMALLY BUCKLED STRUCTURES

by

James Eugene Locke
B.S., December 1981, Oklahoma State University
M.S., July 1983, Oklahoma State University

A Dissertation Submitted to the Faculty of
Old Dominion University in Partial Fulfillment of the
Requirements for the Degree of

DOCTOR OF PHILOSOPHY

in

ENGINEERING MECHANICS

OLD DOMINION UNIVERSITY
July, 1988

Approved by:

Chuh Mei (Director)

John S. Mixson

Thomas E. Alberts

Jean W. Hou

D. M. Dorrepaal

ABSTRACT

A FINITE ELEMENT FORMULATION FOR THE LARGE DEFLECTION
RANDOM RESPONSE OF THERMALLY BUCKLED STRUCTURES

James Eugene Locke
Old Dominion University, 1988
Director: Dr. Chuh Mei

The effects of temperature and acoustic loading are included in a theoretical finite element large deflection formulation for thin, isotropic plate and beam type structures. Thermal loads are applied as steady-state temperature distributions, and acoustic loads are taken to be stationary and Gaussian with zero mean and uniform magnitude and phase over the surface of the structure. Material properties are considered to be independent of temperature. Also, inplane and rotary inertia terms are assumed to be neglegible, and all inplane edge conditions are taken to be immovable. For the random vibration analysis, cross correlation terms are included.

The nature of the loads leads to the solution of two separate problems. First, the problem of thermal postbuckling is solved to determine the deflections and stresses due to the thermal load only. These deflections and stresses are then used as initial deflections and stresses for the random vibration analysis.

Since both analyses are nonlinear, iterative techniques are used to solve each. The solution technique used for the thermal postbuckling analysis is that of Newton-Raphson iteration. This method is found to

always converge; whereas, direct iteration fails to converge. For the large deflection random vibration analysis, the linear mode shapes of the thermally buckled structure are used to reduce the equations of motion to a system of nonlinear modal equations. An equivalent linearization technique is then used to iteratively solve for the mean square deflections. Instead of using direct iteration, an underrelaxation technique is employed to reduce the number of iterations required for a converged solution. In addition to obtaining mean square deflections, the boundary for stable random vibrations for the thermally buckled structure (snap-through boundary) is predicted by considering the incremental equations of motion.

Solutions obtained using these analysis methods are compared with previous solutions to assess the accuracy of the finite element formulation. The thermal postbuckling solution is compared with a 25-mode classical solution for a square plate clamped on all edges, and the random vibration solution is compared with 100-mode classical beam solutions. Excellent agreement with the classical solutions is obtained for each of these problems.

The present study shows that the finite element method can be used to analyze structures subjected to combined thermal/acoustic loads, and the results and analytical methods presented herein should aid in the design of such structures.

DEDICATION

Dedicated to my wife, Mandy.

ACKNOWLEDGEMENTS

To Professor Chuh Mei, Chairman of my Dissertation Committee, I am very grateful for all of the excellent advice and guidance provided during the course of this research. I thank Dr. John S. Mixson who served on my Dissertation Committee for his thorough proofreading of the manuscript and for his enlightening discussions. Drs. Thomas E. Alberts, Jean W. Hou and J. Mark Dorrepaal also served on my Dissertation Committee, and I thank them for their helpful suggestions.

Special thanks are due to Drs. Clemans A. Powell and Dr. Robert L. Ash for their support throughout this effort. I also appreciate the many people at NASA Langley Research Center and Old Dominion University who helped in so many ways. In particular, I thank Diane Riddick for her patience in typing the manuscript and Deborah Price for her assistance in preparing the figures.

I am thankful to my family for providing the moral support necessary to ensure success. This dissertation would have never been completed had it not been for the love and understanding of my wife, Mandy, who constantly encouraged and motivated me; to her I am grateful beyond measure. To my parents, Jim and LuAnn Locke, I am thankful for all of their love and support and for always encouraging me to do my best.

TABLE OF CONTENTS

LIST OF TABLES

LIST OF FIGURES

LIST OF SYMBOLS

a	length of rectangular plate
$\bar{a}$	length of rectangular plate element
$\{a\}$	element nodal displacements
A	planar area of rectangular plate element
A_1	amplitude of linear buckling mode shape to begin thermal postbuckling solution
$[A]$	normal displacement slope matrix in Eq. (2.23)
b	width of rectangular plate
$\bar{b}$	width of rectangular plate element
$[B_b]$	matrix relating generalized coordinates and curvatures in Eq. (2.28)
$[B_m]$	matrix relating generalized coordinates and membrane strains in Eq. (2.22)
$[B_\theta]$	matrix relating generalized coordinates and normal displacement slopes in Eq. (2.24)
c	viscous damping coefficient
$[c]$	element damping matrix
$[C]$	extensional material stiffness matrix
	system damping matrix
$d(\ )$	differential quantity
$[D]$	bending material stiffness matrix
$\{e\}$	membrane strain in Eq. (2.11)
	linearization error in Eq. (3.31)
E	Young's modulus
$[E]$	material stiffness matrix

$E[\ ]$	expected value
$\{f\}$	modal force vector
$\{g(q)\}$	modal force due to deformation only in Eq. (3.29)
h	plate thickness
$[h]$	element consistent stress "stiffness" matrix in Eq. (3.61)
$[H]$	system consistent stress "stiffness" matrix in Eq. (3.60)
$H_j(\omega)$	single degree of freedom transfer function in Eq. (3.41)
$[H_u]$, $[H_v]$, $[H_w]$	matrices relating generalized coordinates and displacements in Eqs. (2.1), (2.2) and (2.3)
I_{jk}	integral given by Eq. (3.41)
$[k]$	element linear stiffness matrix
	diagonal linear modal stiffness matrix
$[K]$	system linear stiffness matrix
$[\bar{k}]$	equivalent linear modal stiffness matrix
$[k1]$, $[k2]$	first- and second-order nonlinear modal stiffness matrices
$[m]$	element mass matrix
	diagonal modal mass matrix
$\{M\}$	bending and twisting moments in Eq. (2.31)
$[M]$	system mass matrix
$[M_c]$	system consistent moment matrix in Eq. (3.60)
$\{N\}$	inplane forces in Eq. (2.31)
$[N]$	inplane force matrix
$[n1]$, $[n2]$	element first- and second-order nonlinear stiffness matrices
$[N1]$, $[N2]$	system first- and second-order nonlinear stiffness matrices
p	random pressure loading

$\{p\}$	element load vector
$\{P\}$	system load vector
$\{q\}$	modal displacements
q_{CR}	single-mode snap-through amplitude in Eq. (3.56)
$\{Q\}$	system nodal displacements
$[r]$	element consistent stress "load" vector in Eq. (3.62)
$[R]$	system consistent stress "load" vector in Eq. (3.60)
S_{CR}	single-mode snap-through sound spectrum level in Eq. (3.57)
S_o	double sided spectral density of applied loading in Eq. (3.41)
S_p	single sided spectral density of applied loading in Eq. (3.43)
$[T_b]$, $[T_m]$	matrices relating element nodal displacements and generalized coordinates in Eqs. (2.9) and (2.10)
u, v	inplane displacements
w	normal displacement
x, y, z	rectangular coordinates

Greek Symbols

α	coefficient of thermal expansion
$\{\alpha\}$, $\{\beta\}$	generalized coordinates in Eqs. (2.4) and (2.5)
β	weighting factor in Eq. (3.50)
$\delta(\ )$	virtual quantity
$\Delta(\ )$	incremental quantity
$\Delta T(x,y)$	planar temperature variation
$\{\varepsilon\}$	total strain in Eq. (2.11)
ζ	damping ratio
$\{\eta\}$	transformed modal displacements

$\{\theta\}$	normal displacement slopes in Eq. (2.23)
$\{\kappa\}$	curvatures in Eq. (2.11)
λ	eigenvalue for thermal buckling in Eq. (3.6)
ν	Poisson's ratio
ξ	coefficient related to viscous damping
ρ	mass density
$\{\sigma\}$	total stress in Eq. (2.29)
$\{\phi\}$	mode shape
$[\Phi]$	modal matrix
$\{\Psi(\ )\}$	sum of internal and external nodal forces
ω	linear frequency, radians per second
Ω	equivalent linear frequency, radians per second

Subscripts

b	bending
c	consistent
m	membrane
N	inplane force
o	initial displacement or stress
T	tangent stiffness
ΔT	thermal

Chapter 1

INTRODUCTION

1.1 Purpose of Study

Modern applications of structural mechanics frequently involve the use of high strength, light weight materials that are designed to endure combinations of severe static and dynamic loadings. These severe loadings can produce nonlinear structural behavior which has typically been dealt with in an empirical fashion by testing various structural components in simulated loading environments. However, with advanced materials structures can be tailored for a specific purpose, and since testing is not practical for every conceivable structural configuration, the best design could be one for which no test data is available. To better evaluate potential designs, nonlinear analysis methods have been developed for particular types of structures and loadings, but situations do occur for which general purpose nonlinear analytical methods are not available, for example, thin structural components subjected to a combined thermal-acoustic loading.

Future aircraft and spacecraft structures can be expected to operate at elevated temperatures and high noise levels [1]*. Numerous experimental studies [2-6] have been conducted to determine the effect

*The numbers in brackets indicate references.

of elevated temperature on aircraft structural components. These studies indicate that aircraft panels subjected to relatively small variations in temperature tend to buckle. Consequently, large deflection postbuckling theory must be used to determine the deflections and stresses. Furthermore, test results [6-18] for various aircraft panels indicate that high noise levels produce large deflections. Again, large deflection theory must be used for the determination of deflection and stresses. It has also been found [7] that buckled panels subjected to high noise levels produce not only large deflections but also become dynamically unstable (snap-through) at sufficiently high noise levels. This instability leads to large stresses and could greatly reduce the sonic fatigue lifetime. Thus, this type of situation should be avoided if at all possible; however, current analytical design methods for sonic fatigue [8, 9, 19-21] are based primarily on linear structural theory with empirical corrections to account for nonlinear behavior and are applicable only for specific applications. It is, therefore, the purpose of this study to develop an analytical formulation to determine the large deflection random response of thermally buckled thin beam and plate type structures. To facilitate the treatment of arbitrary boundary conditions and temperature distributions, the finite element method is used to derive the governing nonlinear equations of motion.

1.2 Literature Review

In 1952, Gossard, Seide and Roberts [2] conducted both experimental and analytical studies to determine the stresses and deflections of a simply supported flat plate subjected to a tent-like temperature

distribution. The theoretical analysis consisted of using approximate methods for determining both the critical buckling temperature and the postbuckling behavior. The critical buckling temperature and corresponding mode shape were determined using a Rayleigh-Ritz formulation. For the postbuckling analysis, appropriate expressions were assumed for both the deflection and the stress function. Galerkin's method was employed for calculation of the resultant deflections and stresses. The analytical results were found to compare quite well with the experimental results, thus demonstrating the accuracy of the analytical solution.

The first investigation of an "exact" nature for the large deflection of heated plates was conducted by Wilcox and Clemmer [22]. Their solution was based on a previous solution developed by Levy [23] for a simply supported square plate. Paul [24] also extended this "exact" solution to a plate clamped on all edges. The Levy solution involved the use of an infinite Fourier series for the transverse deflection, the inplane stress function and the normal pressure with the coefficients of the series being solved for by direct substitution into the von Karman large deflection plate equations. This reduces the system of nonlinear partial differential equations to a system of nonlinear algebraic equations. The accuracy of the solution, of course, depends on the number of terms included in the series, and the exact solution should theoretically be approached as the number of terms in the series approaches infinity. In practice, however, only a finite number of terms may be included, but this does not present any problem since Paul [24] found that only a relatively small number of terms were needed to accurately determine deflections and stresses. Paul's

analytical results were also found to compare favorably with experimental data, thus further confirming the validity of von Karman large deflection plate theory modified to include the effect of thermal stresses. The results of this study also indicate that nonuniform temperature distributions have a significant effect on both the thermal buckling load and the postbuckling deformation and, therefore, should be considered for the most efficient structural design. Additionally, for nonuniform temperature distributions, designs based on the average panel temperature can, in some cases, lead to nonconservative predictions.

Alternative solution techniques such as the finite element method [25-31] have also been successfully applied to the problem of postbuckling. Mechanical postbuckling, which may be treated as a special case of thermal postbuckling, has been treated by Yang et al. [25, 26] using a finite element formulation. These results were found to closely agree with previously obtained classical results [23, 32, 33]. Rao and Raju [27-30] have used the finite element method to investigate both mechanical and thermal postbuckling for circular plates and beams. For thermal postbuckling, only uniform temperature distributions were considered. Again, the finite element results were found to compare very well with results obtained using a classical formulation.

To [34] has recently presented a very comprehensive survey article that reviews techniques for the analysis of nonlinear systems subjected to random excitation. Methods reported to be applicable to both single-degree-of-freedom (SDOF) and multiple-degree-of-freedom (MDOF) systems include statistical or equivalent linearization techniques (EL), the Fokker-Planck-Kolmogorov equation (FPKE) and moment equation (ME) approaches. The FPKE approach [35] has been applied to several

nonlinear problems [36-38], and exact closed-form solutions have been obtained for SDOF systems. However, for MDOF nonlinear systems exact solutions have not been found; hence, approximate methods must be employed. The EL techniques, on the other hand, have been found to be readily applicable to both SDOF and MDOF nonlinear systems; consequently, many studies [7, 13, 39-45] have used EL methods to investigate the large deflection response of structures subjected to random loading.

Since test results [8, 10-14] indicate that there are more than one mode responding, analyses [39, 40, 44, 45] have been conducted to investigate the effect of MDOF solutions on the large deflection random response of flat beams and plates. All of these efforts have started with either the classical von Karman-Herrmann large deflection plate equations or the Woinowsky-Kreiger large deflection beam equation. These partial differential equations were then reduced to ordinary time-dependent differential equations using either Galerkin's method or by direct substitution into the equations. Mei [44] investigated the response of a plate clamped on all edges and demonstrated that, indeed, analytical predictions do improve when multiple modes are included in the analysis. Seide [45] investigated nonlinear stresses and deflections of beams subjected to random loading and indicated that as many as 100-modal functions could be necessary for the accurate determination of stresses. Recently, Prasad [40] used three modal functions to obtain solutions for beams with both nonlinear stiffness and damping. For the case of linear damping only, these three-mode solutions were found to compare reasonably well with Seide's 100-mode solutions for realistic levels of excitation.

Finite element formulations for the nonlinear random vibration of structures have been considered by relatively few researchers [46-49]. Both references [46] and [47] used the EL method. Hwang and Pi [46] found that their proposed method could not be applied for acoustic pressure levels that were too high while Busby and Weingarten [47] did not note such a result for their method. Thus, the applicability of EL methods to nonlinear finite element formulations seems to be questionable. Neither of these studies made any comparisons with any other approximate solutions, and Busby and Weingarten also assumed that the equivalent linear stiffness matrix was diagonal which, in general, is not true. Recently, Chiang and Mei [48] have considered a MDOF solution for large deflection random response. They used an iterative solution technique that assumes that the finite element equations of motion are linearized for a given iteration. Solutions obtained for mean square responses and stresses were found to compare very well with classical results obtained using a SDOF FPKE approach [35] and an EL MDOF approach [40], thus establishing the applicability of the finite element method to the problem of nonlinear random vibration.

In 1957, Bisplinghoff and Pian [5] experimentally and analytically investigated the small amplitude free vibration of plates and beams thermally buckled due to a uniform temperature distribution. Both the plate and the beam were taken to be simply supported, and the plate aspect ratio was three to one. A solution was developed for the plate by using one term for the postbuckled shape and by expressing the vibrating displaced shape as a combination of three symmetric mode shapes. The resulting equations of motion were derived using Lagrange's equation, and results for small amplitude vibration were obtained by

neglecting higher order terms. A similar type of analysis was conducted for the beam. The analytical results were found to be in fair agreement with the experimental data with discrepancies due to both non-ideal support conditions and initial imperfections. Dokmeci and Boley [50] later demonstrated that a better agreement between experiment and theory could be obtained by considering multiple modes for both the postbuckled shape and the vibrating displaced shape. Yang and Han [26] used a finite formulation; the results nicely compared with those obtained by Bisplinghoff and Pian.

The large deflection deterministic vibration of buckled structures has been studied by several researchers [51-57]. Each of these efforts used Galerkin's method in conjunction with the method of harmonic balancing to reduce the governing partial differential equations to a system of nonlinear algebraic equations. Yamaki et al. [51-54] conducted both analytical and experimental studies for clamped circular plates and clamped beams. Tseng and Dugundji [55] considered not only harmonic motions but also dynamic instability (snap-through) for a clamped beam. To investigate the snap-through motion Galerkin's method and the method of Runge-Kutta numerical integration were used. Snap-through was determined to have occurred based on observations of the transient solution. Similar snap-through and dynamic instability problems have also been considered by other researchers [58-66]. As reported by reference [60], due to the lack of a valid definition for "dynamic buckling", dynamic instability is generally considered to have occurred when a small increase in some load parameter produces a large increase in the response. Huang [63] also notes that some structures may deform to an inside-out position without actually snapping-through.

Humphreys [59] investigated whether an energy criteria could be extended from SDOF to MDOF systems for the determination of dynamic instability and found that the energy criteria was not generally extendable to MDOF systems.

Very few analytical studies [67-70] have considered the large deflection random response of either shallow shell type structures or buckled structures. Seide et al. [67-69] has conducted experimental and analytical studies for buckled beams subjected to uniform random pressure. As for previous studies, either Galerkin's method or direct substitution into the governing equation was used to obtain time-dependent ordinary differential equations. These equations were then solved using both an EL technique and Runge-Kutta numerical integration. The snap-through critera used for these studies is based on the numerical integration results and is discussed in Chap. 4. Reference [70] has considered the problem of first-passage time for the snap-through of a shell-type structure using a SDOF system and numerically integrating the equation of motion. For the SDOF system, the free undamped motion can be described in terms of the total energy, that is, the sum of the kinetic and potential energy, and curves of constant energy can be used to determine the regions of stable and unstable motion. Thus, if for a given loading, the system is in the unstable region, snap-through has occurred. However, as mentioned by Seide et al. [67], this method is not readily applicable to a MDOF system.

References [67], [69] and [70] were thought to be the only previous analytical studies to consider the snap-through motion of structures subjected to random excitation. However, as this manuscript was nearing completion, it was noticed that C. F. Ng (also see Ref. [7]) had very

recently completed a snap-through study. He used a SDOF system to model a buckled plate, and EL results were used to derive simple formulas for the prediction of snap-through.

1.3 Scope of Present Study

Considering the results and conclusions obtained by Paul [24], it is apparent that nonuniform temperature distributions have a significant effect on postbuckled stresses and deflections. In addition, Seide and Adami [67] noted the need for improved analytical methods for the large deflection random response and dynamic instability of buckled structures. Mixson and Roussos [1] have also noted that the effects of high temperatures, new materials and complex structural configurations should be taken into account for the proper design of future aerospace vehicles. It was for these reasons that a finite element formulation was chosen for the present study. Following approaches similar to Yang et al. [25, 26] and Wood et al. [71], the governing finite element equations are developed for both thermal postbuckling and large deflection random vibration of thermally buckled structures. The random loading is taken to be a uniformly distributed broadband Gaussian "white noise" with zero mean.

In Chap. 2, the governing variational principles for the present problem are introduced and discussed. These include the principle of virtual work and adjacent-equilibrium criterion. The nonlinear equations of motion and the stability equations for the finite element formulation are developed and include the effects of both thermal and acoustic loads. Large deflection terms are included in first- and second-order nonlinear stiffness matrices.

Computational methods are presented in Chap. 3. A Newton-Raphson iterative solution technique similar to that of Yang and Han [26] is used for the solution of the thermal postbuckling problem. The nonlinear stiffness matrices are of the same form as previous formulations [25, 26, 71, 72]; however, the inclusion of thermal stresses introduces a geometric stiffness matrix and a thermal load vector.

The solution of the large deflection random vibration problem, including snap-through, is the primary objective of the present research. Using the linear mode shapes of the thermally buckled structure, the governing system of finite element equations is reduced to a system of nonlinear modal equations. The resulting system of nonlinear modal equations is solved using the EL method. While Ref. [47] has used the finite element method to obtain a two-mode EL solution for the large deflection random response of a flat, stress free beam, the present study is the first finite element multiple-mode EL solution technique for thermally stressed or buckled structures. In comparison to Ref. [47], the present formulation also includes inplane deformation and a fully populated (nondiagonal) equivalent linear stiffness matrix. Dynamic instability (snap-through) is investigated using the incremental form of the nonlinear modal equations in conjunction with the EL results.

The methodology developed in the present study can be used to obtain nonlinear modal equations for plates and beams subjected to arbitrary temperature distributions with arbitrary boundary conditions. These modal equations can then be solved using any of the solution techniques available for MDOF nonlinear systems. Using a finite element

formulation to derive these nonlinear modal equations is considered to be a significant contribution since for complex boundary conditions classical formulations are very difficult, if not practically impossible, to apply. Previous studies [67, 69, 70], with the exception of C. F. Ng's very recent study, have all used a numerical simulation approach for the determination of the snap-through boundary, and as reported by Ref. [34], numerical (Monte Carlo) simulation solutions for a SDOF system require computational time that is three orders of magnitude greater than that for approximate solutions such as the EL method. Hence, another contribution of the present study is the computational efficiency, as compared to numerical simulation, of the method used for determining the snap-through boundary.

Numerical results are presented in Chap. 4 for plates and beams subjected to both uniform and nonuniform temperature distributions; beam results were obtained by suppressing appropriate plate degrees of freedom. To verify the finite element formulation, results are compared with previous analytical solutions. The thermal postbuckling results are compared with a previous solution [24] for a square plate clamped on all edges, and the large deflection random vibration results are compared with previous beam solutions [45, 67]. A convergence study is included to evaluate the required number of elements and mode shapes necessary to achieve reasonable accuracy. A summary of the present study and possibilities for future research are presented in Chap. 5.

Chapter 2

NONLINEAR FINITE ELEMENT FORMULATION

In this chapter, the governing nonlinear equations of motion are derived for a rectangular plate subjected to a combined thermal/acoustic loading. The thermal loading is taken to be a steady-state temperature distribution, and the acoustic loading is considered to be a stationary Gaussian pressure with zero mean and uniform magnitude and phase over the plate surface. As shown in Fig. 2.1, the plate is considered to be initially deflected by an amount w_0, and the active normal displacement w is measured with respect to the initially deflected shape.

For the derivation of the governing equations the following assumptions are made:

1. The material is homogeneous, isotropic and Hookean with properties that do not depend on temperature.
2. The von Karman large deflection strain-displacement relations are valid.
3. Inplane inertia and rotary inertia are negligible.
4. The temperature does not vary through the thickness of the plate.

The assumption regarding temperature independent material properties is reasonable for the present study since, as reported in Ref. [24], small variations in temperature produce postbuckling behavior in thin panels, and as reported in Ref. [73], the thermomechanical

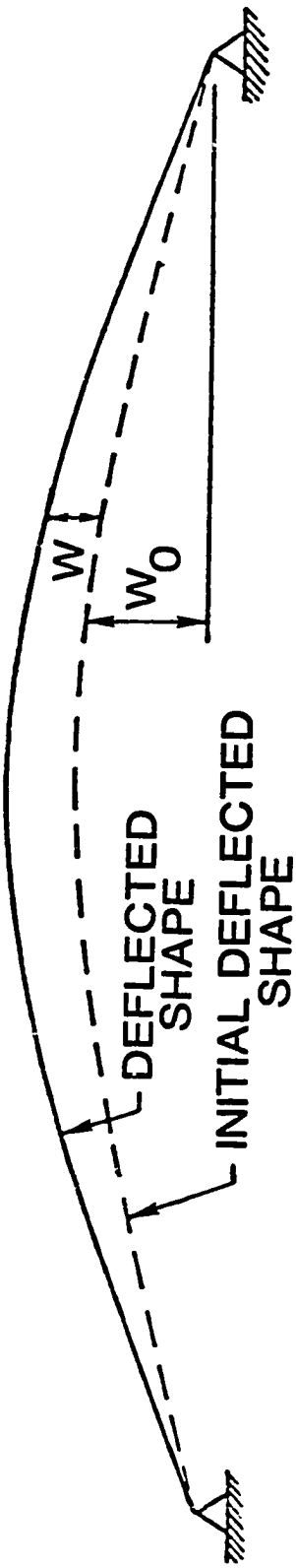

Fig. 2.1 Side view of initially deflected structure.

properties of common structural materials are essentially constant for small changes in temperature.

2.1 Element Displacement Functions

For the selection of a suitable plate element, two things were considered to be important: accuracy and complexity. Higher-order elements, such as the 54 degree-of-freedom triangular plate elements used by Ref. [26], could have been used to obtain a very high degree of accuracy. Such elements, however, are more complex to formulate and apply than elements with fewer degrees-of-freedom. The element chosen for this study is a 24 degree-of-freedom rectangular plate element [74], shown in Fig. 2.2, that is considered to fulfill both of the selection criteria. It is not complex to to formulate and apply but contains a sufficient number of generalized coordinates, at least in the sense that it is a conforming element, to adequately describe the behavior of the plate. Displacement functions for this element are given as

$$\begin{aligned} w = {} & \alpha_1 + \alpha_2 x + \alpha_3 y + \alpha_4 x^2 + \alpha_5 xy + \alpha_6 y^2 \\ & + \alpha_7 x^3 + \alpha_8 x^2 y + \alpha_9 x y^2 + \alpha_{10} y^3 \\ & + \alpha_{11} x^3 y + \alpha_{12} x^2 y^2 + \alpha_{13} x y^3 \\ & + \alpha_{14} x^3 y^2 + \alpha_{15} x^2 y^3 + \alpha_{16} x^3 y^3 = [H_w] \{\alpha\} \end{aligned} \tag{2.1}$$

$$u = \beta_1 + \beta_2 x + \beta_3 y + \beta_4 xy = [H_u] \{\beta\} \tag{2.2}$$

$$v = \beta_5 + \beta_6 x + \beta_7 y + \beta_8 xy = [H_v] \{\beta\} . \tag{2.3}$$

PLATE ELEMENT SUBJECTED TO THERMAL/ACOUSTIC LOADING

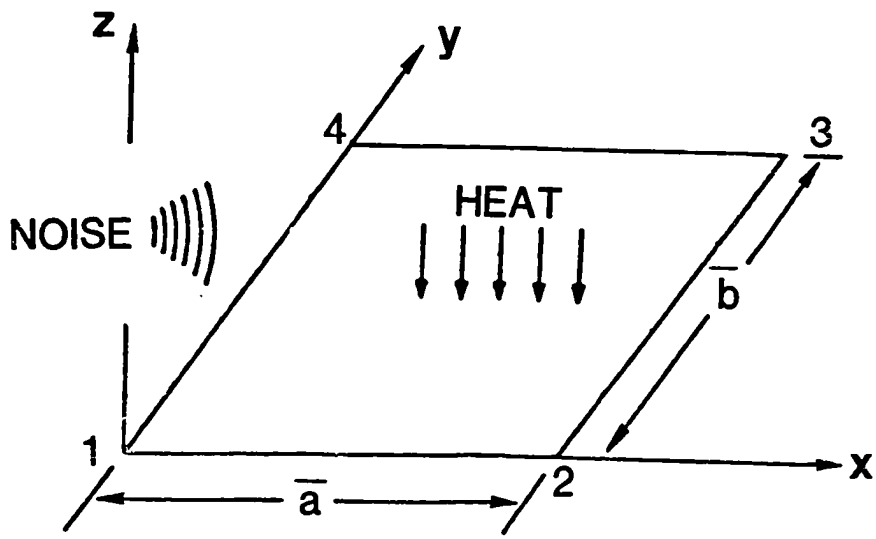

Fig. 2.2 Rectangular plate finite element.

The twenty four generalized coordinates

$$\{\alpha\}^T = [\alpha_1, \alpha_2, \ldots, \alpha_{16}] \tag{2.4}$$

$$\{\beta\}^T = [\beta_1, \beta_2, \ldots, \beta_8] \tag{2.5}$$

can be determined from the nodal displacements

$$\{a\}^T = [\{a_b\}^T, \{a_m\}^T] \tag{2.6}$$

where

$$\{a_b\}^T = [W_1, W_2, W_3, W_4, W_{x1}, \ldots, W_{y1}, \ldots, W_{xy1}, \ldots, W_{xy4}] \tag{2.7}$$

$$\{a_m\}^T = [U_1, U_2, U_3, U_4, V_1, V_2, V_3, V_4] . \tag{2.8}$$

The transformation relating nodal displacements and generalized coordinates can be written as

$$\{\alpha\} = [T_b] \{a_b\} \tag{2.9}$$

$$\{\beta\} = [T_m] \{a_m\} . \tag{2.10}$$

The matrices $[T_b]^{-1}$ and $[T_m]$ are given in Appendix A.

2.2 Nonlinear Strain-Displacement Relations

The von Karman strain-displacement relations modified to include the effect of initial deflections [25] are given by

$$\{\varepsilon\} = \{e\} + z \{\kappa\} \tag{2.11}$$

where

$$\{e\} = \{e_m\} + \{e_b\} \tag{2.12}$$

$$\{e_m\} = \begin{Bmatrix} u_{,x} \\ v_{,y} \\ u_{,y} + v_{,x} \end{Bmatrix} \tag{2.13}$$

$$\{e_b\} = \begin{Bmatrix} \frac{1}{2}\ w_{,x}^2 + w_{,x}\, w_{o,x} \\ \frac{1}{2}\ w_{,y}^2 + w_{,y}\, w_{o,y} \\ w_{,x}\, w_{,y} + w_{,x}\, w_{o,y} + w_{,y}\, w_{o,x} \end{Bmatrix} \tag{2.14}$$

$$\{\kappa\} = - \begin{Bmatrix} w_{,xx} \\ w_{,yy} \\ 2\, w_{,xy} \end{Bmatrix} . \tag{2.15}$$

By using Eqs. (2.1), (2.2) and (2.3) in conjunction with Eqs. (2.13), (2.14) and (2.15), the strains and curvatures can be evaluated as follows:

$$\begin{Bmatrix} u_{,x} \\ u_{,y} \\ v_{,x} \\ v_{,y} \end{Bmatrix} = \begin{bmatrix} \frac{\partial}{\partial x}[H_u] \\ \frac{\partial}{\partial y}[H_u] \\ \frac{\partial}{\partial x}[H_v] \\ \frac{\partial}{\partial y}[H_v] \end{bmatrix} \{\beta\} \tag{2.16}$$

$$\begin{Bmatrix} w_{,x} \\ w_{,y} \end{Bmatrix} = \begin{bmatrix} \frac{\partial}{\partial x}[H_w] \\ \frac{\partial}{\partial y}[H_w] \end{bmatrix} \{\alpha\} \tag{2.17}$$

$$\begin{Bmatrix} w_{o,x} \\ w_{o,y} \end{Bmatrix} = \begin{bmatrix} \frac{\partial}{\partial x}[H_w] \\ \frac{\partial}{\partial y}[H_w] \end{bmatrix} \{\alpha_o\} \tag{2.18}$$

$$\begin{Bmatrix} w_{,xx} \\ w_{,yy} \\ w_{,xy} \end{Bmatrix} = \begin{bmatrix} \frac{\partial^2}{\partial x^2}[H_w] \\ \frac{\partial^2}{\partial y^2}[H_w] \\ \frac{\partial^2}{\partial x \partial y}[H_w] \end{bmatrix} \{\alpha\} \tag{2.19}$$

where

$$\{\alpha_o\} = [T_b]\ \{a_{bo}\} \tag{2.20}$$

and

$$\{a_{bo}\}^T = [W_{o1}, W_{o2}, W_{o3}, W_{o4}, W_{ox1}, \ldots, W_{oy1}, \ldots, W_{oxy1}, \ldots, W_{oxy4}] \tag{2.21}$$

is the initial nodal displacement vector. Using Eq. (2.16), Eq. (2.13) becomes

$$\{e_m\} = \begin{bmatrix} \frac{\partial}{\partial x}[H_u] \\ \frac{\partial}{\partial y}[H_v] \\ \frac{\partial}{\partial y}[H_u] + \frac{\partial}{\partial x}[H_v] \end{bmatrix} \{\beta\}$$

$$= [B_m]\ \{\beta\}\ . \tag{2.22}$$

Using Eqs. (2.17) and (2.18), Eq. (2.14) can be expressed as

$$\begin{aligned}\{e_b\} &= \frac{1}{2}[A]\{\theta\} + [A]\{\theta_o\} \\ &= \frac{1}{2}[A]\{\theta\} + [A_o]\{\theta\}\end{aligned} \tag{2.23}$$

where

$$\{\theta\} = \begin{Bmatrix} w_{,x} \\ w_{,y} \end{Bmatrix} = \begin{bmatrix} \frac{\partial}{\partial x}[H_w] \\ \frac{\partial}{\partial y}[H_w] \end{bmatrix} \{\alpha\}$$

$$= [B_\theta]\{\alpha\} \tag{2.24}$$

$$\{\theta_o\} = \begin{Bmatrix} w_{o,x} \\ w_{o,y} \end{Bmatrix} = \begin{bmatrix} \frac{\partial}{\partial x}[H_w] \\ \frac{\partial}{\partial y}[H_w] \end{bmatrix} \{\alpha_o\}$$

$$= [B_\theta]\{\alpha_o\} \tag{2.25}$$

$$[A] = \begin{bmatrix} w_{,x} & 0 \\ 0 & w_{,y} \\ w_{,y} & w_{,x} \end{bmatrix} = \begin{bmatrix} \theta_x & 0 \\ 0 & \theta_y \\ \theta_y & \theta_x \end{bmatrix} \tag{2.26}$$

$$[A_o] = \begin{bmatrix} w_{o,x} & 0 \\ 0 & w_{o,y} \\ w_{o,y} & w_{o,x} \end{bmatrix} = \begin{bmatrix} \theta_{ox} & 0 \\ 0 & \theta_{oy} \\ \theta_{oy} & \theta_{ox} \end{bmatrix} . \tag{2.27}$$

Finally, using Eq. (2.15) and Eq. (2.19), the curvatures can be expressed as

$$\{\kappa\} = \begin{bmatrix} -\frac{\partial^2}{\partial x^2}[H_w] \\ -\frac{\partial^2}{\partial y^2}[H_w] \\ -2\frac{\partial^2}{\partial x \partial y}[H_w] \end{bmatrix} \{\alpha\}$$

$$= [B_b]\{\alpha\} . \qquad (2.28)$$

The matrices $[B_m]$, $[B_\theta]$, and $[B_b]$ are given in Appendix A.

2.3 Stress Resultants

For an isotropic Hookean material under a state of plane stress and subjected to a temperature variation $\Delta T(x,y)$, the stresses are given by

$$\{\sigma\} = \begin{Bmatrix} \sigma_x \\ \sigma_y \\ \tau_{xy} \end{Bmatrix} = [E]\{\varepsilon\} + \{\sigma_0\} - \{\sigma_{\Delta T}\} \qquad (2.29)$$

where

$$[E] = \frac{E}{1-\nu^2}\begin{bmatrix} 1 & \nu & 0 \\ \nu & 1 & 0 \\ 0 & 0 & \frac{1-\nu}{2} \end{bmatrix}$$

$$\{\sigma_{\Delta T}\} = \frac{E\alpha\Delta T(x,y)}{1-\nu}\begin{Bmatrix} 1 \\ 1 \\ 0 \end{Bmatrix},$$

and $\{\sigma_0\}$ is an initial stress distribution.

The force and moment resultants are defined as

$$\{N,M\} = \int_{-h/2}^{h/2} (1,z)\{\sigma\}\, dz . \qquad (2.30)$$

Using Eqs. (2.11), (2.29) and (2.30) and taking into account that the temperature does not vary through the thickness of the plate, the constitutive equations relating the force and moment resultants to the strains and curvatures become

$$\{N\} = [C]\{e\} + \{N_0\} - \{N_{\Delta T}\}$$
$$\{M\} = [D]\{\kappa\} + \{M_0\} \tag{2.31}$$

where

$$[C] = \frac{Eh}{1-\nu^2}\begin{bmatrix} 1 & \nu & 0 \\ \nu & 1 & 0 \\ 0 & 0 & \frac{1-\nu}{2} \end{bmatrix}$$

$$[D] = \frac{Eh^3}{12(1-\nu^2)}\begin{bmatrix} 1 & \nu & 0 \\ \nu & 1 & 0 \\ 0 & 0 & \frac{1-\nu}{2} \end{bmatrix}$$

$$\{N_{\Delta T}\} = \frac{E\alpha h \Delta T(x,y)}{1-\nu}\begin{Bmatrix} 1 \\ 1 \\ 0 \end{Bmatrix}$$

$$\{N_0, M_0\} = \int_{-h/2}^{h/2} (1,z)\{\sigma_0\}\, dz \ .$$

2.4 Equations of Motion

The equilibrium equations for a structure can be derived using either a Newtonian approach or a variational approach. For complex structural configurations variational methods have proven to be very powerful since the governing equations can be determined entirely through the extremization of a scalar functional. For the present study, the governing equations are derived using the principle of

virtual work which states that for a structure in equilibrium under the action of internal and external forces, the work done by these forces in undergoing an infinitesimal virtual displacement is zero. In the following section, this principle is applied to determine the nonlinear equations of motion. To investigate the stability of an equilibrium configuration, an adjacent-equilibrium method is employed.

2.4.1 Nonlinear Equilibrium Equations

The virtual work principle can be written in the form

$$\delta W = \delta W_{int} - \delta W_{ext} = 0 \tag{2.32}$$

where δW_{int} represents the virtual work of the internal forces and δW_{ext} represents the virtual work of the external forces. Thus, for equilibrium

$$\delta W_{int} = \delta W_{ext} \, . \tag{2.33}$$

For a plate element with forces $\{N\}$ and moments $\{M\}$, the virtual work of the internal forces is given by

$$\delta W_{int} = \int_A (\{\delta e\}^T \{N\} + \{\delta \kappa\}^T \{M\}) \, dA \, . \tag{2.34}$$

Using Eqs. (2.12), (2.22), (2.23) and (2.28), the virtual strains and curvatures are given by

$$\begin{aligned} \{\delta e\} &= \delta\{[B_m] \{\beta\} + \tfrac{1}{2} [A] \{\theta\} + [A] \{\theta_o\}\} \\ &= [B_m] \{\delta\beta\} + \delta\{\tfrac{1}{2} [A] \{\theta\}\} + [\delta A] \{\theta_o\} \\ &= [B_m] \{\delta\beta\} + [A] \{\delta\theta\} + [A_o] \{\delta\theta\} \end{aligned} \tag{2.35}$$

where

$$\delta\{\tfrac{1}{2}\,[A]\,\{\theta\}\} = [A]\,\{\delta\theta\} \tag{2.36}$$

$$[\delta A]\,\{\theta_o\} = [A_o]\,\{\delta\theta\}\ , \tag{2.37}$$

$$\{\delta\kappa\} = \delta\{[B_b]\,\{\alpha\}\} = [B_b]\,\{\delta\alpha\}\ . \tag{2.38}$$

Substituting Eqs. (2.31), (2.35) and (2.38) into (2.34), the virtual work of the internal forces becomes

$$\begin{aligned}
\delta W_{int} &= \int_A \left(\left[\{\delta\beta\}^T\,[B_m]^T + \{\delta\theta\}^T\,[A]^T + \{\delta\theta\}^T\,[A_o]^T\right]\{[C]\,\{e\}\right. \\
&\quad \left. + \{N_o\} - \{N_{\Delta T}\}\right\} + \left[\{\delta\alpha\}^T\,[B_b]^T\right]\{[D]\,\{\kappa\} + \{M_o\}\}\Big)\,dA \\
&= \int_A \left(\{\delta\beta\}^T\,[B_m]^T\,[C]\,\{e\} + \{\delta\beta\}^T\,[B_m]^T\,\{N_o\} - \{\delta\beta\}^T\,[B_m]^T\,\{N_{\Delta T}\}\right. \\
&\quad + \{\delta\theta\}^T\,[A]^T\,[C]\,\{e\} + \{\delta\theta\}^T\,[A]^T\,\{N_o\} - \{\delta\theta\}^T\,[A]^T\,\{N_{\Delta T}\} \\
&\quad + \{\delta\theta\}^T\,[A_o]^T\,[C]\,\{e\} + \{\delta\theta\}^T\,[A_o]^T\,\{N_o\} - \{\delta\theta\}^T\,[A_o]^T\,\{N_{\Delta T}\} \\
&\quad \left. + \{\delta\alpha\}^T\,[B_b]^T\,[D]\,\{\kappa\} + \{\delta\alpha\}^T\,[B_b]^T\,\{M_o\}\right)\,dA\ .
\end{aligned} \tag{2.39}$$

For equilibrium under the action of forces $\{N_o\}$ and moments $\{M_o\}$ with the normal displacement w equal to zero, the virtual strains and curvatures from Eqs. (2.35) and (2.38) are given as

$$\{\delta e\} = [B_m]\,\{\delta\beta\} + [A_o]\,\{\delta\theta\}$$

$$\{\delta\kappa\} = [B_b]\,\{\delta\alpha\}\ ,$$

and the principle of virtual work takes the form

$$\begin{aligned}
&\int_A \left(\{\delta\beta\}^T\,[B_m]^T\,\{N_o\} + \{\delta\theta\}^T\,[A_o]^T\,\{N_o\}\right. \\
&\quad \left. + \{\delta\alpha\}^T\,[B_b]^T\,\{M_o\}\right)\,dA = 0\ .
\end{aligned} \tag{2.40}$$

Enforcing Eq. (2.40) and using Eqs. (2.12), (2.22), (2.23), (2.28) and (2.39), δW_{int} can be expressed as

$$\begin{aligned}\delta W_{int} = \int_A \Big(& \{\delta\beta\}^T [B_m]^T [C] [B_m] \{\beta\} + \{\delta\beta\}^T [B_m]^T [C] \tfrac{1}{2} [A] \{\theta\} \\ & + \{\delta\beta\}^T [B_m]^T [C] [A_o] \{\theta\} - \{\delta\beta\}^T [B_m]^T \{N_{\Delta T}\} \\ & + \{\delta\theta\}^T [A]^T [C] [B_m] \{\beta\} + \{\delta\theta\}^T [A]^T [C] \tfrac{1}{2} [A] \{\theta\} \\ & + \{\delta\theta\}^T [A]^T [C] [A_o] \{\theta\} + \{\delta\theta\}^T [A]^T \{N_o\} - \{\delta\theta\}^T [A]^T \{N_{\Delta T}\} \\ & + \{\delta\theta\}^T [A_o]^T [C] [B_m] \{\beta\} + \{\delta\theta\}^T [A_o]^T [C] \tfrac{1}{2} [A] \{\theta\} \\ & + \{\delta\theta\}^T [A_o]^T [C] [A_o] \{\theta\} - \{\delta\theta\}^T [A_o]^T \{N_{\Delta T}\} \\ & + \{\delta\alpha\}^T [B_b]^T [D] [B_b] \{\alpha\}\Big) \, dA \, . \end{aligned} \tag{2.41}$$

The standard linear stiffness matrices are represented by the first and last terms in Eq. (2.41) as

$$\int_A \left(\{\delta\beta\}^T [B_m]^T [C] [B_m] \{\beta\} + \{\delta\alpha\}^T [B_b]^T [D] [B_b] \{\alpha\} \right) dA \, . \tag{2.42}$$

Using Eqs. (2.9) and (2.10) to transform from generalized coordinates to nodal displacements, Eq. (2.42) becomes

$$\{\delta a_m\}^T [k_m] \{a_m\} + \{\delta a_b\}^T [k_b] \{a_b\} \tag{2.43}$$

where

$$[k_m] = [T_m]^T \int_A [B_m]^T [C] [B_m] \, dA \, [T_m] \tag{2.44}$$

$$[k_b] = [T_b]^T \int_A [B_b]^T [D] [B_b] \, dA \, [T_b] \, . \tag{2.45}$$

Linear stiffness contributions due to the initial deflection w_o are represented by the third, tenth and twelfth terms in Eq. (2.41) as

$$\int_A (\{\delta\beta\}^T [B_m]^T [C] [A_o] \{\theta\} + \{\delta\theta\}^T [A_o]^T [C] [B_m] \{\beta\}$$

$$+ \{\delta\theta\}^T [A_o]^T [C] [A_o] \{\theta\}) \, dA \quad . \tag{2.46}$$

Using Eqs. (2.9), (2.10) and (2.24), Eq. (2.46) becomes

$$\{\delta a_m\}^T [k_{mb}] \{a_b\} + \{\delta a_b\}^T [k_{mb}]^T \{a_m\} + \{\delta a_b\}^T [k_{bo}] \{a_b\} \tag{2.47}$$

where

$$[k_{mb}] = [T_m]^T \int_A [B_m]^T [C] [A_o] [B_\theta] \, dA \, [T_b] \tag{2.48}$$

$$[k_{bo}] = [T_b]^T \int_A [B_\theta]^T [A_o]^T [C] [A_o] [B_\theta] \, dA \, [T_b] \quad . \tag{2.49}$$

Geometric stiffness contributions due to the initial and thermal stresses are given by the eighth, ninth and thirteenth terms in Eq. (2.41) as

$$\int_A (\{\delta\theta\}^T [A]^T \{N_o\} - \{\delta\theta\}^T [A]^T \{N_{\Delta T}\} - \{\delta\theta\}^T [A_o]^T \{N_{\Delta T}\}) \, dA \quad . \tag{2.50}$$

The terms in Eq. (2.50) display the following property

$$\begin{aligned} [A]^T \{N_o\} &= [N_o] \{\theta\} \\ [A]^T \{N_{\Delta T}\} &= [N_{\Delta T}] \{\theta\} \\ [A_o]^T \{N_{\Delta T}\} &= [N_{\Delta T}] \{\theta_o\} \end{aligned} \tag{2.51}$$

where

$$\{N_o\} = \begin{Bmatrix} N_{ox} \\ N_{oy} \\ N_{oxy} \end{Bmatrix}$$

$$[N_o] = \begin{bmatrix} N_{ox} & N_{oxy} \\ N_{oxy} & N_{oy} \end{bmatrix}$$

$$\{N_{\Delta T}\} = \begin{Bmatrix} N_{\Delta Tx} \\ N_{\Delta Ty} \\ 0 \end{Bmatrix}$$

$$[N_{\Delta T}] = \begin{bmatrix} N_{\Delta Tx} & 0 \\ 0 & N_{\Delta Ty} \end{bmatrix} .$$

Using Eqs. (2.9), (2.24) and (2.51), Eq. (2.50) becomes

$$\{\delta a_b\}^T [k_{No}] \{a_b\} - \{\delta a_b\}^T [k_{N\Delta T}] \{a_b + a_{bo}\} \qquad (2.52)$$

where

$$[k_{No}] = [T_b]^T \int_A [B_\theta]^T [N_o] [B_\theta] \, dA \, [T_b] \qquad (2.53)$$

$$[k_{N\Delta T}] = [T_b]^T \int_A [B_\theta]^T [N_{\Delta T}] [B_\theta] \, dA \, [T_b] . \qquad (2.54)$$

First-order stiffness contributions due to coupling between the initial deflection w_o and the deflection w are given by the seventh and eleventh terms in Eq. (2.41) as

$$\int_A (\{\delta\theta\}^T [A]^T [C] [A_o] \{\theta\} + \{\delta\theta\}^T [A_o]^T [C] \tfrac{1}{2} [A] \{\theta\}) \, dA . \qquad (2.55)$$

To transform Eq. (2.55) to a symmetric form, a procedure similar to that given in Ref. [71] is followed. The first term in Eq. (2.55) can be written as

$$\{\delta\theta\}^T [A]^T [C] [A_o] \{\theta\} = \frac{1}{2} \{\delta\theta\}^T [A]^T [C] [A_o] \{\theta\}$$

$$+ \frac{1}{2} \{\delta\theta\}^T [A]^T [C] [A_o] \{\theta\} . \quad (2.56)$$

Letting

$$\{N_{bo}\} = [C] [A_o] \{\theta\} \quad (2.57)$$

and using the same property as given by Eqs. (2.51), the terms on the right hand side of Eq. (2.56) can be expressed as

$$\frac{1}{2} \{\delta\theta\}^T [A]^T [C] [A_o] \{\theta\} = \frac{1}{2} \{\delta\theta\}^T [A]^T \{N_{bo}\}$$

$$= \frac{1}{2} \{\delta\theta\}^T [N_{bo}] \{\theta\} . \quad (2.58)$$

Using Eqs. (2.9), (2.24), (2.56) and (2.58), Eq. (2.55) becomes

$$\frac{1}{2} \{\delta a_b\}^T [nl_{bbo}] \{a_b\} \quad (2.59)$$

where

$$[nl_{bbo}] = [T_b]^T \int_A [B_\theta]^T [[A]^T [C] [A_o] + [A_o]^T [C] [A]$$

$$+ [N_{bo}]] [B_\theta] \, dA \, [T_b] . \quad (2.60)$$

First-order stiffness contributions due to the deflection w are contained in the second and fifth terms of Eq. (2.41) and are given by

$$\int_A (\{\delta\beta\}^T [B_m]^T [C] \frac{1}{2} [A] \{\theta\} + \{\delta\theta\}^T [A]^T [C] [B_m] \{\beta\}) \, dA . \quad (2.61)$$

Equation (2.61) can also be transformed to a symmetric form in the same fashion as Eq. (2.55). The second term in Eq. (2.61) can be expressed as

$$\{\delta\theta\}^T [A]^T [C] [B_m] \{\beta\} = \frac{1}{2} \{\delta\theta\}^T [A]^T [C] [B_m] \{\beta\} + \frac{1}{2} \{\delta\theta\}^T [N_m] \{\theta\} \quad (2.62)$$

where

$$\{N_m\} = [C] [B_m] \{\beta\} . \quad (2.63)$$

Using Eqs. (2.9), (2.10), (2.24) and (2.62), Eq. (2.61) can be written as

$$\frac{1}{2} [\{\delta a_m\}^T [nl_{mb}] \{a_b\} + \{\delta a_b\}^T [nl_{mb}]^T \{a_m\} + \{\delta a_b\}^T [nl_m] \{a_b\}] \quad (2.64)$$

where

$$[nl_{mb}] = [T_m]^T \int_A [B_m]^T [C] [A] [B_\theta] \, dA \, [T_b] \quad (2.65)$$

$$[nl_m] = [T_b]^T \int_A [B_\theta]^T [N_m] [B_\theta] \, dA \, [T_b] . \quad (2.66)$$

The second-order stiffness contribution due to the deflection w can be obtained by examining the sixth term in Eq. (2.41) and is given by

$$\int_A \{\delta\theta\}^T [A]^T [C] \frac{1}{2} [A] \{\theta\} \, dA . \quad (2.67)$$

This term can be transformed in the same manner as Eqs. (2.55) and (2.61) to obtain

$$\{\delta\theta\}^T [A]^T [C] \frac{1}{2} [A] \{\theta\} = \frac{1}{3} \{\delta\theta\}^T [A]^T [C] [A] \{\theta\} + \frac{1}{3} \{\delta\theta\}^T [N_b] \{\theta\} \quad (2.68)$$

where

$$\{N_b\} = [C] \frac{1}{2} [A] \{\theta\} . \quad (2.69)$$

Using Eqs. (2.9), (2.24) and (2.68), Eq. (2.67) takes the form

$$\frac{1}{3} \{\delta a_b\}^T [n2_{bb}] \{a_b\} \tag{2.70}$$

where

$$[n2_{bb}] = [T_b]^T \int_A [B_\theta]^T [[A]^T [C] [A] + [N_b]] [B_\theta] \, dA \, [T_b] \, . \tag{2.71}$$

Finally, the fourth term in Eq. (2.41), given by

$$- \int_A \{\delta\beta\}^T [B_m]^T \{N_{\Delta T}\} \, dA \, , \tag{2.72}$$

represents a thermal load vector. Using Eq. (2.10), Eq. (2.72) becomes

$$- \{\delta a_m\}^T \{p_{m\Delta T}\} \tag{2.73}$$

where

$$\{p_{m\Delta T}\} = [T_m]^T \int_A [B_m]^T \{N_{\Delta T}\} \, dA \, . \tag{2.74}$$

Combining Eqs. (2.43), (2.47), (2.52), (2.59), (2.64), (2.70) and (2.73), Eq. (2.41) can be written as

$$\begin{aligned} \delta W_{int} = {} & \{\delta a_m\}^T [k_m] \{a_m\} + \{\delta a_m\}^T [[k_{mb}] + \tfrac{1}{2} [n1_{mb}]] \{a_b\} \\ & + \{\delta a_b\}^T [[k_{mb}]^T + \tfrac{1}{2} [n1_{mb}]^T] \{a_m\} \\ & + \{\delta a_b\}^T [[k_b] + [k_{bo}] + [k_{No}] \\ & + \tfrac{1}{2} [n1_{bbo}] + \tfrac{1}{2} [n1_m] + \tfrac{1}{3} [n2_{bb}]] \{a_b\} \\ & - \{\delta a_b\}^T [k_{N\Delta T}] \{a_b + a_{bo}\} - \{\delta a_m\}^T \{p_{m\Delta T}\} \, . \end{aligned} \tag{2.75}$$

The virtual work of the inertia and damping forces can be included using D'Alembert's principle; so, the total virtual work of the external forces is due to inertia forces, damping forces and the applied random pressure loading and is given by

$$\delta W_{ext} = \int_A \delta w \, (- \rho h \ddot{w} - c\dot{w} + p) \, dA \, . \tag{2.76}$$

Using Eqs. (2.1) and (2.9), the displacement w is given by

$$w = [H_w] \, [T_b] \, \{a_b\} \, . \tag{2.77}$$

Thus,

$$\delta w = [H_w] \, [T_b] \, \{\delta a_b\} \tag{2.78}$$

$$\dot{w} = [H_w] \, [T_b] \, \{\dot{a}_b\} \tag{2.79}$$

$$\ddot{w} = [H_w] \, [T_b] \, \{\ddot{a}_b\} \, . \tag{2.80}$$

Substituting Eqs. (2.78), (2.79) and (2.80) into Eq. (2.76), the virtual work of the external forces can be expressed as

$$\delta W_{ext} = - \{\delta a_b\}^T [m_b] \{\ddot{a}_b\} - \{\delta a_b\}^T [c_b] \{\dot{a}_b\} + \{\delta a_b\}^T \{p_b\} \tag{2.81}$$

where

$$[m_b] = [T_b]^T \int_A [H_w]^T \rho h \, [H_w] \, dA \, [T_b] \tag{2.82}$$

$$\{p_b\} = [T_b]^T \int_A [H_w]^T \, p \, dA \, , \tag{2.83}$$

and $[c_b]$ is assumed to be proportional to $[m_b]$.

Using Eqs. (2.33), (2.75) and (2.81) and summing the contributions from all elements, the system equations of motion can be expressed as

$$\{\Psi(Q,\dot{Q},\ddot{Q})\} = [K + \frac{1}{2} N1 + \frac{1}{3} N2] \{Q\}$$

$$+ [C] \{\dot{Q}\} + [M] \{\ddot{Q}\}$$

$$- \{P\} = \{0\} \qquad (2.84)$$

where

$$[K] = \begin{bmatrix} [K_b + K_{bo} + K_{No} - K_{N\Delta T}] & [K_{mb}]^T \\ [K_{mb}] & [K_m] \end{bmatrix}$$

$$[N1] = \begin{bmatrix} [N1_{bbo} + N1_m] & [N1_{mb}]^T \\ [N1_{mb}] & 0 \end{bmatrix}$$

$$[N2] = \begin{bmatrix} [N2_{bb}] & 0 \\ 0 & 0 \end{bmatrix}$$

$$[C] = \begin{bmatrix} \xi [M_b] & 0 \\ 0 & 0 \end{bmatrix}$$

$$[M] = \begin{bmatrix} [M_b] & 0 \\ 0 & 0 \end{bmatrix}$$

$$\{P\} = \begin{Bmatrix} \{P_b\} + [K_{N\Delta T}] \{Q_{bo}\} \\ \{P_{m\Delta T}\} \end{Bmatrix}$$

$$_tQ\} = \begin{Bmatrix} \{Q_b\} \\ \{Q_m\} \end{Bmatrix} .$$

2.4.2 Stability Equations

The adjacent-equilibrium criterion [75] can be used to investigate the stability of a given equilibrium configuration. This involves giving small increments to the displacements and examining the two adjacent configurations. Letting

$$\begin{aligned} \{Q\} &\rightarrow \{Q_1 + \Delta Q\} \\ \{\dot{Q}\} &\rightarrow \{\dot{Q}_1 + \Delta\dot{Q}\} \\ \{\ddot{Q}\} &\rightarrow \{\ddot{Q}_1 + \Delta\ddot{Q}\} \end{aligned} \tag{2.85}$$

where the incremental quantities $\{\Delta Q\}$, $\{\Delta\dot{Q}\}$ and $\{\Delta\ddot{Q}\}$ are arbitrarily small and $\{\Psi(Q_1,\dot{Q}_1,\ddot{Q}_1)\}$ is an equilibrium configuration. $\{\Psi(Q_1 + \Delta Q, \dot{Q}_1 + \Delta\dot{Q},\ddot{Q}_1 + \Delta\ddot{Q})\}$ can be investigated using a curtailed Taylor series as

$$\{\Psi(Q_1 + \Delta Q,\dot{Q}_1 + \Delta\dot{Q},\ddot{Q}_1 + \Delta\ddot{Q})\} = [\frac{d\Psi}{dQ}(Q_1,\dot{Q}_1,\ddot{Q}_1)]\ \{\Delta Q\}$$

$$+ [\frac{d\Psi}{d\dot{Q}}(Q_1,\dot{Q}_1,\ddot{Q}_1)]\ \{\Delta\dot{Q}\} + [\frac{d\Psi}{d\ddot{Q}}(Q_1,\dot{Q}_1,\ddot{Q}_1)]\ \{\Delta\ddot{Q}\} = \{0\}\ . \tag{2.86}$$

From Eq. (2.84), the total differential of $\{\Psi(Q,\dot{Q},\ddot{Q})\}$ is

$$\{d\Psi(Q,\dot{Q},\ddot{Q})\} = [K]\ \{dQ\} + d\{[\tfrac{1}{2}\ N1 + \tfrac{1}{3}\ N2]\ \{Q\}\}$$

$$+ [C]\ \{d\dot{Q}\} + [M]\ \{d\ddot{Q}\}\ . \tag{2.87}$$

Evaluating the term $d\{[\frac{1}{2}\ N1 + \frac{1}{3}\ N2]\ \{Q\}\}$ requires an examination of the corresponding terms in the element equilibrium equations. Using Eqs. (2.9), (2.10), (2.24), (2.55), (2.61) and (2.67), the contributions to

the element equilibrium equations due to first-order coupling terms, first-order terms and second-order terms, respectively, are

$$[T_b]^T \int_A ([B_\theta]^T [A]^T [C] [A_o] \{\theta\} + [B_\theta]^T [A_o]^T [C] \tfrac{1}{2} [A] \{\theta\}) \, dA \tag{2.88}$$

$$[T_b]^T \int_A [B_\theta]^T [A]^T [C] [B_m] \{\beta\} \, dA$$

$$+ [T_m]^T \int_A [B_m]^T [C] \tfrac{1}{2} [A] \{\theta\} \, dA \tag{2.89}$$

$$[T_b]^T \int_A [B_\theta]^T [A]^T [C] \tfrac{1}{2} [A] \{\theta\} \, dA \, . \tag{2.90}$$

The incremental forms of Eqs. (2.88) through (2.90) can be found by taking the derivatives of the equations with respect to the generalized coordinates which can be accomplished by considering the total differential of each equation. The total differential of Eq. (2.88) is

$$[T_b]^T \int_A ([B_\theta]^T [dA]^T [C] [A_o] \{\theta\} + [B_\theta]^T [A]^T [C] [A_o] \{d\theta\}$$

$$+ [B_\theta]^T [A_o]^T [C] \, d\{\tfrac{1}{2} [A] \{\theta\}\}) \, dA \, . \tag{2.91}$$

Using Eq. (2.36),

$$d\{\tfrac{1}{2} [A] \{\theta\}\} = [A] \{d\theta\} \, , \tag{2.92}$$

and using Eq. (2.57) in conjunction with the property displayed by Eqs. (2.51),

$$[dA]^T [C] [A_o] \{\theta\} = [dA]^T \{N_{bo}\} = [N_{bo}] \{d\theta\} \, . \tag{2.93}$$

Combining Eqs. (2.9), (2.24), (2.60), (2.92) and (2.93), Eq. (2.91) can be written as

$$[nl_{bbo}] \{da_b\} . \tag{2.94}$$

The total differential of Eq. (2.89) is given by

$$[T_b]^T \int_A ([B_\theta]^T [dA]^T [C] [B_m] \{\beta\} + [B_\theta]^T [A]^T [C] [B_m] \{d\beta\}) dA$$
$$+ [T_m]^T \int_A [B_m]^T [C] d\{\tfrac{1}{2} [A] \{\theta\}\} dA . \tag{2.95}$$

Using Eq. (2.63) and considering Eqs. (2.51),

$$[dA]^T [C] [B_m] \{\beta\} = [dA]^T \{N_m\} = [N_m] \{d\theta\} . \tag{2.96}$$

Combining Eqs. (2.9), (2.10), (2.24), (2.65), (2.66), (2.92) and (2.96), Eq. (2.95) can be expressed as

$$[nl_m] \{da_b\} + [nl_{mb}]^T \{da_m\} + [nl_{mb}] \{da_b\} . \tag{2.97}$$

Finally, the total differential of Eq. (2.90) is

$$[T_b]^T \int_A ([B_\theta]^T [dA]^T [C] \tfrac{1}{2} [A] \{\theta\}$$
$$+ [B_\theta]^T [A]^T [C] d\{\tfrac{1}{2} [A] \{\theta\}\}) dA . \tag{2.98}$$

Using Eq. (2.69) and again considering Eqs. (2.51),

$$[dA]^T [C] \tfrac{1}{2} [A] \{\theta\} = [dA]^T \{N_b\} = [N_b] \{d\theta\} . \tag{2.99}$$

Combining Eqs. (2.9), (2.24), (2.71), (2.92) and (2.99), Eq. (2.98) can be written as

$$[n2_{bb}] \{da_b\} . \tag{2.100}$$

Summing the contributions from all elements, the total differential of the system equations of motion related to the first- and second-order stiffness matrices becomes

$$d\{[\tfrac{1}{2} N1 + \tfrac{1}{3} N2] \{Q\}\} = [N1 + N2] \{dQ\} \quad . \qquad (2.101)$$

Combining Eqs. (2.87) and (2.101), the incremental equilibrium equations expressed by Eq. (2.86) can be written as

$$[K + N1 + N2] \{\Delta Q\} + [C] \{\Delta \dot{Q}\} + [M] \{\Delta \ddot{Q}\} = \{0\} \quad . \qquad (2.102)$$

where [K], [N1], [N2], [C] and [M] are as given by Eq. (2.84).

Chapter 3

COMPUTATIONAL PROCEDURE

This chapter presents a detailed description of the computational methods used to solve the problems of thermal postbuckling and large deflection random vibration. Each of these problems is nonlinear and, therefore, must be solved using an iterative solution technique with the iterative solution being terminated when the appropriate convergence criteria are satisfied.

3.1 Thermal Postbuckling Solution

The method of Newton-Raphson iteration is a well established procedure for solving time independent, nonlinear problems [25, 26, 76, 77]. This method requires that the loading be applied in a series of increments. For sufficiently small loading increments convergence can be achieved even when severe nonlinearities are present [76, 77]. In addition, any level of accuracy can be obtained depending on the convergence criteria. Therefore, this method was chosen to solve the nonlinear thermal postbuckling equations.

For the thermal postbuckling of an initially flat plate with no initial stresses, the equations of motion and the incremental stability equations are given by Eqs. (2.84) and (2.102), respectively, where w_o, $\{N_o\}$ and $\{M_o\}$ are taken to be zero and the dynamic terms are not included. Equations (2.84) and (2.102) for this case can be written as

$$\{\Psi(Q)\} = [K + \frac{1}{2} N1 + \frac{1}{3} N2] \{Q\} - \{P\} = \{0\} \tag{3.1}$$

$$[\frac{d\Psi(Q)}{dQ}] \{\Delta Q\} = [K + N1 + N2] \{\Delta Q\} = \{0\} \tag{3.2}$$

where

$$[K] = \begin{bmatrix} [K_b - K_{N\Delta T}] & 0 \\ 0 & [K_m] \end{bmatrix}$$

$$[N1] = \begin{bmatrix} [N1_m] & [N1_{mb}]^T \\ [N1_{mb}] & 0 \end{bmatrix} \tag{3.3}$$

$$\{P\} = \begin{Bmatrix} 0 \\ \{P_{m\Delta T}\} \end{Bmatrix}$$

and [N2] and {Q} are defined by Eq. (2.84).

3.1.1 Determination of Critical Buckling Temperature

If an initially unstressed flat plate is subjected to a temperature distribution that varies only in the plane of the plate and is uniform through the plate thickness, the relationship between the applied temperature and the inplane deformation is given by Eq. (3.1) as

$$[K_m] \{Q_m\} = \{P_{m\Delta T}\} . \tag{3.4}$$

For a temperature variation $\Delta T_o(x,y)$, the thermal load vector $\{P_{m\Delta T}\}$ can be formed and Eq. (3.4) can be solved for the inplane displacements $\{Q_m\}$ which can be used in conjunction with Eqs. (2.10), (2.22) and (2.31) to determine the resulting inplane forces. The stability of this equilibrium configuration can be investigated using Eq. (3.2), which takes the form

$$\begin{bmatrix} [K_b - K_{N\Delta T} + Nl_m] & 0 \\ 0 & [K_m] \end{bmatrix} \begin{Bmatrix} \{\Delta Q_b\} \\ \{\Delta Q_m\} \end{Bmatrix} = \{0\} \quad . \tag{3.5}$$

Obviously, $\{\Delta Q_m\}$ is zero, but do temperature distributions exist for which $\{\Delta Q_b\}$ is nonzero? To answer this question, first consider that since Eq. (3.4) is linear, the inplane displacements for any variation in temperature can be expressed as a scale factor λ times the inplane displacements due to $\Delta T_o(x,y)$; therefore, since the first-order stiffness matrix $[Nl_m]$ is linearly dependent on the inplane displacements, $[Nl_m]$ for any temperature is given by λ times $[Nl_m]$ due to $\Delta T_o(x,y)$. In addition, the geometric stiffness matrix $[K_{N\Delta T}]$ is linearly dependent on temperature, hence for an arbitrary temperature variation $\lambda\ \Delta T_o(x,y)$ Eq. (3.5) can be written as

$$[K_b - \lambda\ K_{N\Delta T} + \lambda\ Nl_m]\ \{\Delta Q_b\} = \{0\}\ ,$$

or

$$[K_b]\ \{\phi\} = \lambda\ [K_{N\Delta T} - Nl_m]\ \{\phi\}\ . \tag{3.6}$$

Thus, the determination of the critical temperature variation, if one exists, reduces to the solution of the eigenvalue problem given by Eq. (3.6). The critical temperature at which buckling occurs correpsonds to the first value of λ for which $\{\phi\}$ is nontrivial and is given by $\Delta T_{CR}(x,y) = \lambda_1\ \Delta T_o(x,y)$, and $\{\phi\}_1$ is the buckling mode shape associated with λ_1. The flow-chart for the thermal buckling solution is shown in Fig. 3.1.

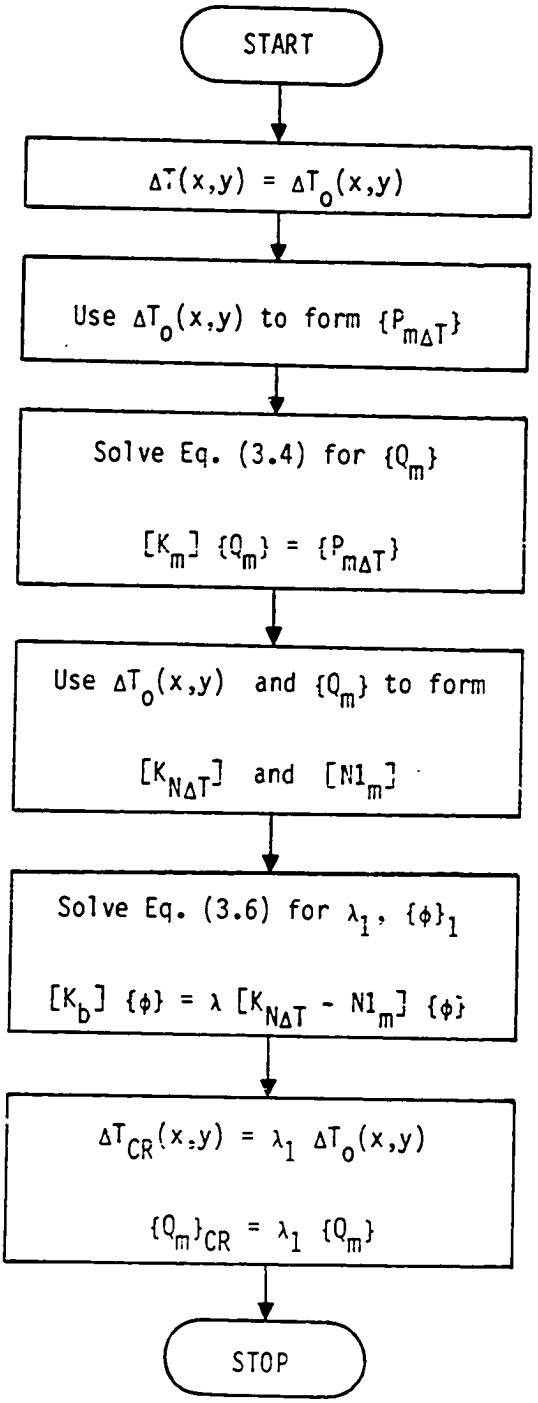

Fig. 3.1 Computer flow-chart for thermal buckling solution.

3.1.2 Solution of Thermal Postbuckling Equations

Equation (3.1) can be solved for a given thermal loading by using the method of Newton-Raphson iteration. If a solution is known for configuration $\{Q\}$, then the solution at configuration $\{Q + \Delta Q\}$ can be approximated using a curtailed Taylor expansion of Eq. (3.1) given as

$$\{\Psi(Q + \Delta Q)\} = \{\Psi(Q)\} + [\frac{d\Psi(Q)}{dQ}] \{\Delta Q\} = \{0\} . \tag{3.7}$$

Equation (3.7) can be rewritten in terms of the tangent stiffness matrix $[K_T]$ and the incremental load vector $\{\Delta P\}$ as

$$[K_T] \{\Delta Q\} = \{\Delta P\} \tag{3.8}$$

where from Eqs. (3.1) and (3.2)

$$[K_T] = [\frac{d\Psi(Q)}{dQ}] = [K + N1 + N2]$$

$$\{\Delta P\} = - \{\Psi(Q)\} = \{P\} - [K + \frac{1}{2} N1 + \frac{1}{3} N2] \{Q\} .$$

The incremental load vector $\{\Delta P\}$ represents the equilibrium equation at configuration $\{Q\}$; hence, as $\{Q\}$ approaches the true solution, $\{\Delta P\}$ approaches zero. Equation (3.8) can be solved in an iterative fashion for a given thermal loading with the iterative process being terminated whenever the convergence criteria (Appendix B) are satisfied.

Typically, solutions are sought for several temperature variations $\Delta T(x,y)_j$ $(j = 1,\ldots, m)$ above the critical buckling temperature $\Delta T_{CR}(x,y)$; these temperature variations can be expressed as

$$\Delta T(x,y)_j = (T/T_{CR})_j \Delta T_{CR}(x,y) \tag{3.9}$$

where $(T/T_{CR})_j$ is a scale factor (> 1. for postbuckling). To begin the iterative process for a given thermal loading corresponding to $\Delta T(x,y)_j$, initial deflections $\{Q\}$ are necessary to evaluate $[K_T]$ and $\{\Delta P\}$. For j = 1 (the first solution in the postbuckling region) special care must be taken in estimating $\{Q\}$, and the following procedure has been found to be satisfactory. Take

$$\{Q\} = \begin{Bmatrix} \{Q_b\} \\ \{Q_m\} \end{Bmatrix} \tag{3.10}$$

where

$$\{Q_b\} = A_1 \{\phi\}_1$$

$$\{Q_m\} = (T/T_{CR})_1 \{Q_m\}_{CR}$$

with $\{\phi\}_1$ and $\{Q_m\}_{CR}$, respectively, being the buckling mode shape (normalized to a maximum value equal to the plate thickness) and the inplane displacements corresponding to $\Delta T_{CR}(x,y)$. Satisfactory results have been obtained for $A_1 = 0.50$ and $(T/T_{CR})_1 = 1.05$. For j > 1, the displacements $\{Q\}$ to begin the iterative process can be updated using the previous solution as

$$\{Q\} = \frac{(T/T_{CR})_j}{(T/T_{CR})_{j-1}} \{Q\} \ . \tag{3.11}$$

The flow-chart of this solution process is shown in Fig. 3.2.

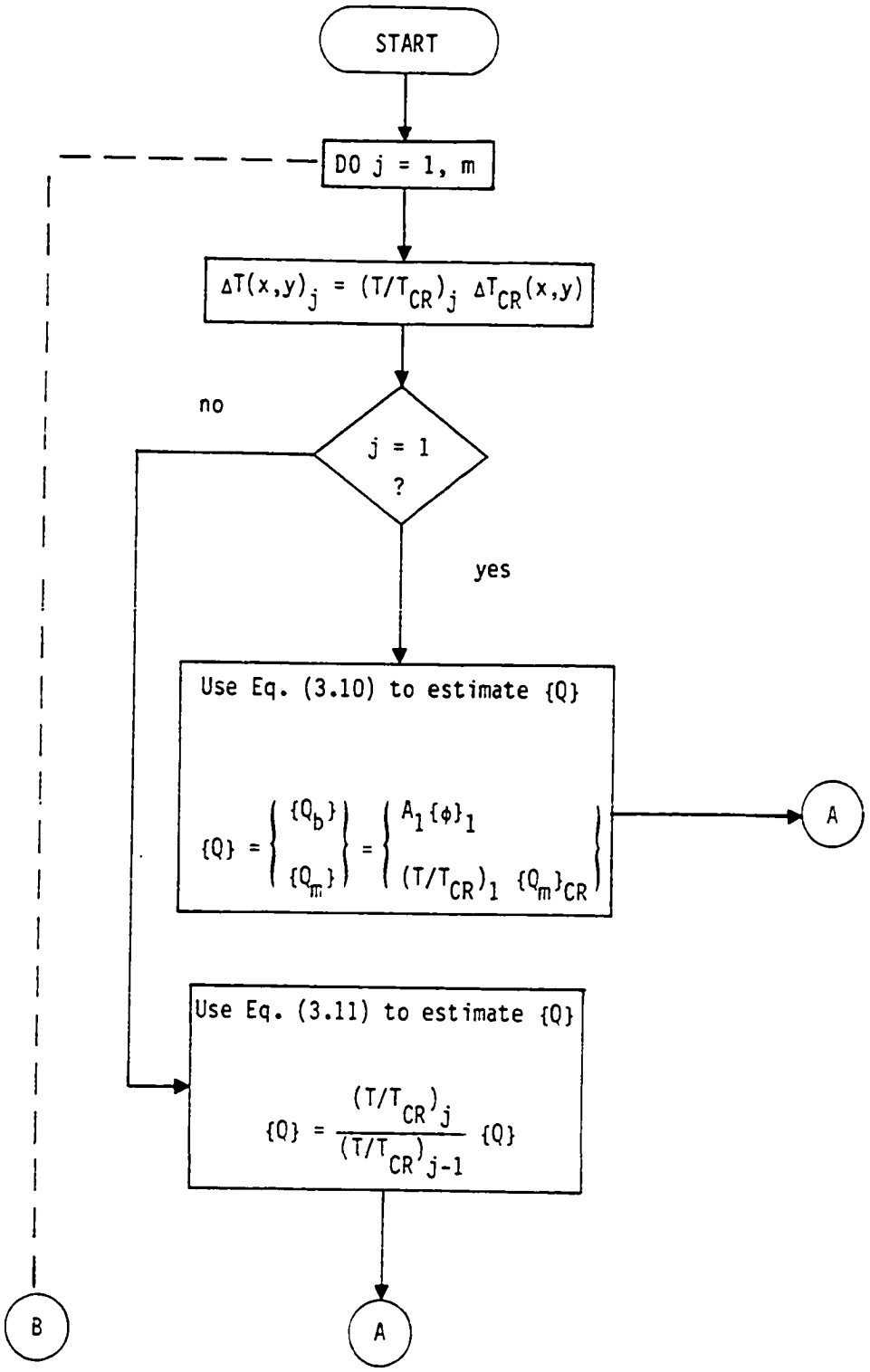

Fig. 3.2 Computer flow-chart for thermal postbuckling solution.

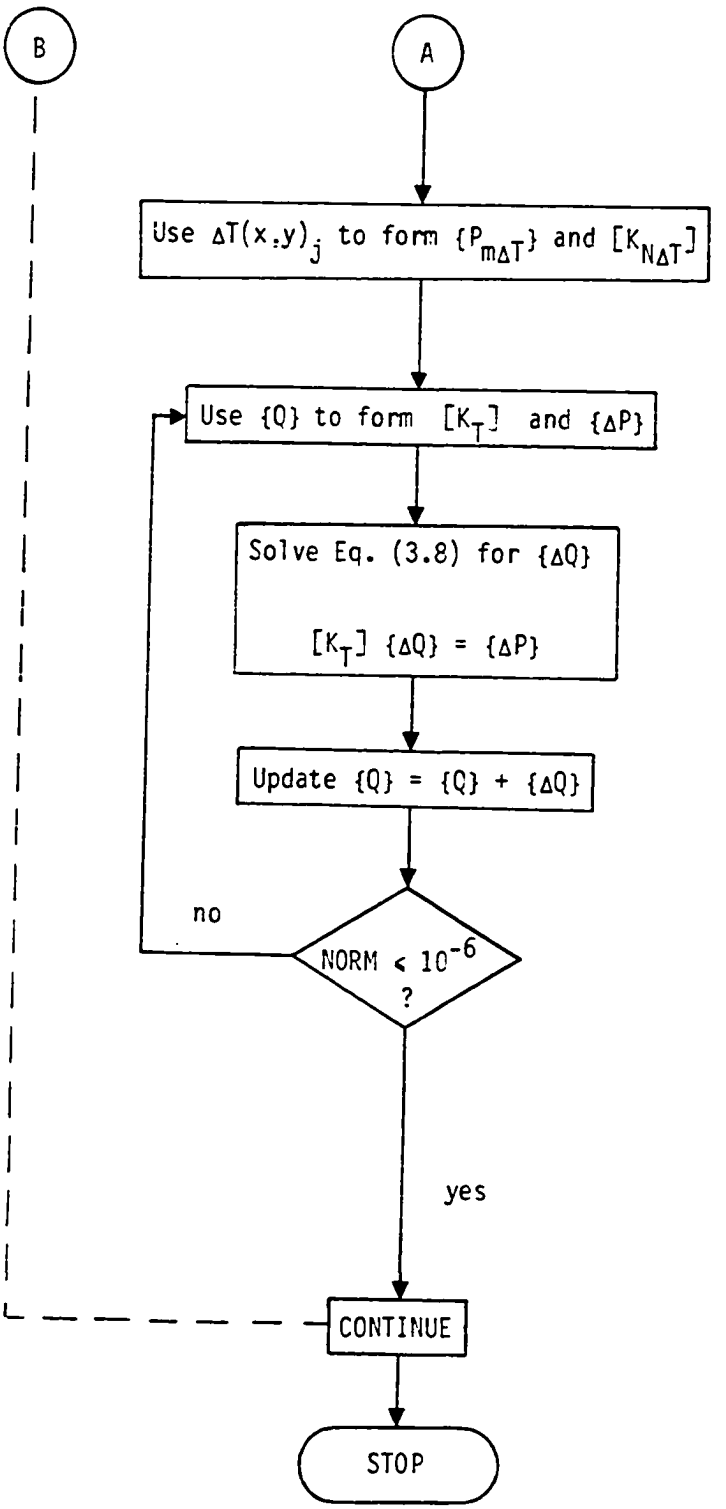

Fig. 3.2 Concluded.

3.2 Large Deflection Random Vibration Solution

Finite element solution methods for nonlinear random vibration are not nearly so well developed as solution methods for thermal postbuckling, and any of several approximate methods [34] could have been used, at least in theory, for the present formulation. Since satisfactory results have been obtained using the EL technique in conjunction with classical formulations, this technique was employed for the present study. Following an approach similar to Busby and Weingarten [47], the nonlinear equations of motion are reduced to a system of modal equations using the linear mode shapes of the thermally stressed or buckled structure to transfer from system to modal coordinates. The resulting modal equations are then solved using the EL method [78].

Equations (2.84) and (2.102) can be specialized for the large deflection random vibration of thermally buckled plates by setting the temperature distribution $\Delta T(x,y)$ equal to zero. For this case, w_o represents the initial buckled shape with corresponding initial inplane forces and moments $\{N_o\}$ and $\{M_o\}$; the equations of motion and the incremental equations given by Eqs. (2.84) and (2.102) become

$$[K + \tfrac{1}{2} N1 + \tfrac{1}{3} N2] \{Q\} + [C] \{\dot{Q}\} + [M] \{\ddot{Q}\} = \{P\} \tag{3.12}$$

$$[K + N1 + N2] \{\Delta Q\} + [C] \{\Delta\dot{Q}\} + [M] \{\Delta\ddot{Q}\} = \{0\} \tag{3.13}$$

where

$$[K] = \begin{bmatrix} [K_b + K_{bo} + K_{No}] & [K_{mb}]^T \\ [K_{mb}] & [K_m] \end{bmatrix}$$

$$\{P\} = \begin{Bmatrix} \{P_b\} \\ 0 \end{Bmatrix} \tag{3.14}$$

and [N1], [N2], [C], [M] and {Q} are defined by Eq. (2.84). Using Eq. (3.12), the inplane displacements can be written in terms of the bending displacements as

$$\{Q_m\} = -[K_m^{-1} K_{mb}]\{Q_b\} - \frac{1}{2}[K_m^{-1} N1_{mb}]\{Q_b\} . \tag{3.15}$$

Using Eq. (3.15), Eq. (3.12) can be written as

$$\begin{aligned}&[[K_b + K_{bo} + K_{No} - K_{mb}^T K_m^{-1} K_{mb}] \\ &\quad + \frac{1}{2}[N1_{bbo} + N1_m - K_{mb}^T K_m^{-1} N1_{mb} - N1_{mb}^T K_m^{-1} K_{mb}] \\ &\quad + [\frac{1}{3} N2_{bb} - \frac{1}{4} N1_{mb}^T K_m^{-1} N1_{mb}]]\{Q_b\} \\ &\quad + \xi[M_b]\{\dot{Q}_b\} + [M_b]\{\ddot{Q}_b\} = \{P_b\} .\end{aligned} \tag{3.16}$$

From Eq. (3.16), the linear frequencies and mode shapes of the thermally buckled structure can be obtained by solving the eigenvalue problem

$$[K_b + K_{bo} + K_{No} - K_{mb}^T K_m^{-1} K_{mb}]\{\phi\} = \omega^2 [M_b]\{\phi\} . \tag{3.17}$$

Solving Eq. (3.17), the truncated modal matrix is given by

$$[\Phi] = [\{\phi\}_1, \ldots, \{\phi\}_N] \tag{3.18}$$

where N is the number of modes to be used for the nonlinear analysis. Now $\{Q_b\}$ can be written in terms of the linear mode shapes as

$$\begin{aligned}\{Q_b\} &= [\Phi]\{q\} \\ &= \sum_{j=1}^{N} q_j \{\phi\}_j .\end{aligned} \tag{3.19}$$

Using Eq. (3.19), the nonlinear stiffness matrices can be written in terms of {q} as

$$[N1_{bbo}] = \sum_{j=1}^{N} q_j \, [N1_{bbc}]_j \tag{3.20}$$

$$[N1_{mb}] = \sum_{j=1}^{N} q_j \, [N1_{mb}]_j \tag{3.21}$$

$$[N2_{bb}] = \sum_{j=1}^{N} \sum_{k=1}^{N} q_j \, q_k \, [N2_{bb}]_{jk} \tag{3.22}$$

where $[N1_{bbo}]_j$, $[N1_{mb}]_j$ and $[N2_{bb}]_{jk}$ represent the sums of the element matrices $[n1_{bbo}]_j$, $[n1_{mb}]_j$ and $[n2_{bb}]_{jk}$, respectively. Using Eqs. (2.57), (2.60), (2.65), (2.69) and (2.71), the element matrices can be defined as

$$\begin{aligned}
[n1_{bbo}]_j &= [T_b]^T \int_A [B_\theta]^T \left[[A]_j^T [C] [A_o] + [A_o]^T [C] [A]_j \right. \\
&\quad \left. + [N_{bo}]_j \right] [B_\theta] \, dA \, [T_b] \\
[n1_{mb}]_j &= [T_m]^T \int_A [B_m]^T [C] [A]_j [B_\theta] \, dA \, [T_b] \\
[n2_{bb}]_{jk} &= [T_b]^T \int_A [B_\theta]^T \left[[A]_j^T [C] [A]_k + [N_b]_{jk} \right] [B_\theta] \, dA \, [T_b]
\end{aligned} \tag{3.23}$$

where the entries in $[A]_j$ correspond to $\{Q_b\} = \{\phi\}_j$ and the entries in $[N_{bo}]_j$ and $[N_b]_{jk}$ are for

$$\begin{aligned}
\{N_{bo}\}_j &= [C] [A_o] \{\theta\}_j \\
\{N_b\}_{jk} &= [C] \tfrac{1}{2} [A]_j \{\theta\}_k \, .
\end{aligned} \tag{3.24}$$

Substituting Eqs. (3.19) and (3.21) into Eq. (3.15), the expression for the inplane displacements becomes

$$\{Q_m\} = -\sum_{j=1}^{N} q_j \left[K_m^{-1} K_{mb}\right] \{\phi\}_j - \frac{1}{2} \sum_{j=1}^{N} \sum_{k=1}^{N} q_j q_k \left[K_m\right]^{-1} \left[N1_{mb}\right]_j \{\phi\}_k$$

$$= \sum_{j=1}^{N} q_j \{Q_m\}_j + \frac{1}{2} \sum_{j=1}^{N} \sum_{k=1}^{N} q_j q_k \{Q_m\}_{jk} \qquad (3.25)$$

where

$$\{Q_m\}_j = -\left[K_m^{-1} K_{mb}\right] \{\phi\}_j$$

$$\{Q_m\}_{jk} = -\left[K_m\right]^{-1} \left[N1_{mb}\right]_j \{\phi\}_k \ .$$

Using Eqs. (3.25), $[N1_m]$ can be expressed as

$$\left[N1_m\right] = \sum_{j=1}^{N} q_j \left[N1_m\right]_j + \frac{1}{2} \sum_{j=1}^{N} \sum_{k=1}^{N} q_j q_k \left[N1_m\right]_{jk} \qquad (3.26)$$

where $[N1_m]_j$ corresponds to $[N1_m]$ for $\{Q_m\} = \{Q_m\}_j$, of Eq. (3.25), $[N1_m]_{jk}$ corresponds to $[N1_m]$ for $\{Q_m\} = \{Q_m\}_{jk}$, of Eq. (3.25), and $[N1_m]$ is composed of element matrices $[n1_m]$ given by Eq. (2.66). Using Eqs. (3.19) through (3.22) and (3.26), Eq. (3.16) can be written as

$$\left[[k] + \frac{1}{2} \sum_{j=1}^{N} q_j \left[k1\right]_j + \sum_{j=1}^{N} \sum_{k=1}^{N} q_j q_k \left[k2\right]_{jk}\right] \{q\}$$

$$+ \xi \left[m\right] \{\dot{q}\} + \left[m\right] \{\ddot{q}\} = \{f\} \qquad (3.27)$$

where

$$\left[k\right] = \left[\phi\right]^T \left[K_b + K_{bo} + K_{No} - K_{mb}^T K_m^{-1} K_{mb}\right] \left[\phi\right]$$

$$= \begin{bmatrix} \omega_1^2 m_1 & & 0 \\ & \ddots & \\ 0 & & \omega_N^2 m_N \end{bmatrix}$$

$$[k1]_j = [\phi]^T \left[[N1_{bbo}]_j + [N1_m]_j - [K_{mb}^T K_m^{-1}] [N1_{mb}]_j \right.$$

$$\left. - [N1_{mb}]_j^T [K_m^{-1} K_{mb}] \right] [\phi]$$

$$[k2]_{jk} = [\phi]^T \left[\frac{1}{3} [N2_{bb}]_{jk} + \frac{1}{4} [N1_m]_{jk} - \frac{1}{4} [N1_{mb}]_j^T [K_m]^{-1} [N1_{mb}]_k \right] [\phi]$$

$$[m] = \begin{bmatrix} m_1 & \cdot & \cdot & 0 \\ & \cdot & & \\ & & \cdot & \\ 0 & & & m_N \end{bmatrix}$$

$$\{f\} = [\phi]^T \{P_b\} \quad .$$

Similarly, the incremental equations expressed by Eq. (3.13) can be written as

$$\left[[k] + \sum_{j=1}^{N} q_j [k1]_j + \sum_{j=1}^{N} \sum_{k=1}^{N} q_j q_k [k2_T]_{jk} \right] \{\Delta q\}$$

$$+ \xi [m] \{\Delta \dot{q}\} + [m] \{\Delta \ddot{q}\} = \{0\} \qquad (3.28)$$

where

$$[k2_T]_{jk} = [\phi]^T \left[[N2_{bb}]_{jk} + [N1_m]_{jk} - [N1_{mb}]_j^T [K_m]^{-1} [N1_{mb}]_k \right] [\phi] \quad .$$

3.2.1 Method of Equivalent Linearization

Consider that Eq. (3.27) can be written in the form

$$\{g(q)\} + \xi [m] \{\dot{q}\} + [m] \{\ddot{q}\} = \{f\}$$

where

$$\{g(q)\} = \left[[k] + \frac{1}{2} \sum_{j=1}^{N} q_j [k1]_j + \sum_{j=1}^{N} \sum_{k=1}^{N} q_j q_k [k2]_{jk} \right] \{q\} \quad . \qquad (3.29)$$

If Eq. (3.29) were linear, it could be expressed in the form

$$[\bar{k}] \{q\} + \xi [m] \{\dot{q}\} + [m] \{\ddot{q}\} = \{f\} \qquad (3.30)$$

where $[\bar{k}]$ is an equivalent linear stiffness matrix. The error involved in using Eq. (3.30) instead of Eq. (3.29) is given by the difference between the two equations as

$$\{e\} = \{g(q)\} - [\bar{k}]\{q\} . \tag{3.31}$$

The equivalent linear stiffness can be found by requiring that the mean square value of $\{e\}$ be a minimum, that is

$$E[\{e\}^T \{e\}] \rightarrow \text{minimum} . \tag{3.32}$$

For Eq. (3.32) to be true

$$\frac{\partial E[\{e\}^T \{e\}]}{\partial \bar{k}_{ij}} = 0 . \tag{3.33}$$

Substituting Eq. (3.31) into Eq. (3.32) and applying Eq. (3.33), the equivalent linear stiffness can be determined from the equation [78]

$$E[\{q\}\{q\}^T][\bar{k}] = E[\{q\}\{g(q)\}^T] . \tag{3.34}$$

Substituting from Eq. (3.29) for $\{g(q)\}$, the right hand side of Eq. (3.34) can be evaluated as

$$E[\{q\}\{g(q)\}^T] = E[\{q\}\{q\}^T][k] + \frac{1}{2}\sum_{j=1}^{N} E[q_j \{q\}\{q\}^T][k1]_j^T$$

$$+ \sum_{j=1}^{N}\sum_{k=1}^{N} E[q_j q_k \{q\}\{q\}^T][k2]_{jk}^T . \tag{3.35}$$

Since Eq. (3.30) is a linear equation and the excitation $\{f\}$ is Gaussian, it follows that $\{q\}$ is Gaussian, and for a Gaussian process with zero mean, the modal amplitudes follow the relations [48]

$$E[q_i\ q_j\ q_k] = 0$$

$$E[q_i\ q_j\ q_k\ q_l] = E[q_i\ q_j]\ E[q_k\ q_l] \tag{3.36}$$

$$+ E[q_i\ q_k]\ E[q_j\ q_l] + E[q_i\ q_l]\ E[q_j\ q_k]\ .$$

Applying Eqs. (3.36), Eq. (3.35) becomes

$$E[\{q\}\ \{g(q)\}^T] = E[\{q\}\ \{q\}^T]\ [k] + \sum_{j=1}^{N}\ \sum_{k=1}^{N} E[q_j\ q_k\ \{q\}\ \{q\}^T]\ [k2]^T_{jk} \tag{3.37}$$

since

$$E[q_j\ \{q\}\ \{q\}^T] = 0\ .$$

Therefore, if the covariance matrix $E[\{q\}\ \{q\}^T]$ is known, then Eqs. (3.34), (3.36) and (3.37) can be used to determine the equivalent linear stiffness $[\bar{k}]$. Conversely, if $[\bar{k}]$ is known then Eq. (3.30) can be used to determine the covariance matrix. The equivalent linear frequencies and mode shapes for the system described by Eq. (3.30) can be determined from the equation

$$[\bar{k}]\ \{\tilde{\phi}\} = \Omega^2\ [m]\ \{\tilde{\phi}\}\ . \tag{3.38}$$

Applying the coordinate transformation

$$\{q\} = [\tilde{\phi}]\ \{\eta\} \tag{3.39}$$

where

$$[\tilde{\phi}] = [\{\tilde{\phi}\}_1, \ldots, \{\tilde{\phi}\}_N]\ ,$$

Eq. (3.30) becomes uncoupled yielding the modal equations

$$\ddot{\eta}_j + \xi\ \dot{\eta}_j + \Omega_j^2\ \eta_j = \tilde{f}_j \tag{3.40}$$

where

$$\tilde{f}_j = \frac{\{\tilde{\phi}\}_j^T \{f\}}{\tilde{m}_j}$$

$$\tilde{m}_j = \{\tilde{\phi}\}_j^T [m] \{\tilde{\phi}\}_j .$$

Solutions for the system described by Eq. (3.40) are given in Ref. [79], and if the applied external loading p, of Eq. (2.76), is uniform, then the covariance terms for the case of ideal white noise can be expressed as

$$E[\eta_j \eta_k] = S_o \tilde{f}_j \tilde{f}_k I_{jk} \tag{3.41}$$

where

$$H_j(\omega) = \frac{1}{\Omega_j^2 - \omega^2 + i \xi \omega}$$

$$I_{jk} = \int_{-\infty}^{\infty} H_j(\omega) H_k(-\omega) d\omega ,$$

S_o is the double sided spectral density of the applied loading p in units of (pressure)^2/radian/sec and the nodal forces $\{P_b\}$, of Eq. (3.16), correspond to a unit pressure (p = 1.0).

Using the Residue Theorem, I_{jk} is found to be

$$I_{jk} = \frac{4 \pi \xi}{(\Omega_k^2 - \Omega_j^2)^2 + 2 \xi^2 (\Omega_j^2 + \Omega_k^2)} . \tag{3.42}$$

Typically, the spectral density of the excitation is single sided and is given in terms of (presssure)^2/Hz; Equation (3.41) modified for this case becomes

$$E[\eta_j \eta_k] = S_p \tilde{f}_j \tilde{f}_k \left[\frac{\xi}{(\Omega_k^2 - \Omega_j^2)^2 + 2 \xi^2 (\Omega_j^2 + \Omega_k^2)}\right] \tag{3.43}$$

where S_p is the single sided spectral density of the applied loading p in units of (pressure)^2/Hz.

Using Eq. (3.39), the covariance matrix $E[\{q\}\ \{q\}^T]$ becomes

$$E[\{q\}\ \{q\}^T] = E[[\tilde{\Phi}]\ \{\eta\}\ \{\eta\}^T\ [\tilde{\Phi}]^T]$$

$$= [\tilde{\Phi}]\ E[\{\eta\}\ \{\eta\}^T]\ [\tilde{\Phi}]^T \qquad (3.44)$$

where the terms for the covariance matrix $E[\{\eta\}\ \{\eta\}^T]$ are given by Eq. (3.43). Therefore, Eqs. (3.34), (3.36), (3.37), (3.38), (3.40), (3.43) and (3.44) can be used to determine $[\bar{k}]$ and $E[\{q\}\ \{q\}^T]$. However, since each of these quantities is dependent on the other, these equations are nonlinear and, consequently, must be solved using an iterative method. As a first approximation consider neglecting all cross correlation terms, i.e. $E[q_i\ q_j] = 0$ for $i \neq j$, and assuming that all of the equations are completely uncoupled. For this case, the diagonal terms in the equivalent linear stiffness matrix can be computed from Eqs. (3.34), (3.36) and (3.37) as

$$\bar{k}_{jj} = k_j + 3\ k2_{jjjj}\ E[q_j^2] \qquad (3.45)$$

where k_j and $k2_{jjjj}$ can be determined from Eq. (3.27). Alternatively, Eq. (3.45) can be written as

$$\Omega_j^2 = \frac{\bar{k}_{jj}}{m_j} = \omega_j^2 + 3\ k2_{jjjj}\ E[q_j^2] / m_j\ . \qquad (3.46)$$

Since all of the modes are assumed to be uncoupled, the equivalent linear stiffness matrix $[\bar{k}]$ is diagonal and $\eta_j = q_j$. As a result of this $\tilde{f}_j = f_j/m_j$, and $E[q_j^2]$ can be found from Eq. (3.43) to be

$$E[q_j^2] = S_p \frac{f_j^2}{m_j^2} \left(\frac{1}{4 \xi \Omega_j^2}\right) . \tag{3.47}$$

Using Eqs. (3.46) and (3.47), $E[q_j^2]$ can be determined to be

$$E[q_j^2] = (\sqrt{B^2 + 4C} - B)/2 \tag{3.48}$$

where

$$B = \frac{k_j}{3\ k2_{jjjj}}$$

$$C = \frac{S_p\ f_j^2}{12\ \xi\ m_j\ k2_{jjjj}} .$$

The covariance matrix of the displacements $\{Q_b\}$ can be found using Eq. (3.19) which yields

$$E[\{Q_b\}\ \{Q_b\}^T] = [\Phi]\ E[\{q\}\ \{q\}^T]\ [\Phi]^T . \tag{3.49}$$

To begin the coupled solution, the cross correlation terms $E[q_i\ q_j]$ for the covariance matrix can be evaluated using Eq. (3.43) with the equivalent linear frequencies given by Eq. (3.46). Using Eqs. (3.34), (3.36) and (3.37), the equivalent linear stiffness can be computed. Equations (3.38), (3.40), (3.43) and (3.44) can then be used to determine a new covariance matrix, and Eq. (3.49) can be used to compute the nodal displacement covariance matrix. If the convergence criteria (Appendix B) are satisfied then the iterative process is terminated.

This direct iteration method can be used to determine the mean square response; however, it is slow to converge. An improved method to

use for hardening type structures [76] is an underrelaxation approach where displacements are not updated to full values after an iteration. For the present problem, this method can be used for the covariance matrix as

$$E[\{q\}\ \{q\}^T]_{i+1} = (1-\beta)\ E[\{q\}\ \{q\}^T]_i + \beta\ E[\{q\}\ \{q\}^T]_{i+1} \qquad (3.50)$$

where $E[\{q\}\ \{q\}^T]_{i+1}$ is the computed covariance matrix for the current iteration and $E[\{q\}\ \{q\}^T]_i$ is for the previous iteration. This method was found to work very well with $\beta = 0.5$.

3.2.2 Snap-Through Boundary

To determine the possibility of a given configuration becoming unstable and snapping-through, the incremental equilibrium equations, Eq. (3.28), are considered. These equations, however, require the displacements $\{q\}$, and the method of equivalent linearization only provides the mean square displacements. For a harmonic steady-state loading, the relationship between the displacement amplitude and the root-mean-square displacement is

$$q = \sqrt{2}\ (E[q^2])^{1/2} \ . \qquad (3.51)$$

If the amplitude of the displacements is approximated using Eq. (3.51) and the incremental motion is taken to be harmonic then the frequency equation for incremental harmonic motion is

$$[k_T]\ \{\Delta q\} = \Delta\omega^2\ [m]\ \{\Delta q\} \qquad (3.52a)$$

where the tangent stiffness matrix in linear normal coordinates is given by

$$[k_T] = [[k] + \sum_{j=1}^{N} q_j [k1]_j + \sum_{j=1}^{N} \sum_{k=1}^{N} q_j q_k [k2_T]_{jk}] . \quad (3.52b)$$

Solutions to Eqs. (3.52) such that any of the incremental frequencies are zero would indicate that the incremental motion of the system is unbounded. Therefore, the stability boundary for snap-through is assumed to be that point at which any of the incremental frequencies vanish, which corresponds to the tangent stiffness matrix $[k_T]$ becoming singular, that is

$$|[k_T]| = 0 . \quad (3.53)$$

But $[k_T]$ is dependent on the displacements $\{q\}$; so, to evaluate the determinant of $[k_T]$, the displacements must first be determined. Equation (3.51) can be used to determine the displacement amplitudes, but the signs (positive or negative) must also be known. The mode shapes used for the present formulation are all scaled so that the maximum displacement component at the center of the structure is positive. As a result, the maximum center deflection occurs when all of the displacements $\{q\}$ are the same sign. For a structure such as the one shown in Fig. 2.1, the deflection w for snap-through motion is negative, and the maximum negative center deflection is obtained when all of the displacements $\{q\}$ are less than zero. This particular combination of displacements is assumed to be the configuration for which snap-through motion first occurs. So, to determine the stability of a given configuration, the displacements q_j $(j = 1,\ldots, N)$ are taken to be

$$q_j = - \sqrt{2}\ (E[q_j^2])^{1/2}, \tag{3.54}$$

$[k_T]$ is computed from Eq. (3.52b) and the determinant is computed. If the determinant is identically zero, then the corresponding configuration defines a snap-through boundary; if, however, the determinant is less than zero then the sound spectrum level at which snap-through occurs has already been exceeded. Although the displacements given by Eq. (3.54) do represent a possible configuration for which $[k_T]$ is singular, other configurations for which all of the displacements are not less than zero could also produce a singular $[k_T]$ since the matrices $[k1]_j$ and $[k2_T]_{jk}$ both contain positive and negative entries. In fact, there is no guarantee that the displacements given by Eq. (3.54) will produce a singular $[k_T]$. However, requiring the center deflection to obtain a maximum negative value is considered to be a reasonable method for predicting the onset of snap-through motion.

To determine the critical sound spectrum level at which the determinant of $[k_T]$ vanishes, the following procedure is employed. First, the snap-through boundary is determined for a single-mode solution as being the point at which $k_T = 0$. From Eq. (3.52b), the equation describing this condition is

$$k + q\ k1 + q^2\ k2_T = 0 \tag{3.55}$$

where

$$k = k_j$$

$$k1 = k1_{jjj}$$

$$k2_T = k2_{Tjjjj}$$

$$q = q_j$$

and $$j = 1 \ .$$

Solving Eq. (3.55), the critical value of q is given by

$$q_{CR} = (\sqrt{B^2 - 4C} - B)/2 \tag{3.56}$$

where

$$B = \frac{k1}{k2_T}$$

$$C = \frac{k}{k2_T} \ .$$

Using Eqs. (3.47), (3.54) and (3.56), the critical sound spectrum level is given by

$$S_{CR} = \frac{2\, q_{CR}^2\, m_1^2\, \xi\, \Omega_1^2}{f_1^2} \tag{3.57}$$

where Ω_1^2 is given by Eq. (3.46) for j = 1. Equation (3.57) can be used as an initial estimate of the critical snap-through sound spectrum level for multiple-mode solutions. To obtain a more accurate multiple-mode solution for the critical sound spectrum level, several EL solutions with sound spectrum levels close to that predicted by Eq. (3.57) can be computed, and the point at which the determinant of $[k_T]$ changes sign from positive to negative defines the snap-through boundary. The accuracy of this process is limited only by the difference in sound spectrum levels used to compute the various EL solutions. A computer flow-chart for large deflection random vibration, including snap-through, is shown in Fig. 3.3.

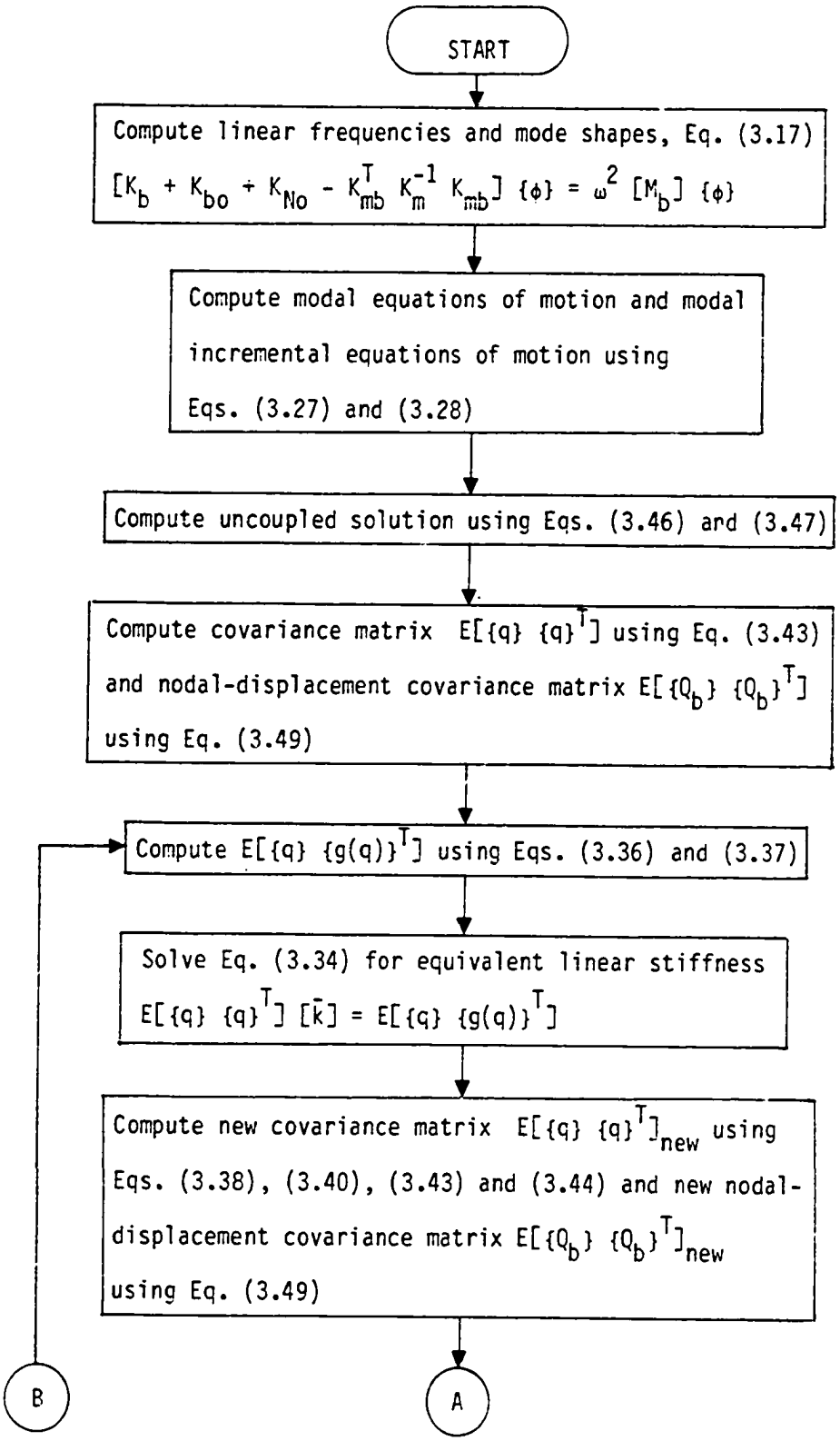

Fig. 3.3 Computer flow-chart for large deflection random vibration.

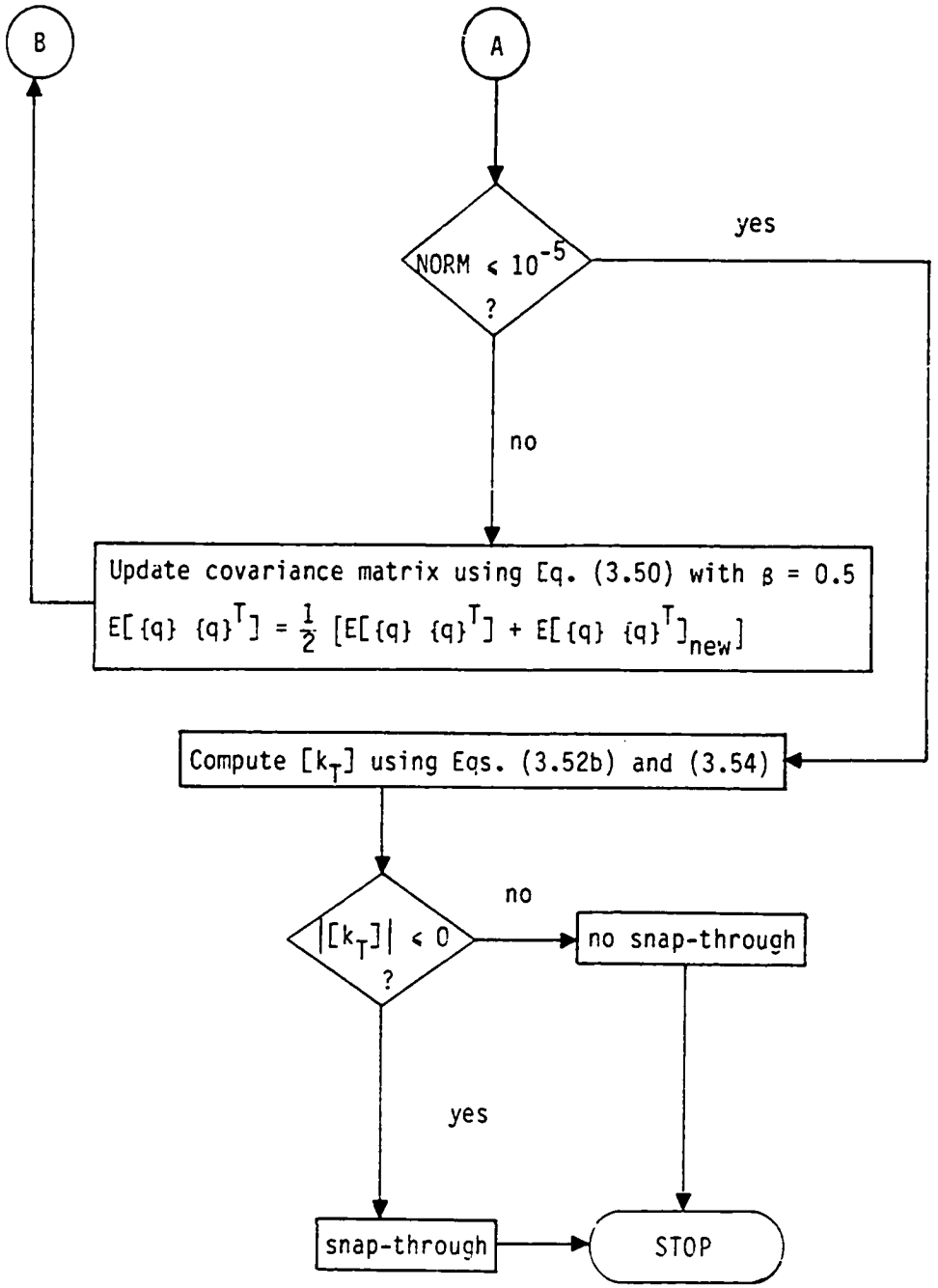

Fig. 3.3 Concluded.

3.3 Consistent Stresses/Strains

After the displacements for a given equilibrium configuration are known, the element strains and curvatures can be calculated using Eqs. (2.9), (2.10), (2.22) and (2.23) through (2.28). For this particular element, both the strains due to inplane displacements and the curvatures are discontinuous; hence, the computed stresses will also be discontinuous. To avoid this difficulty, Oden et al. [80] proposed a method for obtaining continuous stresses that are consistent with the displacements. Using this formulation, a discontinuous stress field can be transformed to a continuous stress field by assuming that the element displacement functions given by Eqs. (2.1), (2.2) and (2.3) can also be used to describe the stresses.

3.3.1 Stresses

The conventional element discontinuous inplane forces and moments can be calculated using Eqs. (2.9), (2.10), (2.12), (2.22), (2.28) and (2.31) as

$$\{\bar{N}\} = [C]\,[B_m]\,[T_m]\,\{a_m\} \tag{3.58}$$

$$\{\bar{M}\} = [D]\,[B_b]\,[T_b]\,\{a_b\}\ . \tag{3.59}$$

Following Ref. [80], the consistent nodal moments can be calculated using

$$[H]\,[M_c] = [R] \tag{3.60}$$

where the system matrix [H] is composed of the element matrices

$$[h] = [T_b]^T \int_A [H_w]^T\,[H_w]\,dA\,[T_b]\ , \tag{3.61}$$

[R] is composed of the element matrices

$$[r] = [T_b]^T \int_A [H_w]^T \{\bar{M}\}^T \, dA \, , \tag{3.62}$$

and the unknown nodal moments $\{M_c\}$ are contained in the matrix $[M_c]$ which can be obtained from Eq. (3.60), once [H] and [R] are formed. Applying this same type of procedure to compute the consistent nodal inplane forces $\{N_c\}$ and using Eqs. (2.11), (2.12), and (2.29) through (2.31), the extreme fiber stresses can be expressed as

$$\{\sigma\}_{\pm h/2} = \frac{1}{h} \{N\} \pm \frac{6}{h^2} \{M\} \tag{3.63}$$

where

$$\{N\} = \{N_c\} + [C] \{e_b\} + \{N_o\} - \{N_{\Delta T}\}$$

$$\{M\} = \{M_c\} + \{M_o\}$$

and all quantities are evaluated at the element nodes.

3.3.2 Root-Mean-Square Strains

The same procedure as used in the previous section can be applied to compute the consistent inplane strains $\{e_{mc}\}$ and curvatures $\{\kappa_c\}$ for a given displacement. Using Eqs. (2.11), (2.12) and (2.23), the extreme fiber strains can be expressed as

$$\{\varepsilon\}_{\pm h/2} = \{e_{mc}\} + \frac{1}{2} [A] \{\theta\} + [A_o] \{\theta\} \pm \frac{h}{2} \{\kappa_c\} \, . \tag{3.64}$$

Considering Eqs. (3.19) and (3.25), the terms in Eq. (3.64) can be written as

$$\{e_{mc}\} = \sum_{j=1}^{N} \{e_{mc}\}_j \, q_j + \sum_{j=1}^{N} \sum_{k=1}^{N} \{e_{mc}\}_{jk} \, q_j \, q_k$$

$$\frac{1}{2} [A] \{\theta\} = \sum_{j=1}^{N} \sum_{k=1}^{N} \frac{1}{2} [A]_j \{\theta\}_k \, q_j \, q_k$$

$$[A_o] \{\theta\} = \sum_{j=1}^{N} [A_o] \{\theta\}_j \, q_j \qquad (3.65)$$

$$\{\kappa_c\} = \sum_{j=1}^{N} \{\kappa_c\}_j \, q_j$$

where

$\{e_{mc}\}_j$ corresponds to $\{e_{mc}\}$ for $\{Q_m\} = \{Q_m\}_j$

$\{e_{mc}\}_{jk}$ corresponds to $\{e_{mc}\}$ for $\{Q_m\} = \frac{1}{2} \{Q_m\}_{jk}$

$[A]_j$ corresponds to $[A]$ for $\{Q_b\} = \{\phi\}_j$

$\{\theta\}_k$ corresponds to $\{\theta\}$ for $\{Q_b\} = \{\phi\}_k$

$\{\kappa_c\}_j$ corresponds to $\{\kappa_c\}$ for $\{Q_b\} = \{\phi\}_j$.

Combining Eqs. (3.64) and (3.65), the extreme fiber strains can be written in terms of first- and second-order terms as

$$\{\varepsilon\}_{\pm h/2} = \{\varepsilon_1\} + \{\varepsilon_2\} \qquad (3.66)$$

where

$$\{\varepsilon_1\} = \sum_{j=1}^{N} \left\{ \{e_{mc}\}_j + [A_o] \{\theta\}_j \pm \frac{h}{2} \{\kappa_c\}_j \right\} q_j = \sum_{j=1}^{N} \{\varepsilon_1\}_j \, q_j$$

$$\{\varepsilon_2\} = \sum_{j=1}^{N} \sum_{k=1}^{N} \left\{ \{e_{mc}\}_{jk} + \frac{1}{2} [A]_j \{\theta\}_k \right\} q_j \, q_k$$

$$= \sum_{j=1}^{N} \sum_{k=1}^{N} \{\varepsilon_2\}_{jk} \, q_j \, q_k \, .$$

The mean-square strains can be determined by evaluating

$$E[\{\varepsilon\}_{\pm h/2}\ \{\varepsilon\}^T_{\pm h/2}] = E[\{\varepsilon_1\}\ \{\varepsilon_1\}^T] + E[\{\varepsilon_2\}\ \{\varepsilon_2\}^T] \qquad (3.67)$$

since for a Gaussian process with zero mean $E[q_i\ q_j\ q_k] = 0$. Using Eq. (3.66), the terms in Eq. (3.67) can now be evaluated as

$$E[\{\varepsilon_1\}\ \{\varepsilon_1\}^T] = \sum_{i=1}^{N}\sum_{j=1}^{N} \{\varepsilon_1\}_i\ \{\varepsilon_1\}_j^T\ E[q_i\ q_j]$$

$$E[\{\varepsilon_2\}\ \{\varepsilon_2\}^T] = \sum_{i=1}^{N}\sum_{j=1}^{N}\sum_{k=1}^{N}\sum_{l=1}^{N} \{\varepsilon_2\}_{ij}\ \{\varepsilon_2\}_{kl}^T\ E[q_i\ q_j\ q_k\ q_l] \qquad (3.68)$$

where $E[q_i\ q_j\ q_k\ q_l]$ can be evaluated using Eq. (3.36). Equations (3.66), (3.67) and (3.68) can now be combined to determine the mean-square strains and the root-mean-square strains.

Chapter 4

NUMERICAL RESULTS AND DISCUSSION

The primary objectives of this study are to develop a finite element formulation for the large deflection random response of thermally buckled structures and to predict regions of stable vibrations for such structures. Since the stiffness matrices of a thermally buckled structure depend on both the initial deflections and stresses and since very little of this data is available, a secondary objective is to develop a finite element formulation to accurately predict the postbuckled deflections and stresses of structures subjected to arbitrary temperature distributions. To verify the finite element formulations, results are compared with multiple-mode classical solutions [24, 45, 67] that are considered to be a comparison standard. Convergence studies are included to evaluate the required number of elements and mode shapes necessary to achieve reasonable accuracy.

4.1 Boundary Conditions

Thin plate boundary conditions are typically defined as being either simply supported or clamped with respect to transverse deflections and moveable or immovable with respect to inplane deflections. Immovable inplane edges require that the inplane deflections u and v be equal to zero at a boundary; whereas, u and v are free at a boundary for moveable inplane edges. Simply supported boundary conditions are obtained by setting the transverse deflection equal to zero at an edge,

and clamped boundary conditions require that both the transverse deflection and its associated slope be equal to zero at an edge. For the present study, all inplane boundary conditions are taken to be immovable.

4.2 Thermal Postbuckling

The thermal postbuckling results are compared with a previous solution for a square plate clamped on all edges for both uniform and nonuniform temperature distributions. For the present study, the plate is considered to be aluminum with the following properties:

Young's modulus	$E = 10.0 \times 10^6$ psi
Poisson's ratio	$\nu = 0.3$
coefficient of thermal expansion	$\alpha = 12.5 \times 10^{-6}$ in./in./°F .

However, any representative properties can be used, with the exception of Poisson's ratio, since the results are nondimensional.

4.2.1 Convergence of Thermal Postbuckling Formulation

Solution convergence is examined by using various degrees of mesh refinement for a plate subjected to a uniform temperature distribution and observing the change in deflections and stresses. All elements are taken to be square and of equal size, and due to symmetry considerations, only 1/4 of the plate is modeled. Figures 4.1-4.5 illustrate the convergence of the thermal postbuckling formulation. As indicated in Fig. 4.1, the center deflection converges very rapidly, and the 16, 25 and 36 element results are essentially the same. Convergence for the stresses in the center of the plate is also quite rapid as illustrated in Figs. 4.2 and 4.3. The edge stresses (Figs. 4.4 and 4.5) are much

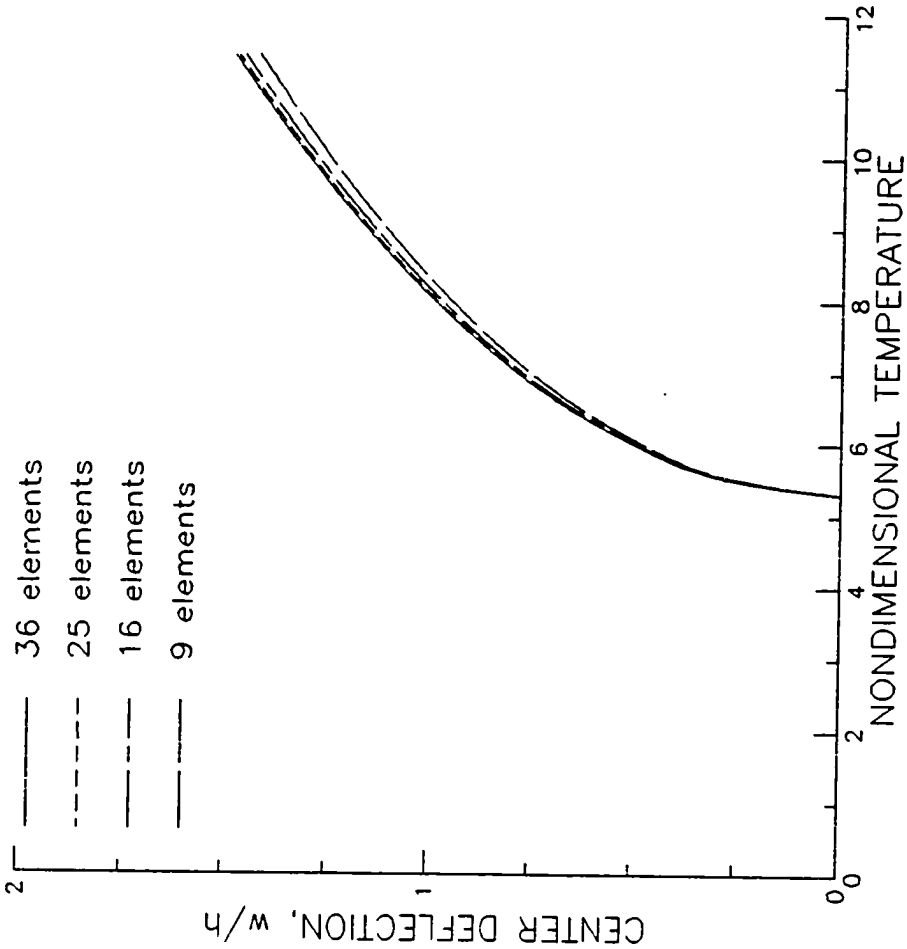

Fig. 4.1 Convergence of center deflection for a clamped square plate subjected to a uniform temperature distribution

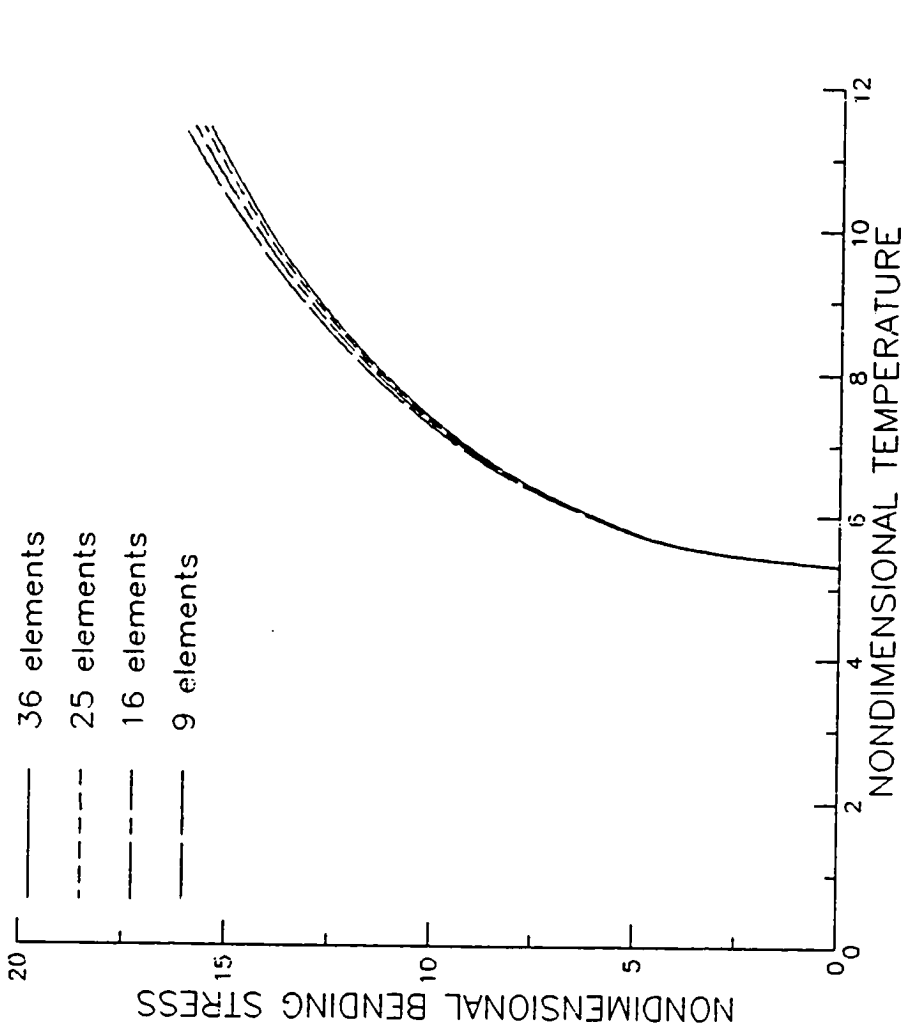

Fig. 4.2 Convergence of extreme-fiber bending stress, plate center, for a clamped square plate subjected to a uniform temperature distribution

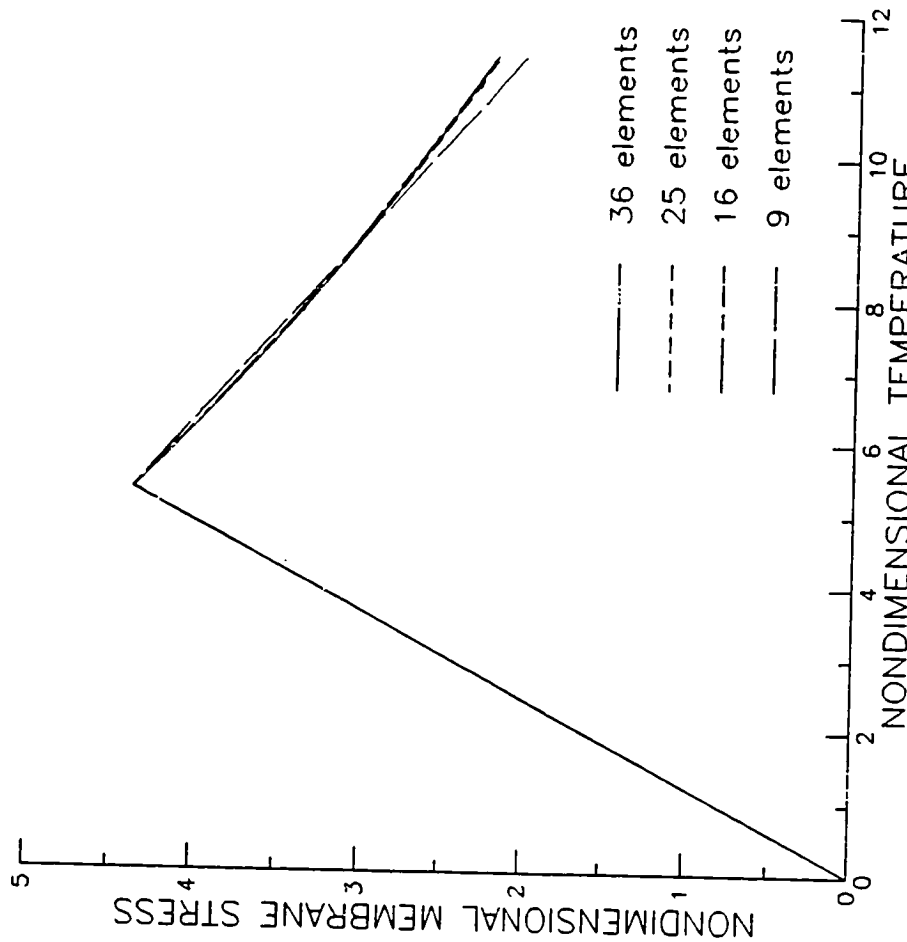

Fig. 4.3 Convergence of membrane stress, plate center, for a clamped square plate subjected to a uniform temperature distribution

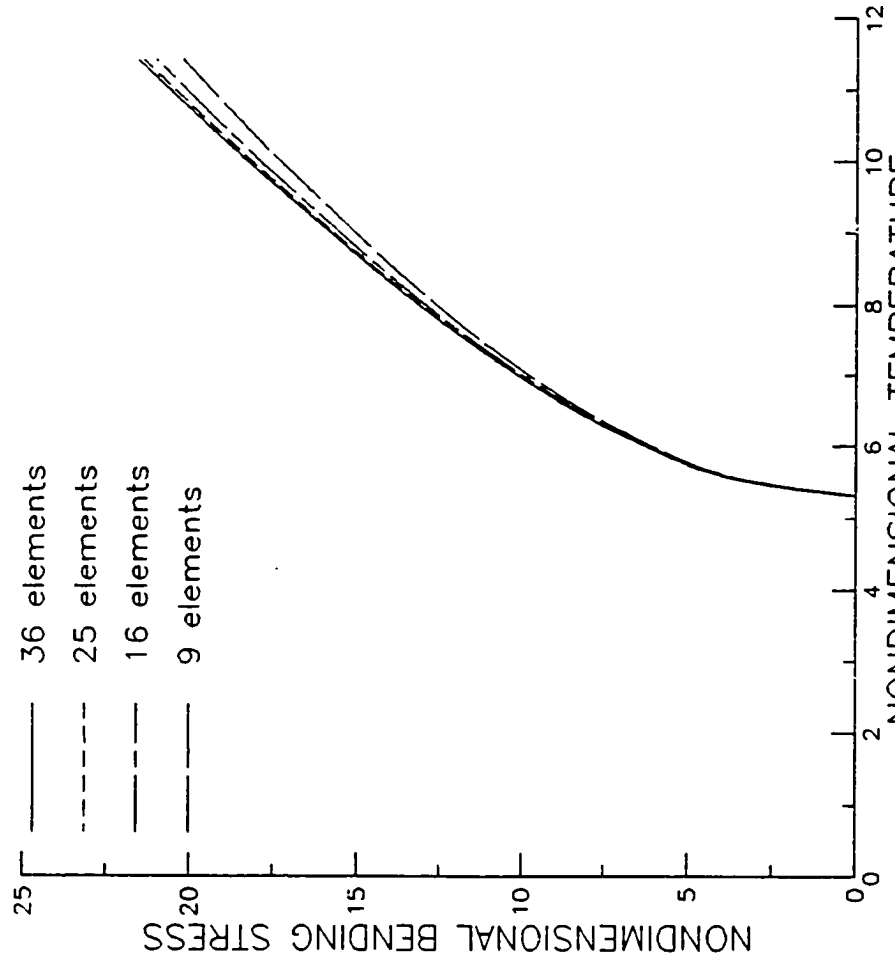

Fig. 4.4 Convergence of extreme-fiber bending stress, plate edge midpoint, for a clamped square plate subjected to a uniform temperature distribution

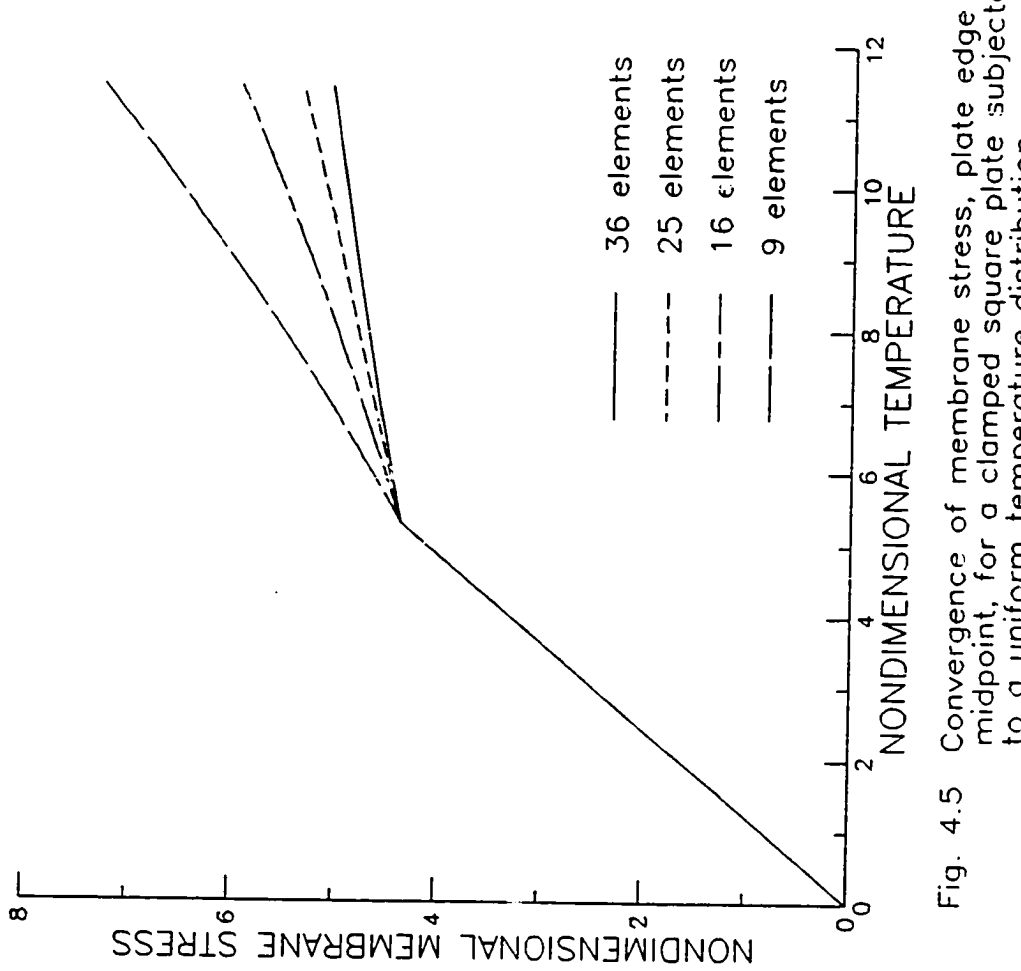

Fig. 4.5 Convergence of membrane stress, plate edge midpoint, for a clamped square plate subjected to a uniform temperature distribution

slower to converge with the edge membrane stress being the slowest. This is probably due to the high stress gradients near the edge of the plate coupled with the fact that the inplane element displacement functions are only C° continuous.

4.2.2 Accuracy of Thermal Postbuckling Formulation

Since the 25 and 36 element results appear to be reasonably close for both deflections and stresses, the 36 element model is considered to be accurate enough to compare with Paul [24]. Paul's classical solution is chosen to compare with because it uses 25 modal functions to determine the postbuckled deflections and stresses and should be very accurate. Figures 4.6-4.10 illustrate the comparison of the results obtained using 36 elements to Paul's results for the case of a uniform temperature distribution. The deflection results (Fig. 4.6) and the center stress results (Figs. 4.7 and 4.8) are very nearly identical with Paul's solution, and the edge stresses (Figs. 4.9 and 4.10) are very close. For the case of a nonuniform temperature distribution ($\Delta T(x,y) = T_0 (1 - \cos \frac{2\pi x}{a}) (1 - \cos \frac{2\pi y}{b})$), the results are shown in Figs. 4.11-4.15. As for the case of a uniform temperature distribution, the center deflections and stresses compare more favorably, and the edge stresses are in error the most when compared with Paul's solution. For the edge membrane stress (Fig. 4.15), the 36 element results compare poorly with Paul's solution. However, the results obtained using 64 and 100 elements tend to converge to the classical solution indicating that better accuracy can be obtained by using more elements. Higher order inplane element displacement functions could also be used to improve the accuracy of the present formulation.

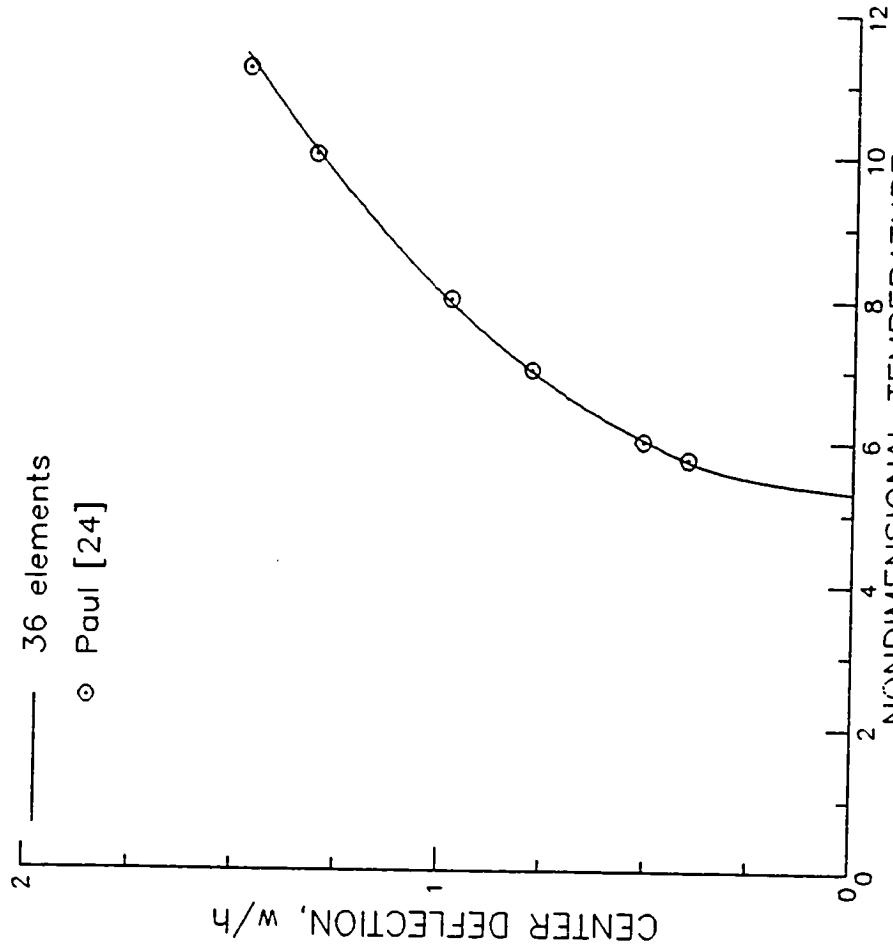

Fig. 4.6 Center deflection for a clamped square plate subjected to a uniform temperature distribution

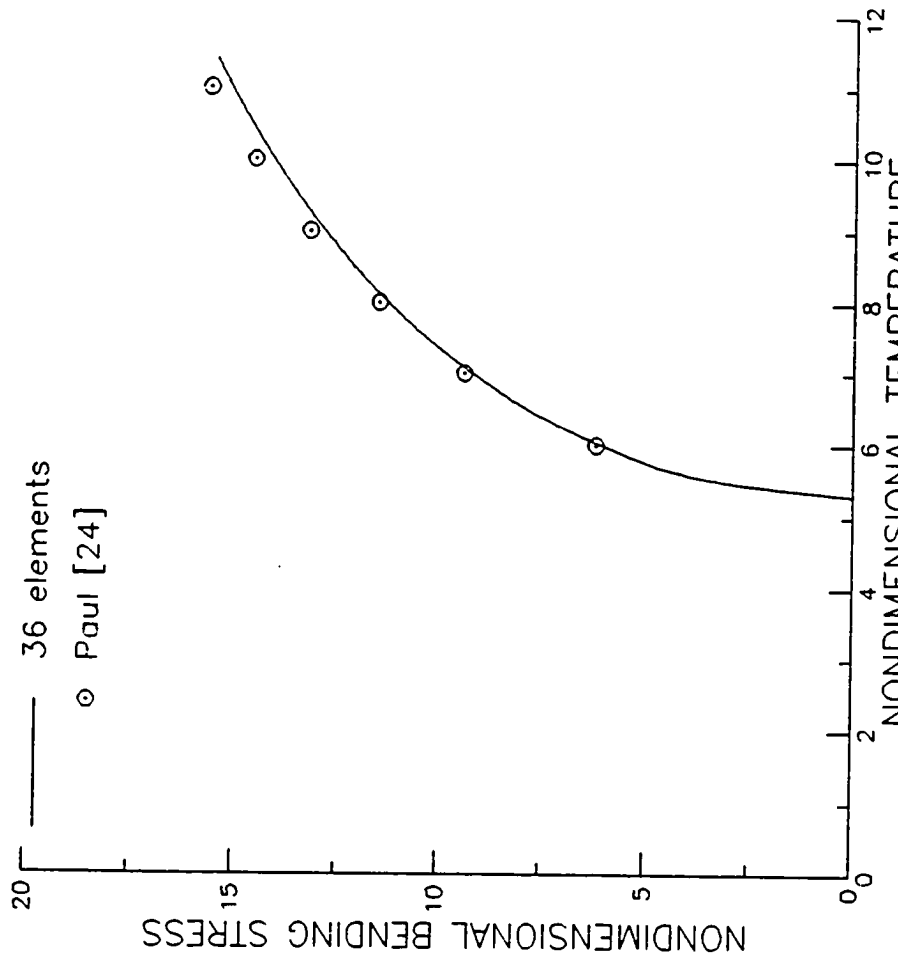

Fig. 4.7 Extreme-fiber bending stress, plate center, for a clamped square plate subjected to a uniform temperature distribution

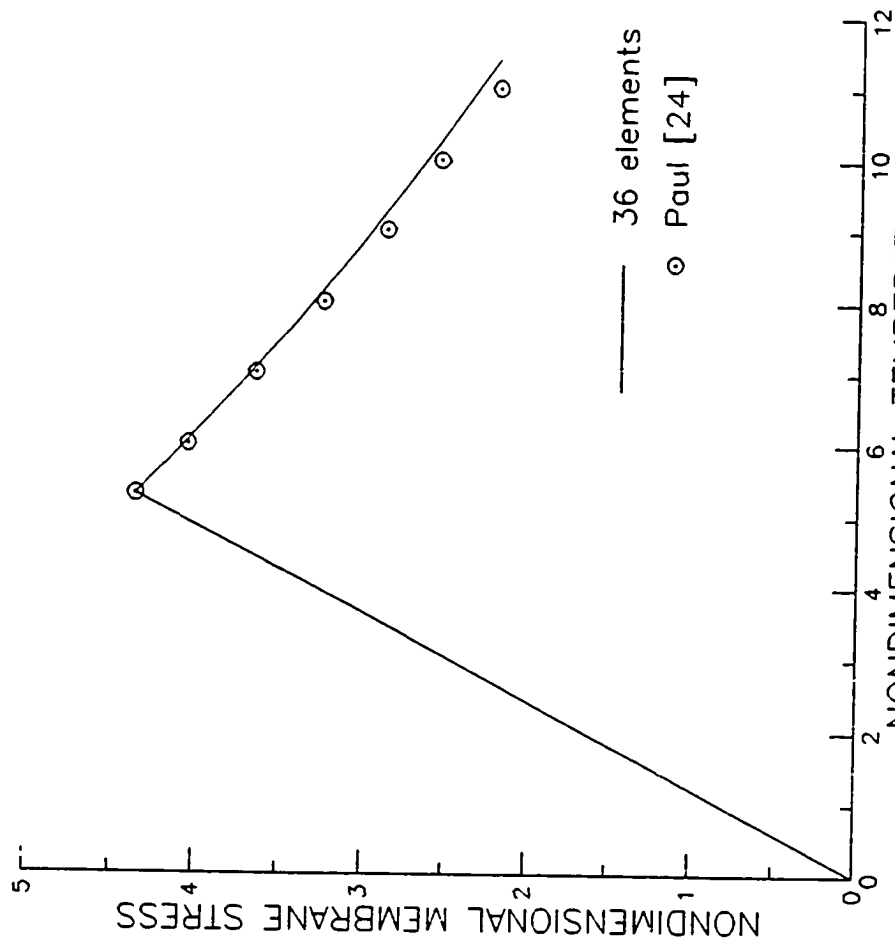

Fig. 4.8 Membrane stress, plate center, for a clamped square plate subjected to a uniform temperature distribution

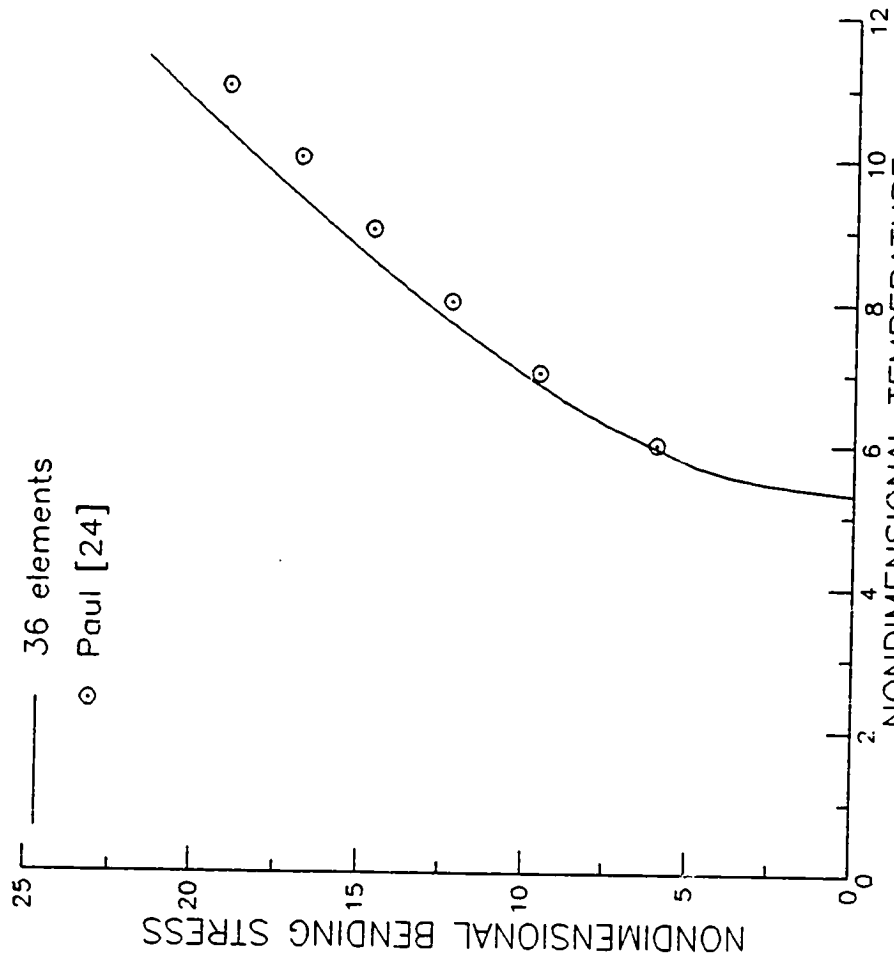

Fig. 4.9 Extreme-fiber bending stress, plate edge midpoint, for a clamped square plate subjected to a uniform temperature distribution

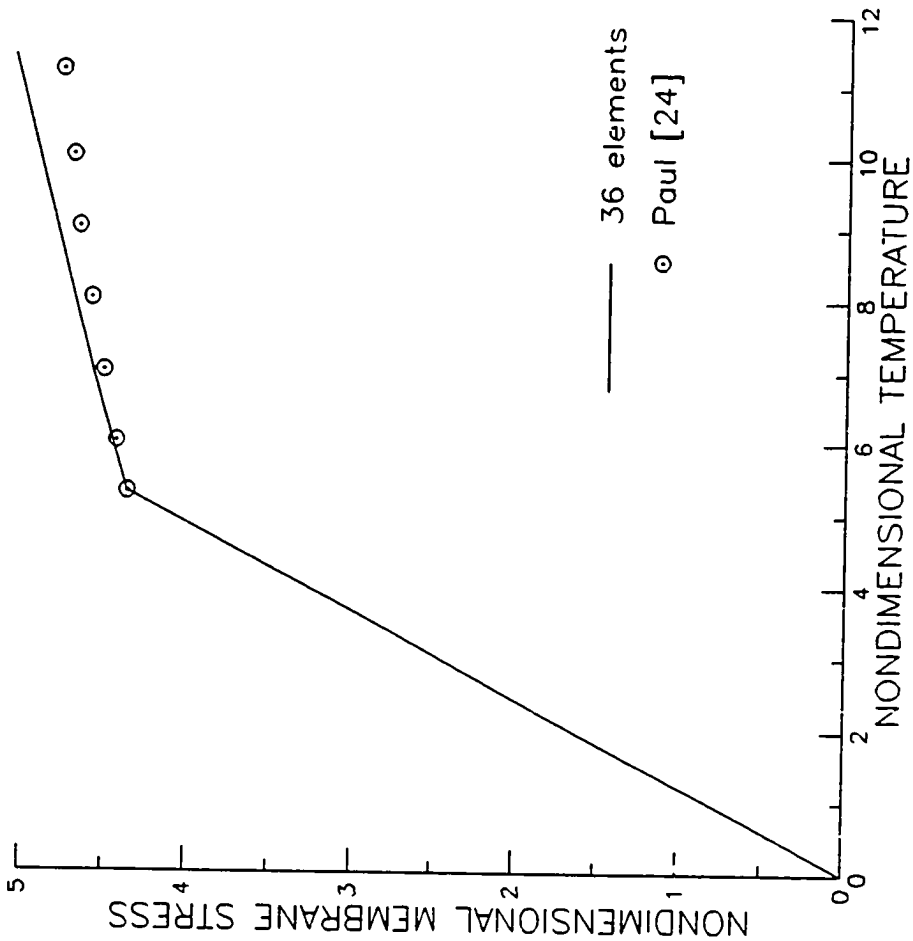

Fig. 4.10 Membrane stress, plate edge midpoint, for a clamped square plate subjected to a uniform temperature distribution

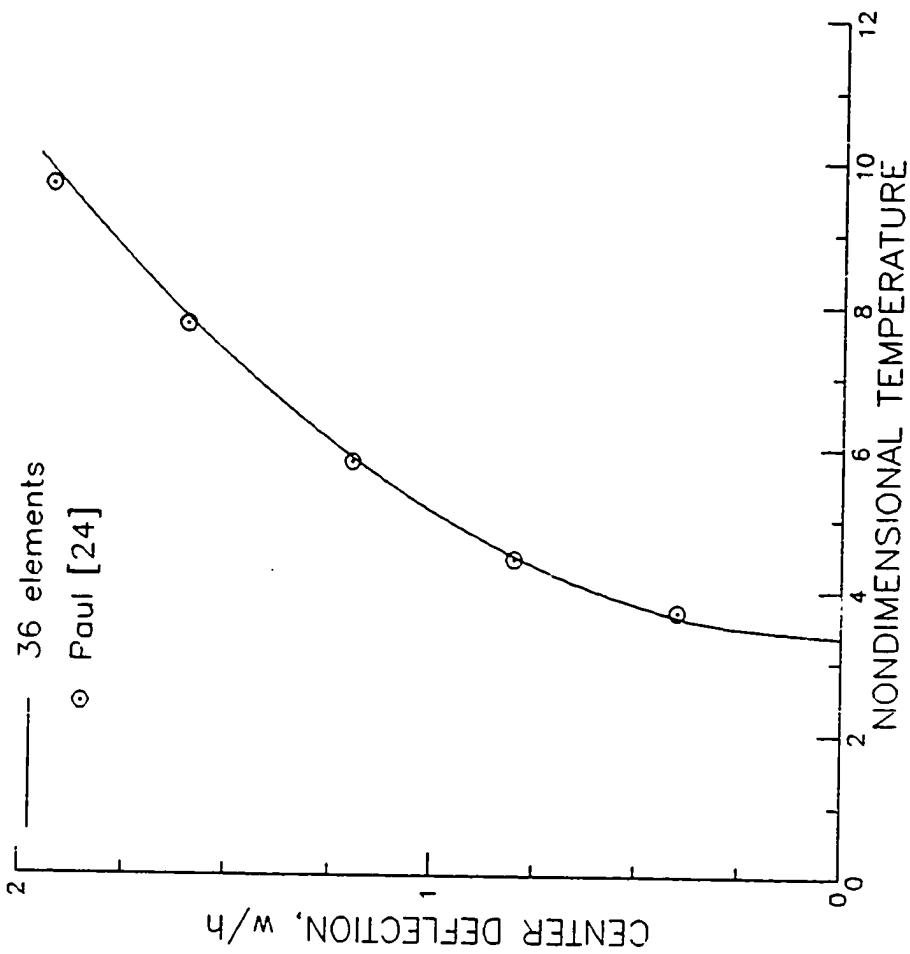

Fig. 4.11 Center deflection for a clamped square plate subjected to a nonuniform temperature distribution

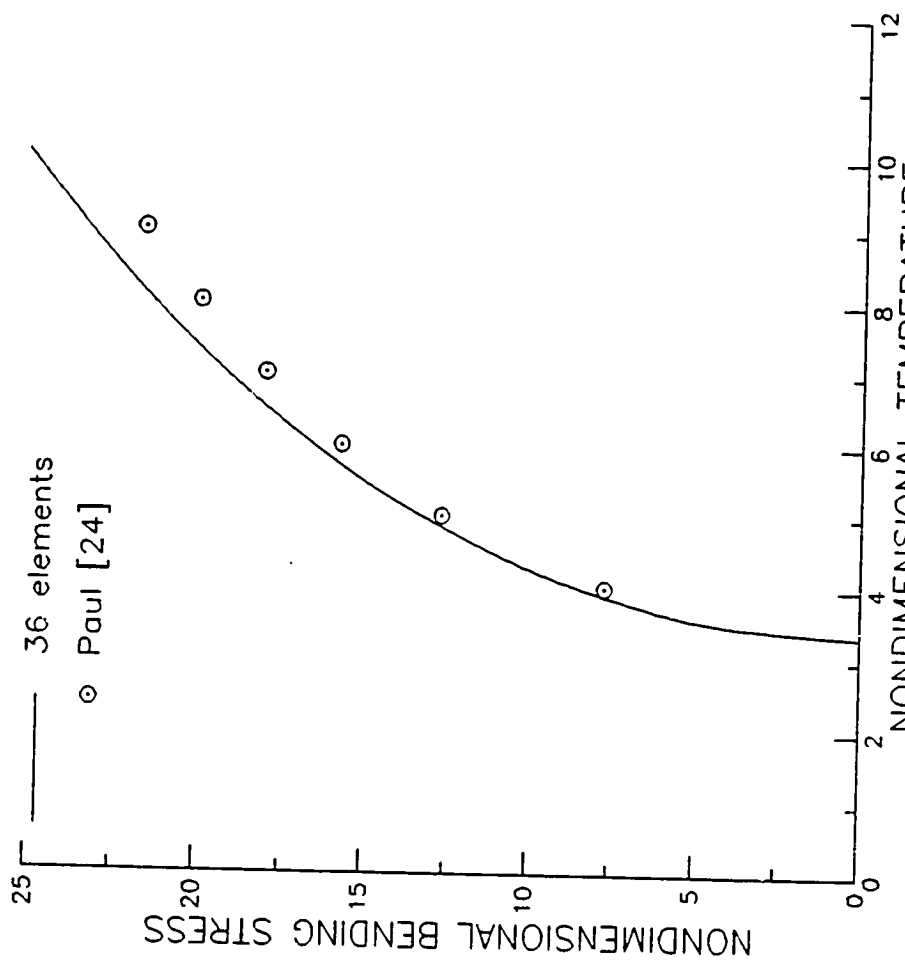

Fig. 4.12 Extreme-fiber bending stress, plate center, for a clamped square plate subjected to a nonuniform temperature distribution

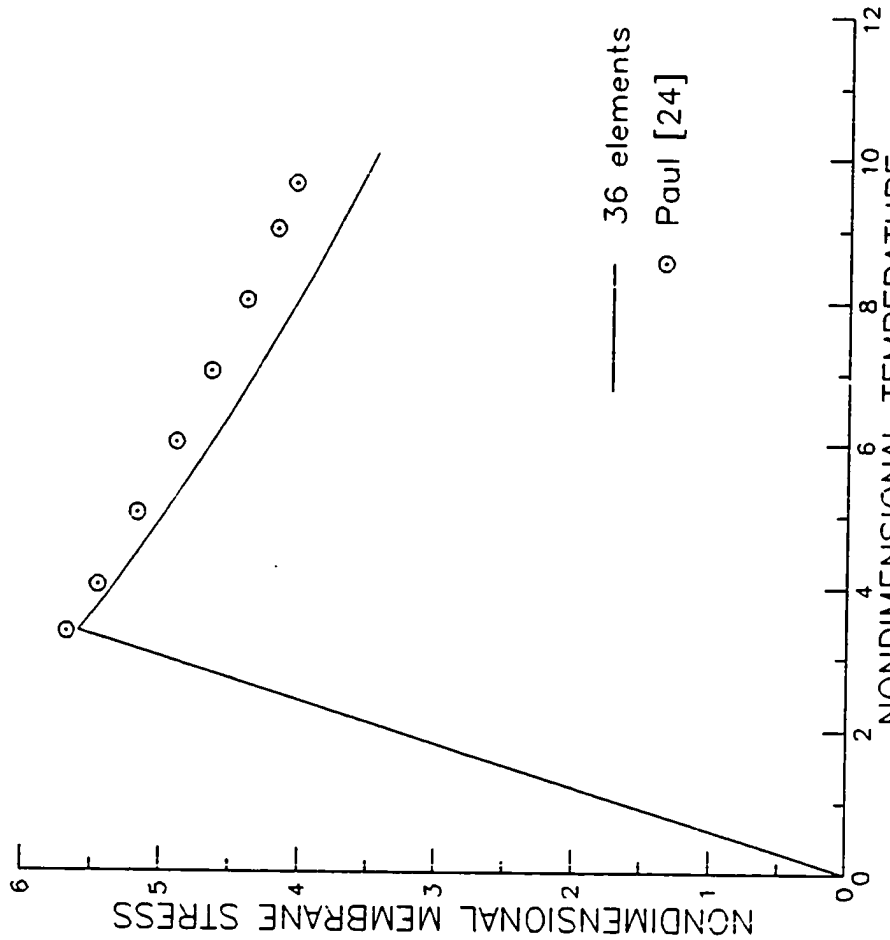

Fig. 4.13 Membrane stress, plate center, for a clamped square plate subjected to a nonuniform temperature distribution

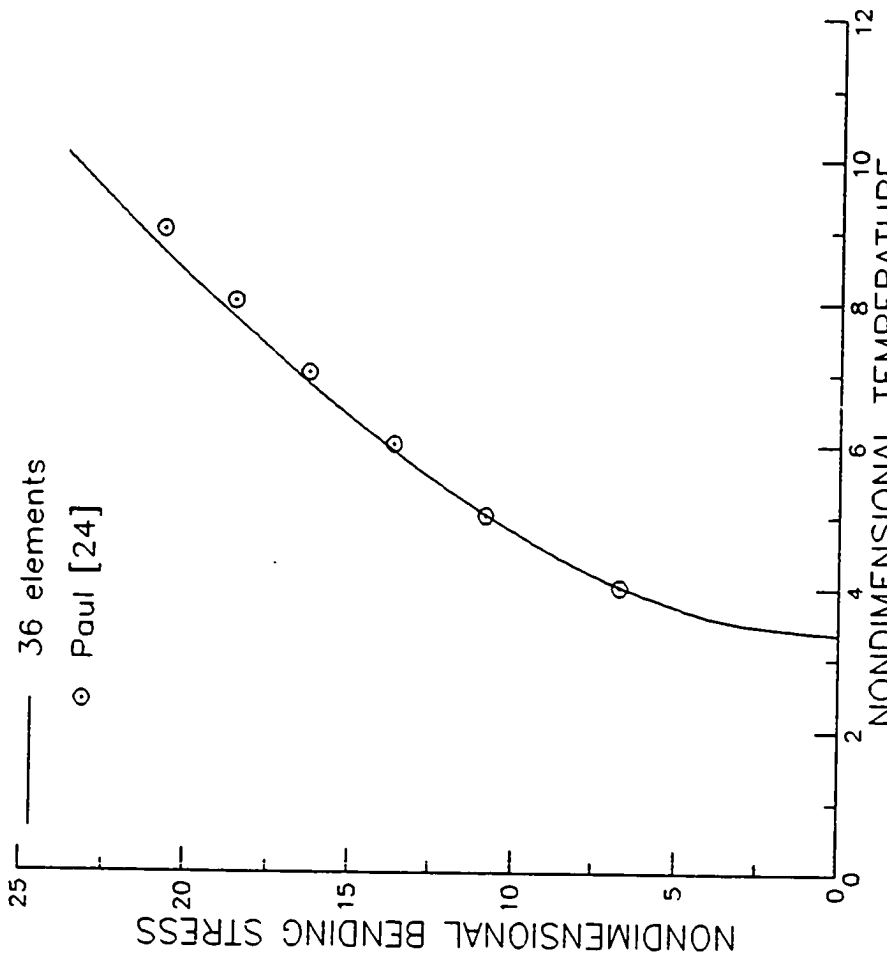

Fig. 4.14 Extreme-fiber bending stress, plate edge midpoint, for a clamped square plate subjected to a nonuniform temperature distribution

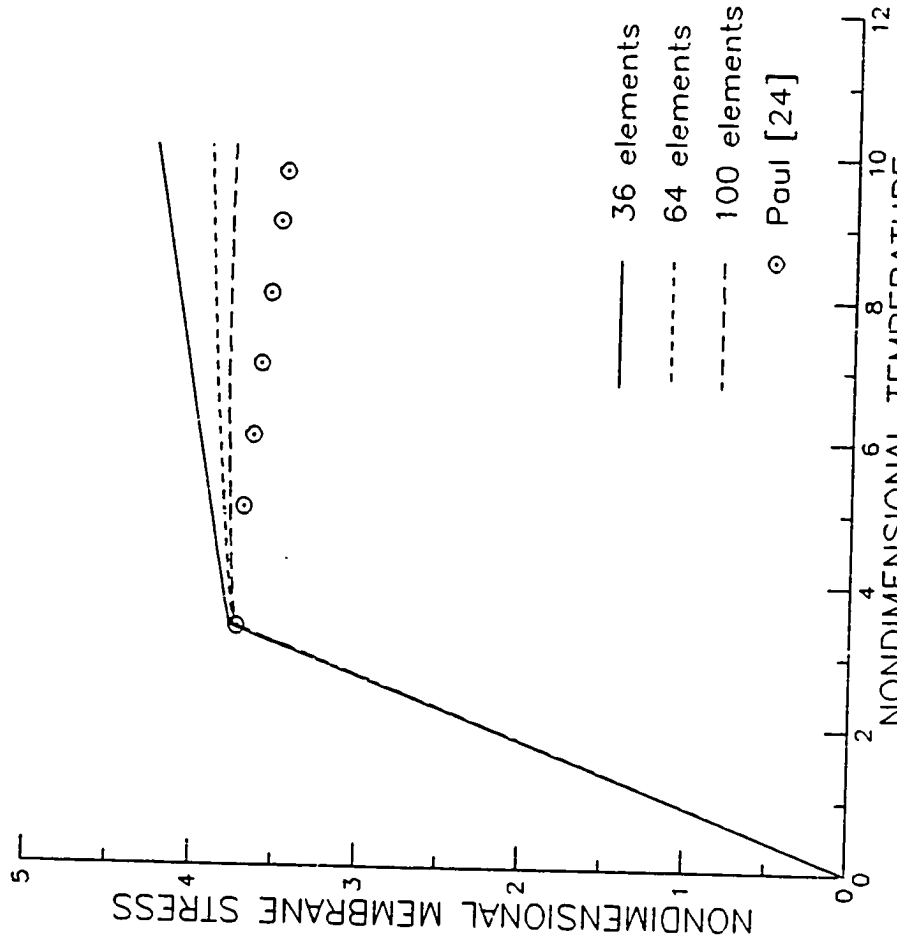

Fig. 4.15 Membrane stress, plate edge midpoint, for a clamped square plate subjected to a nonuniform temperature distribution

4.3 Large Deflection Random Response

Results for large deflection random vibration are compared with previous solutions for flat, stress free beams. For a simply supported beam buckled by a uniform temperature distribution, the deflection response, strain response and snap-through boundary are compared with a previous study. Also, the strain response is evaluated at various sound spectrum levels for simply supported beams and clamped rectangular plates buckled by both uniform and nonuniform temperature distributions. The damping ξ is taken to be equal to $2\zeta\omega_0$ where ζ is the damping ratio and ω_0 is the fundamental frequency of the initially flat, stress free structure. The material properties, mass density and damping ratio are taken as

Young's modulus	$E = 10.5 \times 10^6$ psi
Poisson's ratio	$\nu = 0.3$
coefficient of thermal expansion	$\alpha = 12.5 \times 10^{-6}$ in./in./°F
mass density	$\rho = .2588 \times 10^{-3}$ lb-sec^2/in.^{4}
damping ratio	$\zeta = .01$,

with the dimensions of the beam being

length	a = 12 in.
width	b = 2 in.
thickness	h = 0.064 in.,

and the dimensions of the plate being

length	a = 15 in.
width	b = 12 in.
thickness	h = 0.040 in.

4.3.1 Convergence of Random Vibration Formulation

A 16 element, half-beam model is used to evaluate the convergence characteristics of the present formulation and determine the required number of modes for reasonable accuracy. The half-beam model was chosen since both the thermal and random loading are considered to be symmetric. As a result, only the symmetric mode shapes are used for the random vibration analysis. Sixteen elements were chosen since a high degree of mesh refinement is necessary to accurately determine the higher frequencies and mode shapes used for the convergence study.

The root-mean-square deflections obtained using one, two, three and four symmetric mode shapes for flat, unstressed beams are shown in Table 4.1. As indicated, the maximum deflection for the simply supported beam converges very rapidly, and the single-mode deflection is virtually the same as the multiple-mode deflection. For the clamped beam, the maximum deflection is slower to converge, but the three- and four-mode solutions are almost identical even for high sound spectrum levels. Root-mean-square maximum strains, shown in Figs. 4.16 and 4.17, are slower to converge, but the three- and four-mode solutions are still very close for both the simply supported and clamped beams. As for the thermal postbuckling solution, the slower convergence of the strains can be partially attributed to the low-order inplane element displacement functions.

4.3.2 Accuracy of Random Vibration Formulation

Based on the results of the convergence studies, the four-mode, 16 element solution is considered accurate enough to compare with other solutions and is used for the remainder of the random vibration beam

Table 4.1 Convergence of RMS maximum deflections for simply supported and clamped flat, stress free beams ($\xi = 2\zeta\omega_0$, $\zeta = .01$)

SSL (dB)	Single Mode	Two Modes	Three Modes	Four Modes
		Simply Supported		
90	0.3194	0.3196	0.3196	0.3196
100	0.8454	0.8456	0.8455	0.8455
110	1.7932	1.7924	1.7920	1.7918
120	3.3830	3.3768	3.3740	3.3731
130	6.1301	6.1082	6.0957	6.0917
		Clamped		
90	0.1005	0.1008	0.1008	0.1008
100	0.3154	0.3161	0.3162	0.3162
110	0.9351	0.9350	0.9356	0.9355
120	2.2830	2.2680	2.2768	2.2753
130	4.5887	4.5057	4.5704	4.5608

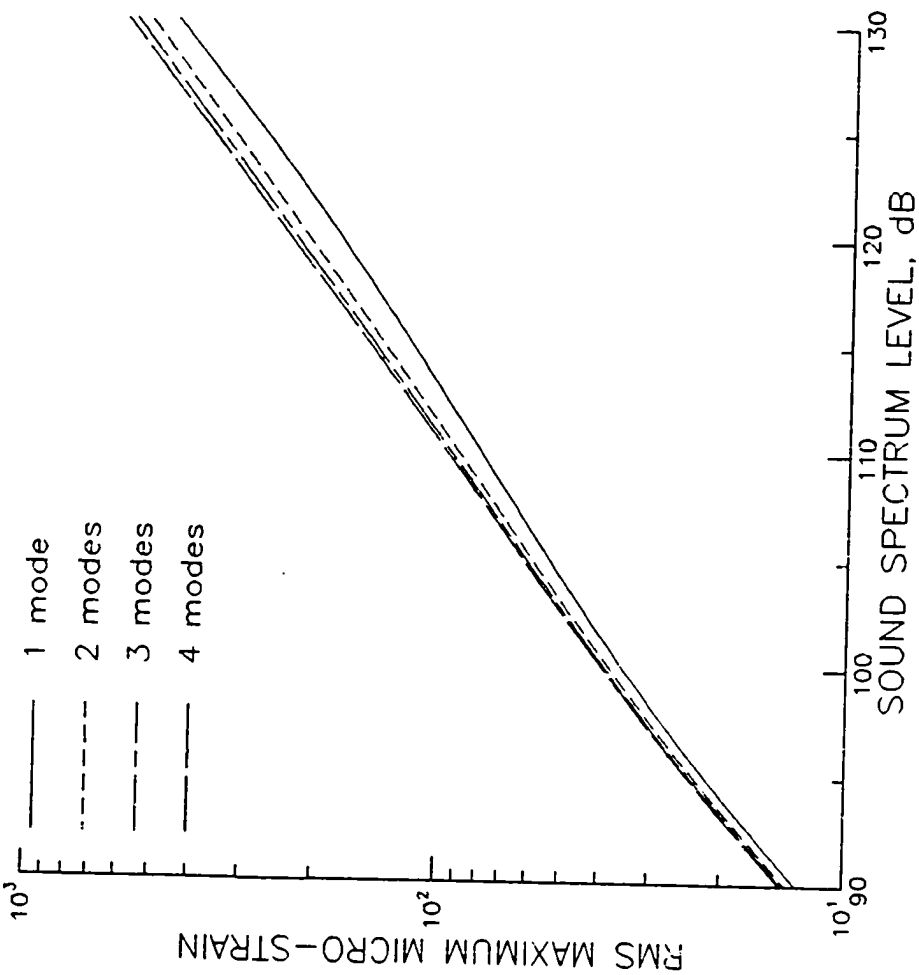

Fig. 4.16 Convergence of RMS maximum micro-strain for flat, stress free simply supported beam

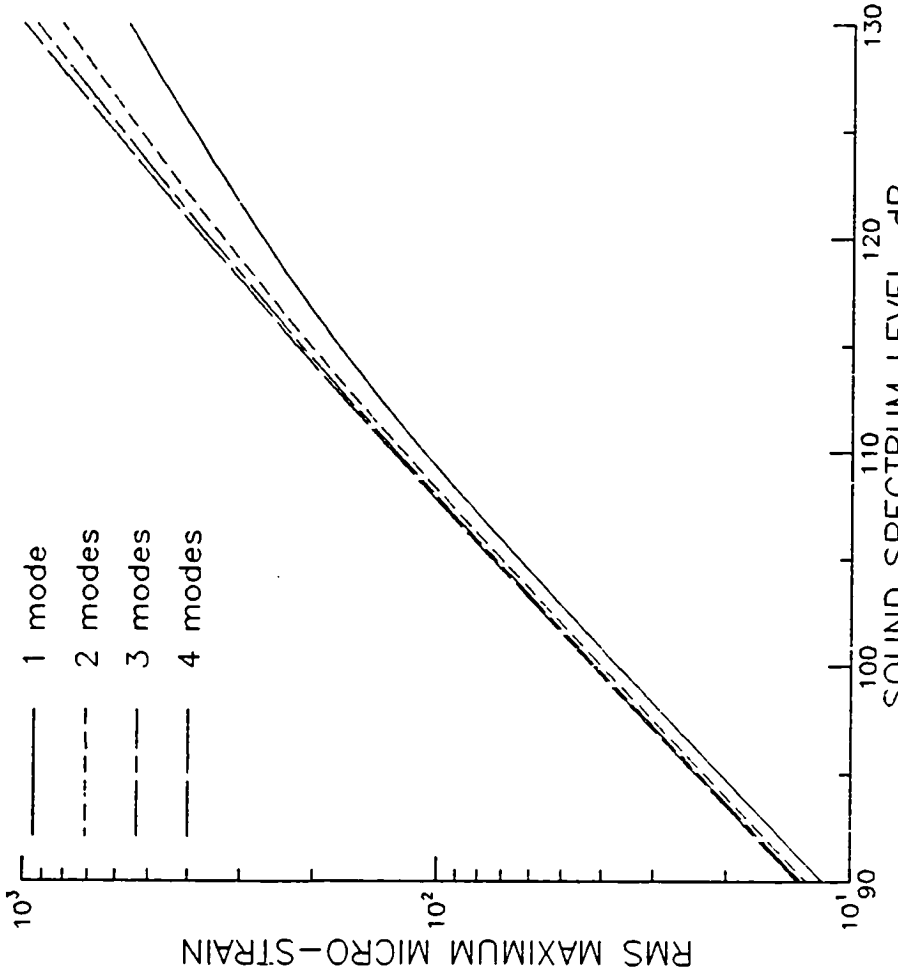

Fig. 4.17 Convergence of RMS maximum micro-strain for flat, stress free clamped beam

studies. Comparisons are made with Refs. [45] and [67] which both use a 100-mode classical approach in conjunction with the EL method. For the case of flat, unstressed beams, the present results are in excellent agreement with the classical solutions as illustrated by Figs. 4.18 and 4.19. The maximum deflections for both the simply supported and clamped beams are seen to be identical with those obtained using the classical 100-mode formulations. Strains, although not as close as deflections, still compare very well with the classical solutions. Discrepancies can be attributed to the element inplane displacement functions as well as the fact that the classical solutions use such a high number of modes. Furthermore, the method of equivalent linearization used for the present study does not make the restrictive assumption that the equivalent linear stiffness matrix is diagonal which, in general, is not true.

The only previous studies to consider the large deflection multiple-mode random vibration of buckled structures are those conducted by Seide et al. [67-69] with Ref. [67] being the most comprehensive. All of these studies considered the random vibration of beams buckled by a uniform temperature distribution. Comparisons with the EL results for a thermally buckled simply supported beam [67] are shown in Figs. 4.20 and 4.21 for selected values of T/T_{CR}. As for the case of flat, unstressed beams, the deflections are in exact agreement with the 100-mode classical solution, and the strains compare very closely.

Results for the snap-through boundary of a thermally buckled simply supported beam are compared in Fig. 4.22. Two different snap-through boundaries are shown from Ref. [67]. Both were determined by using a numerical simulation technique to generate a time dependent random loading. Three modal functions were used, and the resulting equations

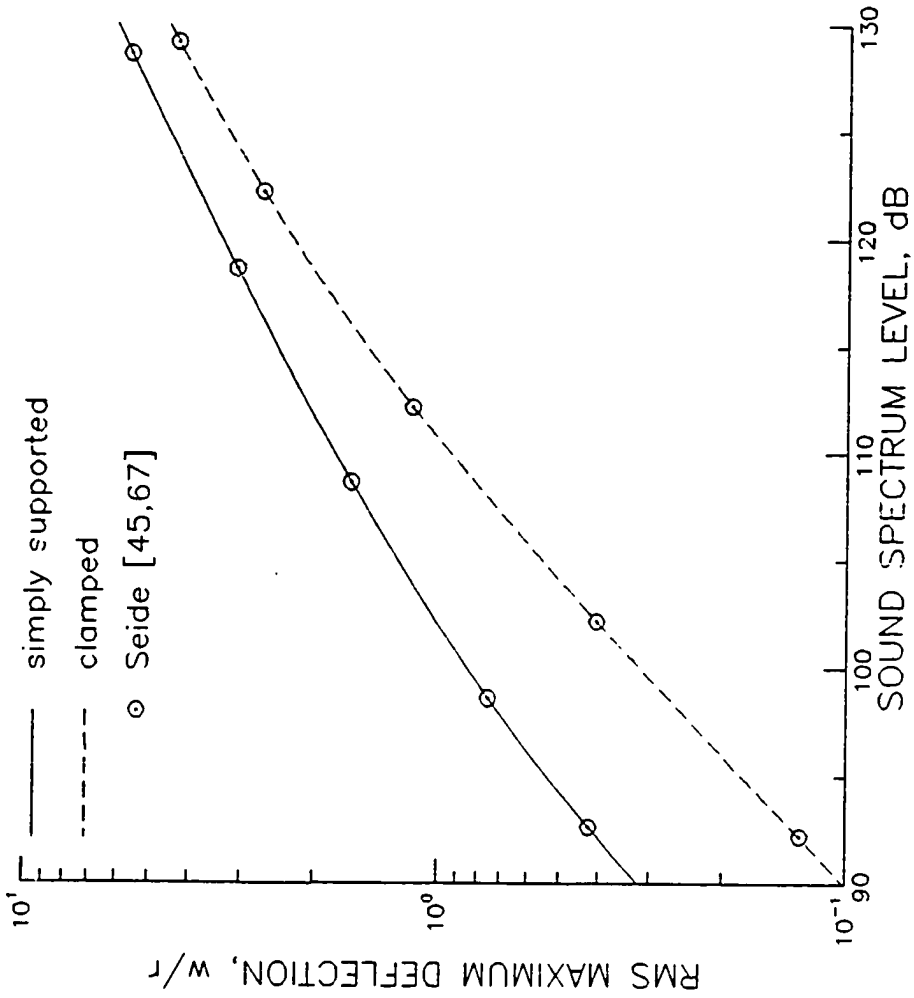

Fig. 4.18 RMS maximum deflection for flat, stress free beams

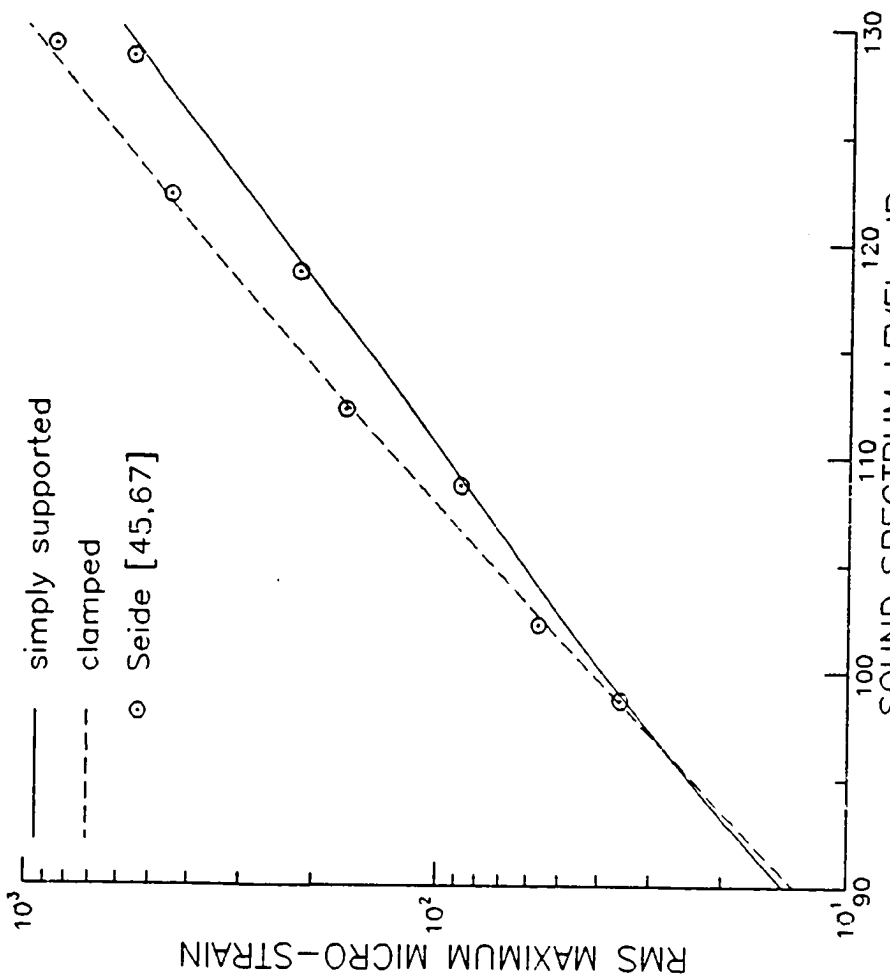

Fig. 4.19 RMS maximum micro-strain for flat, stress free beams

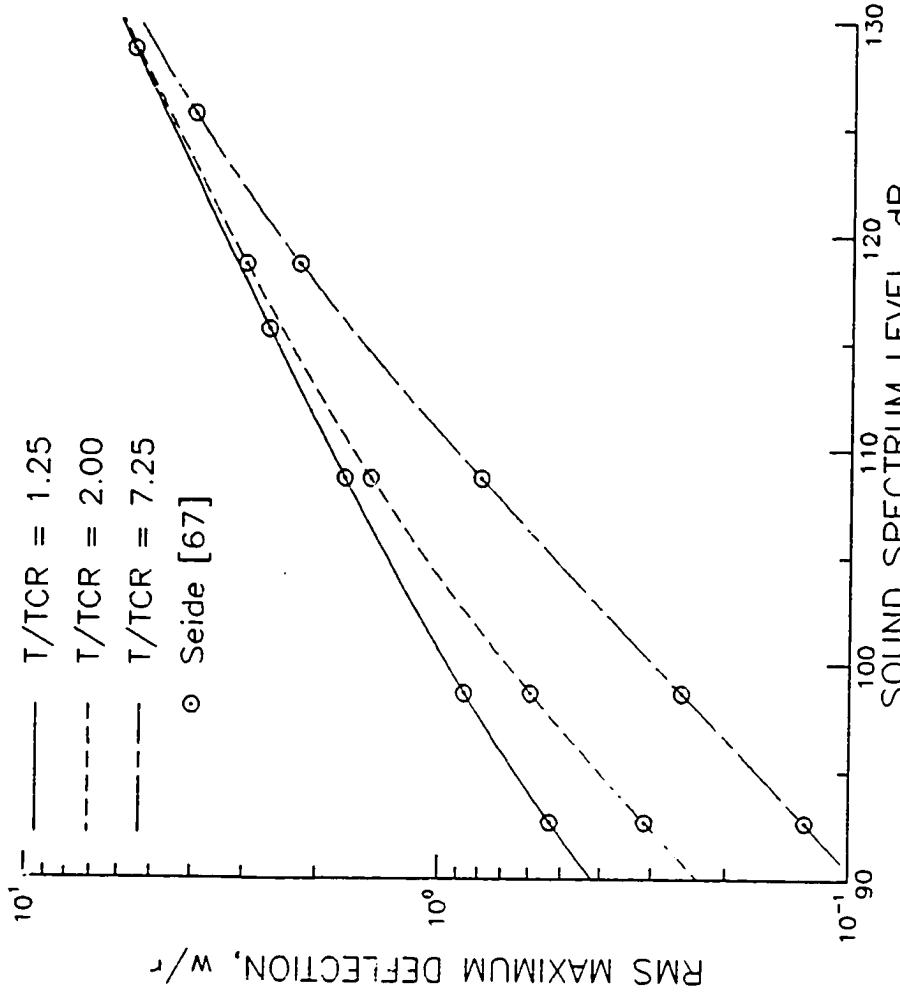

Fig. 4.20 RMS maximum deflection for a simply supported beam subjected to a uniform temperature distribution

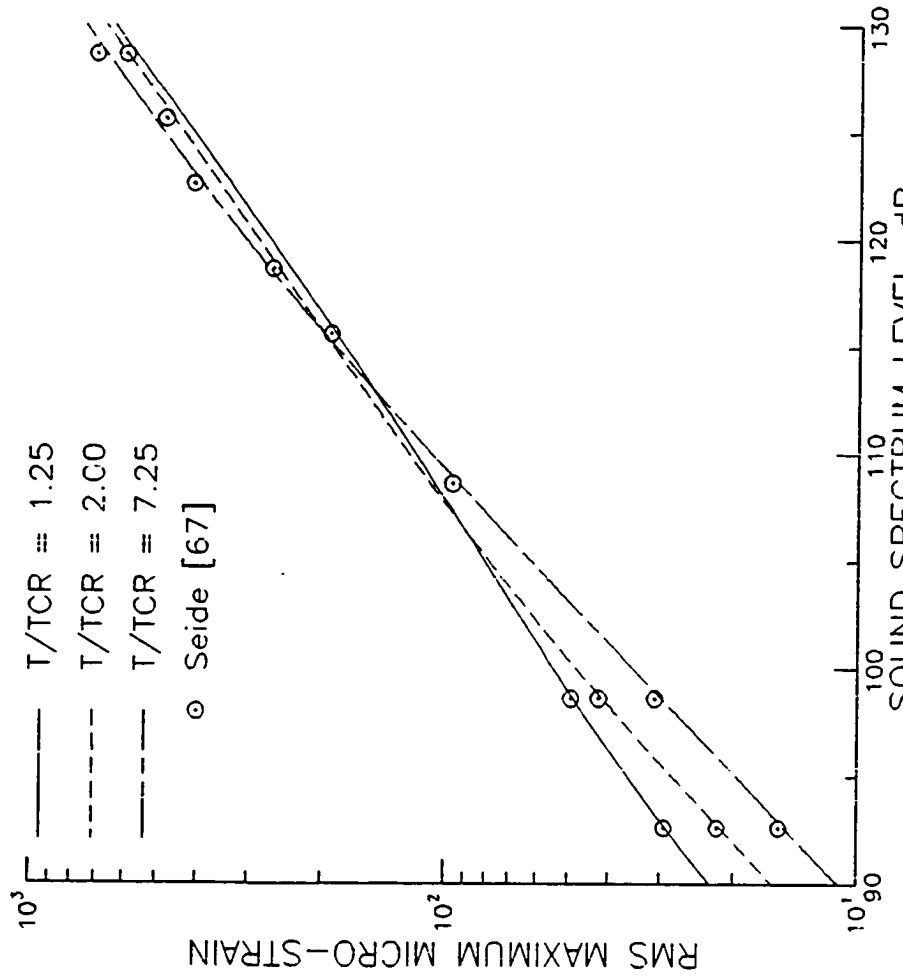

Fig. 4.21 RMS maximum micro-strain for a simply supported beam subjected to a uniform temperature distribution

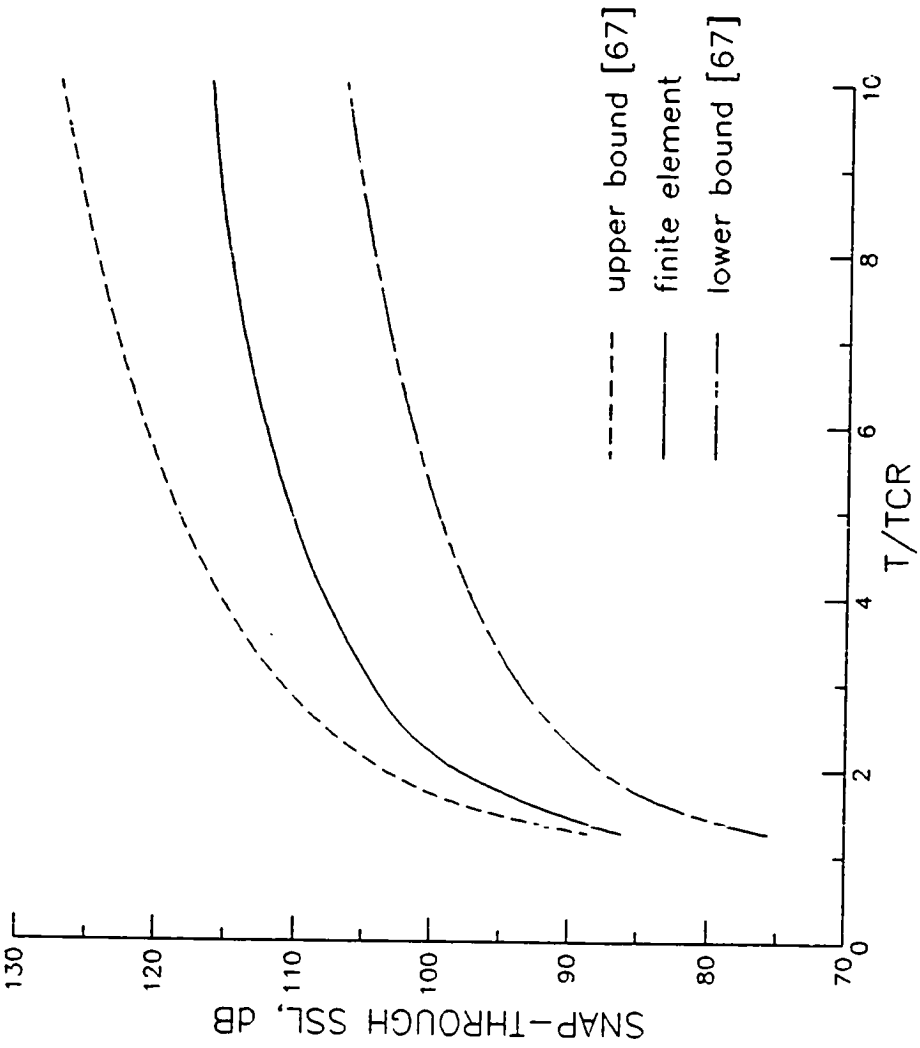

Fig. 4.22 Snap-through sound spectrum level for a simply supported beam subjected to a uniform temperature distribution

of motion were then solved using numerical integration. Snap-through was considered to have occurred when the random center deflection of the beam became greater than the initial static center deflection. This criterion for snap-through would seem to be very conservative, in an average sense, because for random vibration the peak response can greatly exceed the average response. The strict use of this criterion produces the lower bound depicted in Fig. 4.22. This same criterion was also used to determine the probability of the first-passage time for snap-through. If the probability of the first-passage time is relatively low for all time, then the probability of snap-through is also low but is not equal to zero; therefore, this condition was considered to represent an upper bound for snap-through as shown in Fig. 4.22. The present formulation is seen to predict a snap-through boundary that falls between these two bounds. There is a considerable difference between the snap-through boundary predicted using the present formulation and the boundaries taken from Ref. [67]. A large part of this difference is due to two things. First, the snap-through boundary calculated using the present formulation is based on EL results instead of numerical simulation results. Secondly, the snap-through criteria used for this study is different than the criteria used by Ref. [67].

4.3.3 Strain Response of Thermally Buckled Beams

Having verified the accuracy of the present formulation, the root-mean-square strain response at the center of a thermally buckled simply supported beam is computed at various sound spectrum levels for two conditions: a uniform temperature distribution and a nonuniform temperature distribution. For the case of a uniform temperature

distribution ($\Delta T(x) = T_o$), the temperature T_o necessary to produce buckling was found to be 1.87°F; whereas, for the nonuniform temperature distribution ($\Delta T(x) = T_o \sin \frac{\pi x}{a}$) the temperature T_o to produce buckling was found to be 2.94°F. Although the maximum temperature at the center of the beam is higher for the nonuniform temperature distribution, the average temperature is the same (T_{AVG} = 1.87°F) for both cases. The results for the two different cases are shown in Figs. 4.23 and 4.24, and as illustrated, at low sound spectrum levels the maximum strain occurs at or near T/T_{CR} equal to one. However, at higher sound spectrum levels, the maximum strain is seen to occur at higher values of T/T_{CR}. This indicates that even though the beams become stiffer in the post-buckling region, the maximum strains occur at temperatures well beyond the buckling temperature for sufficiently high sound spectrum levels. This type of strain response is due to the coupling terms, of Eq. (2.23), that depend on both the initial deflection w_o as well as the random deflection w and is discussed in more detail in the next section. The snap-through boundary of Fig. 4.22 is also included in Fig. 4.23 to show that at higher sound spectrum levels for $T/T_{CR} > 1$, snap-through motion can be expected to occur.

A comparison of the maximum strain versus sound spectrum level for each of the temperature distributions is shown in Fig. 4.25. For this particular beam subjected to the two different types of temperature distributions, the maximum strains are virtually the same. This is due to the fact that even though the initial stresses for the two temperature distributions are different, the initial deflections w_o differ by a very small amount. Hence, the stiffness matrices for the two different cases contain significant differences only in the terms involving the

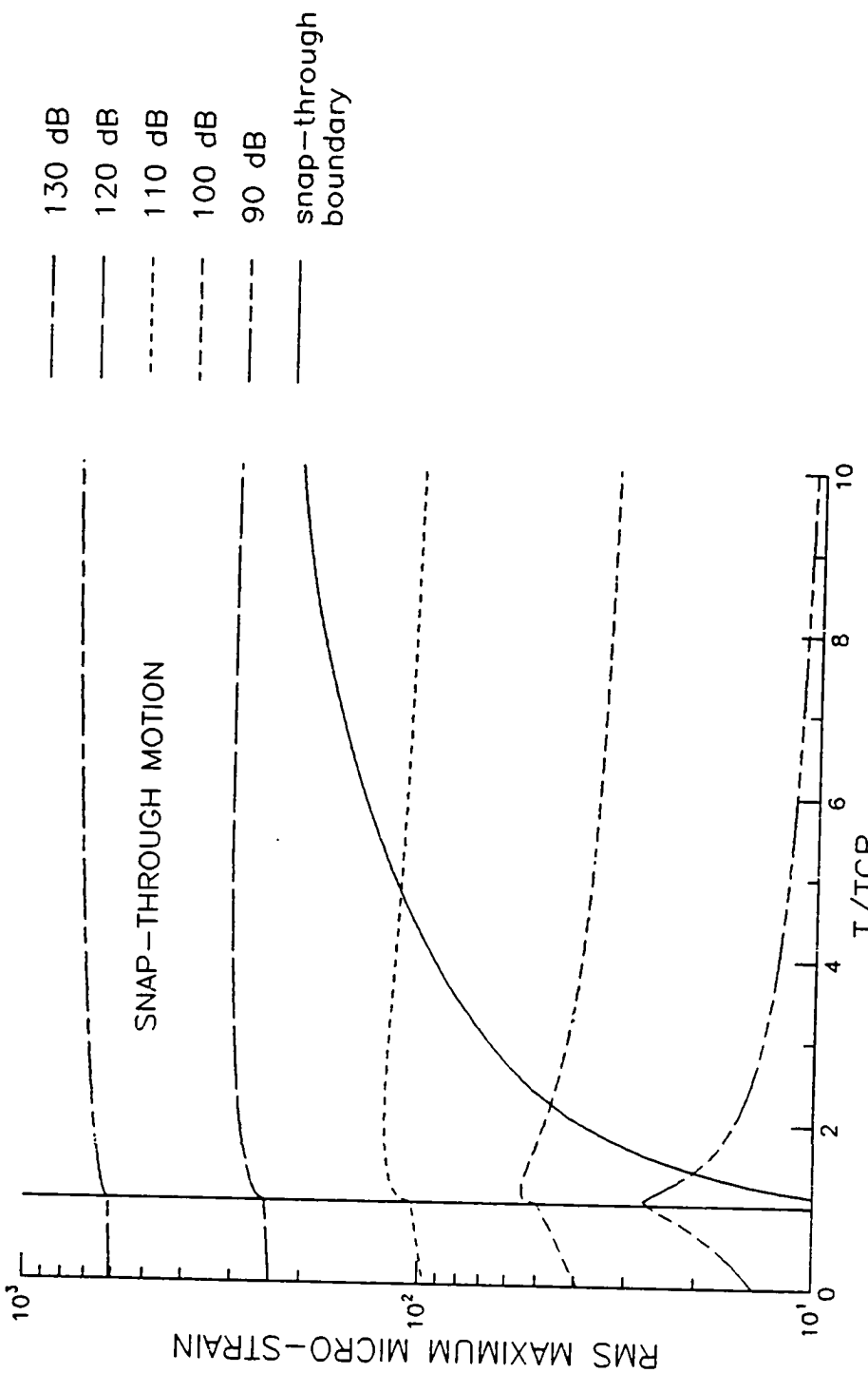

Fig. 4.23 RMS maximum micro-strain versus temperature for a simply supported beam subjected to a uniform temperature distribution

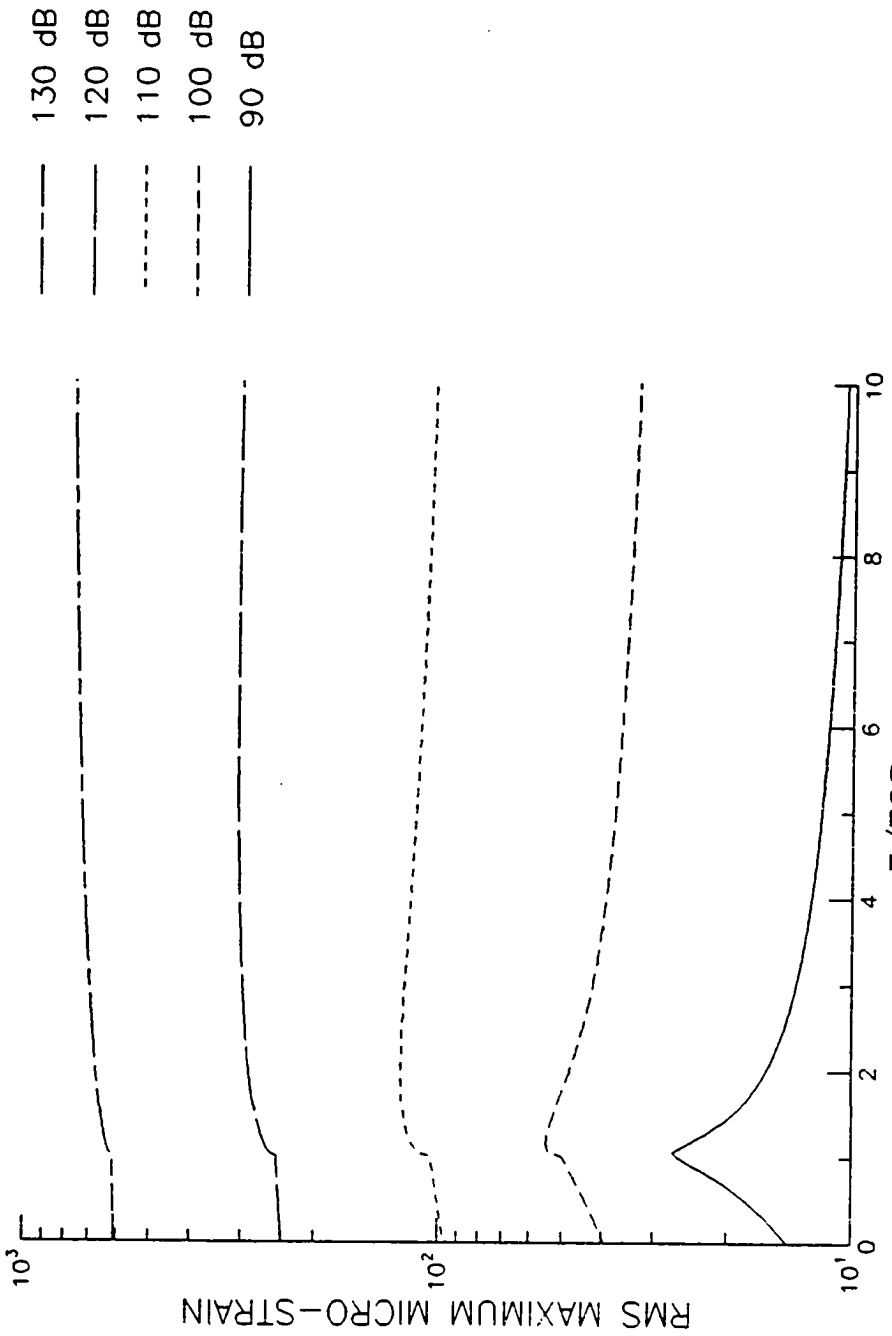

Fig. 4.24 RMS maximum micro-strain versus temperature for a simply supported beam subjected to a nonuniform temperature distribution

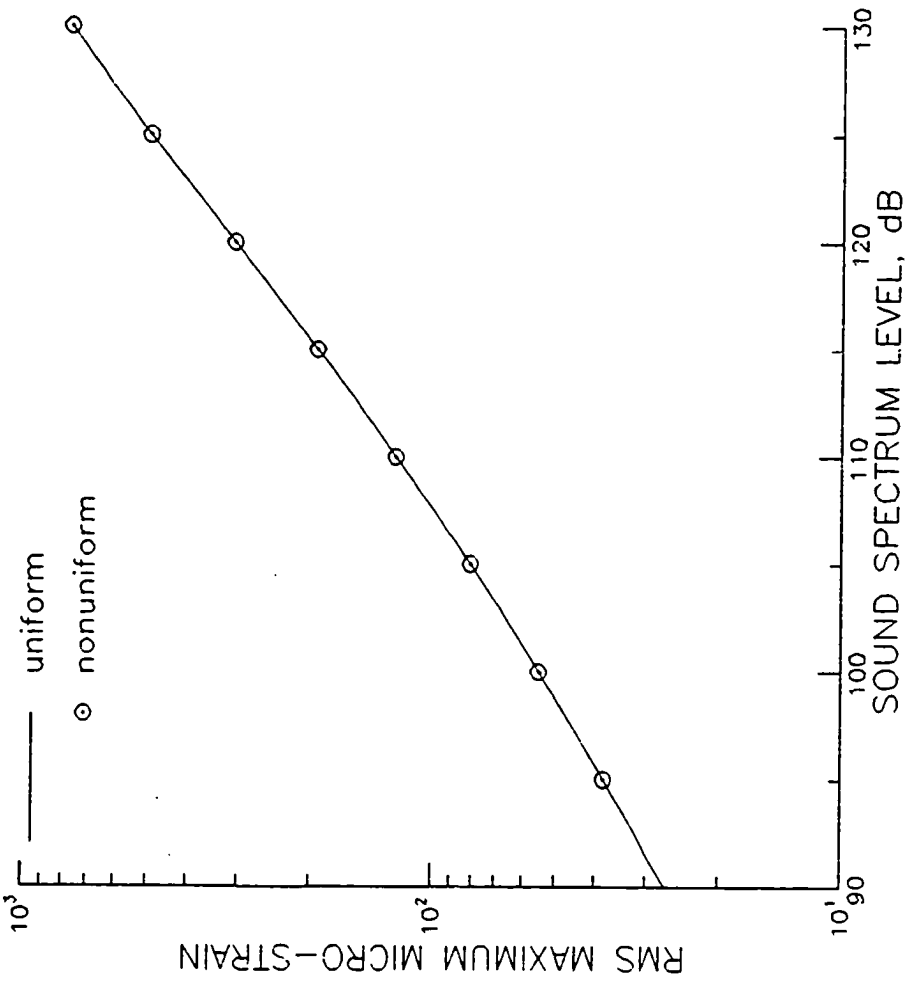

Fig. 4.25 Comparison of RMS maximum micro-strain for a simply supported beam subjected to different temperature distributions

initial inplane force N_o, and the change in the total stiffness is very small. As a result, the random deflections and strains are very nearly equal for the two cases.

4.3.4 Strain Response of Thermally Buckled Plates

A clamped rectangular plate is modeled using 36 equal sized elements for 1/4 of the plate, and four mode shapes are used for the random vibration analysis. Two different temperature distributions are considered: a uniform distribution ($\Delta T(x,y) = T_o$) and a nonuniform distribution ($\Delta T(x,y) = T_o (1 - \cos \frac{2\pi x}{a}) (1 - \cos \frac{2\pi y}{b})$) with T_o being the average temperature for each case. The average temperature necessary to produce buckling was found to be 2.51 °F for the uniform distribution and 1.58 °F for the nonuniform distribution. Thus, as noted by reference [24], buckling occurs at a lower average temperature for the nonuniform distribution.

Results for the root-mean-square strain response at various sound spectrum levels for each of these cases are shown in Figs. 4.26 and 4.27. The plate results are seen to be very similar to the beam results of the previous section even though the values of T/T_{CR} are much lower. This is because the initial plate deflection w_o at T/T_{CR} equal to three is of the same order as the initial beam deflection at T/T_{CR} equal to ten. Hence, for a given value of T/T_{CR}, the plate is stiffer than the beam. Again, the maximum strain occurs at lower temperatures for low sound spectrum levels and at higher temperatures for high sound spectrum levels. Behavior of this type is due to the coupling term $[A_o]\{\theta\}$ of Eq. (2.23) with $[A_o]$ being dependent on the initial deflection w_o and $\{\theta\}$ being dependent on the random deflection w. For a given sound

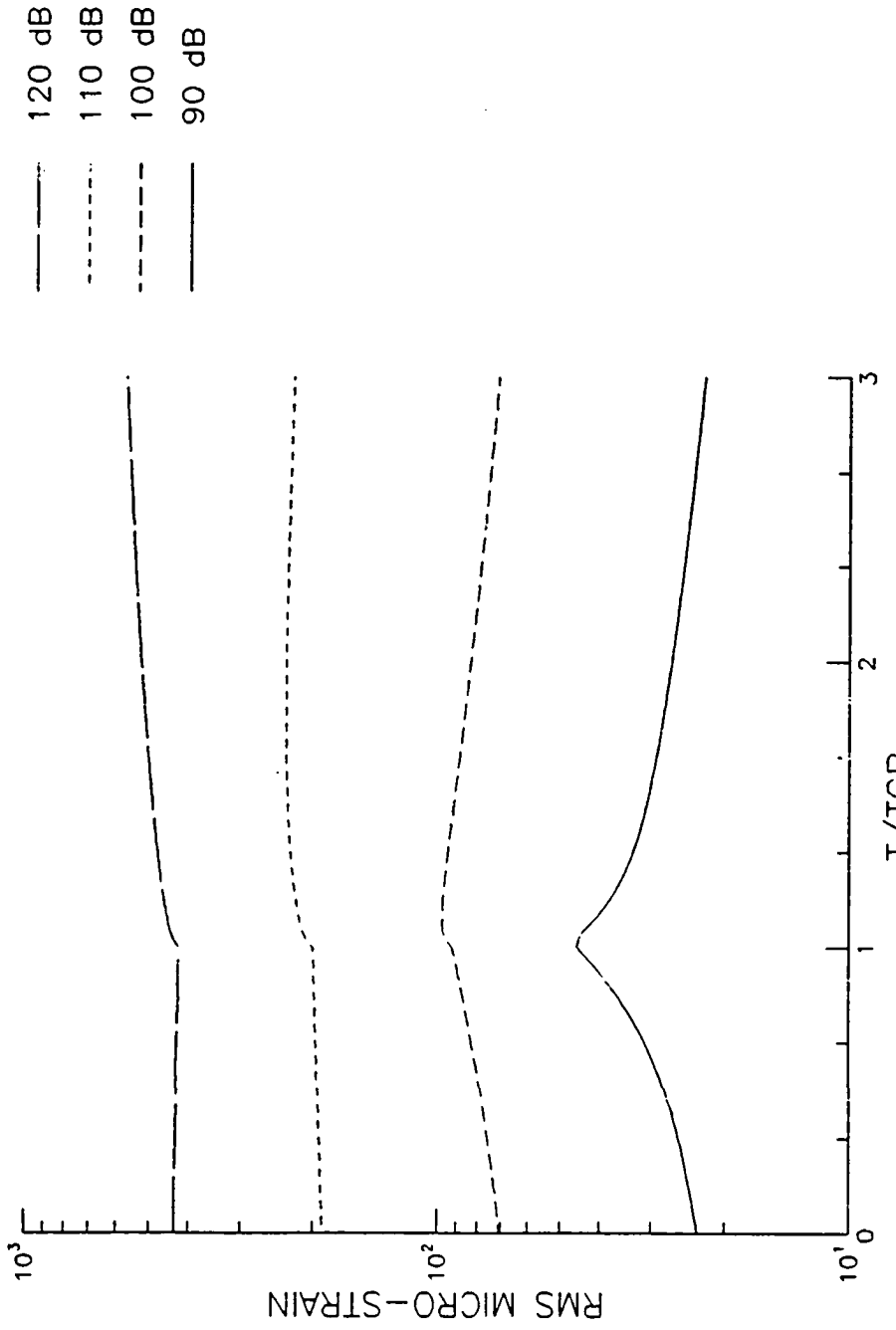

Fig. 4.26 RMS micro-strain, long edge midpoint, versus temperature for a clamped plate subjected to a uniform temperature distribution

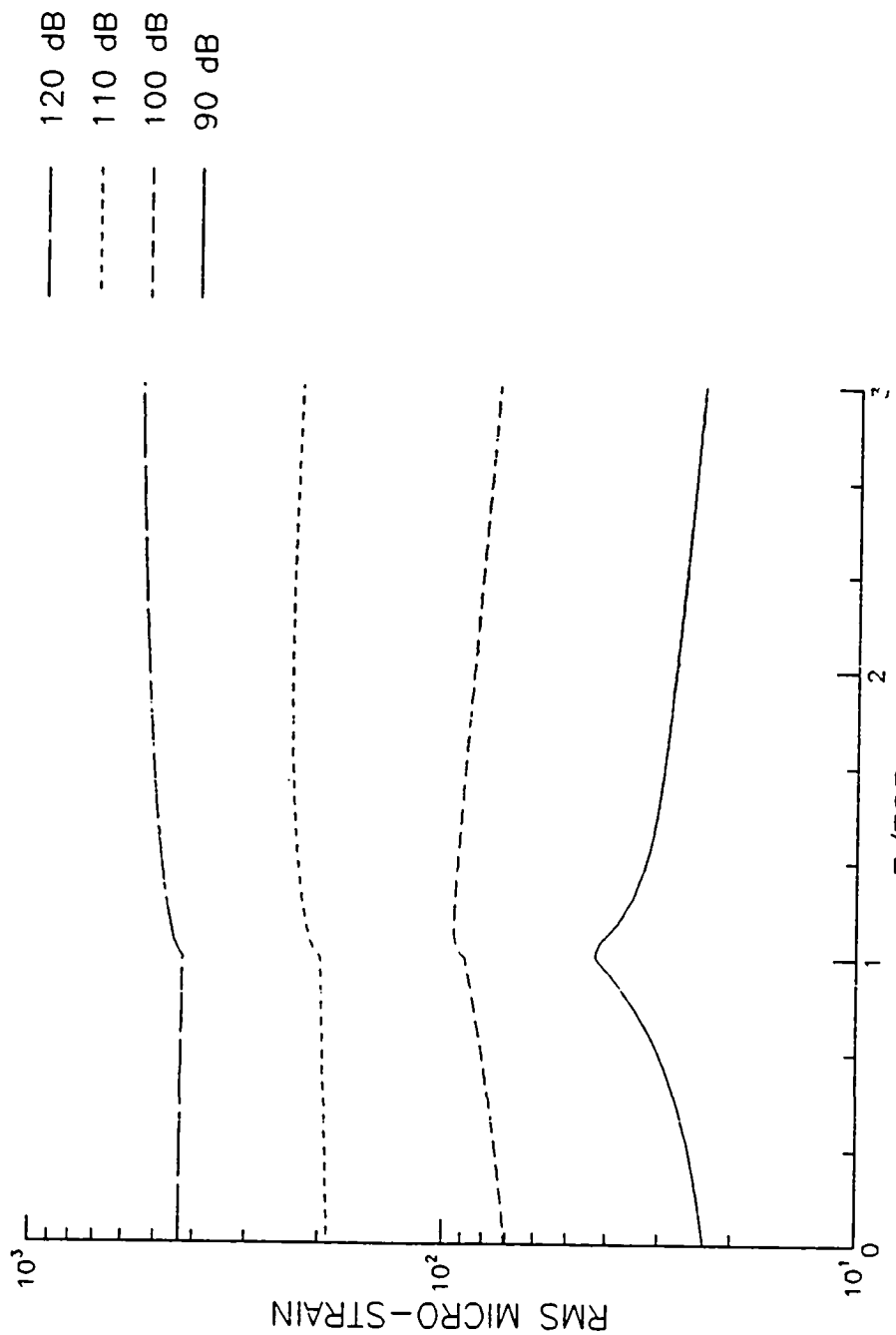

Fig. 4.27 RMS micro-strain, long edge midpoint, versus temperature for a clamped plate subjected to a nonuniform temperature distribution

spectrum level as T/T_{CR} increases, the initial deflection increases, and the structure becomes stiffer. As a result, the random deflection decreases. But for a given value of T/T_{CR}, the random deflection increases with sound spectrum level. So, with increasing T/T_{CR}, $\{\theta\}$ decreases and $[A_o]$ increases, and with increasing sound spectrum level $\{\theta\}$ increases. Thus, at high sound spectrum levels $\{\theta\}$ is sufficiently large for the term $[A_o]\{\theta\}$ to become large, and the strain response increases with temperature until the structure becomes stiff enough for $\{\theta\}$ to become small.

Maximum strain versus sound spectrum level for each of the temperature distributions is shown in Fig. 4.28. As for the beam results of the previous section, the different temperature distributions have a very small effect on the strain response since the postbuckled deflections w_o are very nearly equal, in an average sense, for the two different cases.

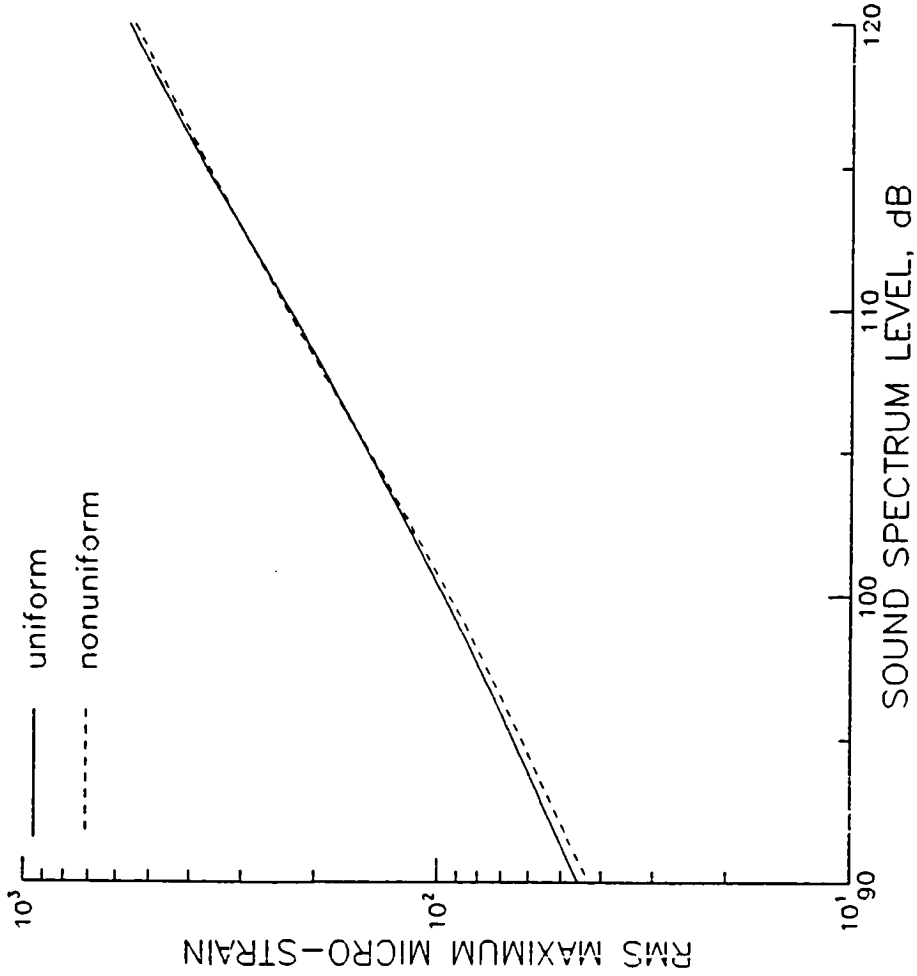

Fig. 4.28 Comparison of RMS maximum micro-strain, long edge midpoint, for a clamped plate subjected to different temperature distributions

Chapter 5

CONCLUSIONS

Using a finite element formulation, the governing nonlinear equations of motion have been derived for thin structural components subjected to a combined thermal/acoustic loading. Considering that thin panels buckle when subjected to small variations in temperature and exhibit large deflection response when exposed to moderately high sound spectrum levels, the nonlinear equations of motion were specialized for the specific applications of thermal postbuckling and large deflection random vibration of thermally buckled structures.

The critical temperature variation that produced panel buckling was determined using the incremental equations of motion. Corresponding to the critical buckling temperature are both inplane deflections and a buckling mode shape which were used to estimate the initial deflected shape to begin the postbuckling solution. Newton-Raphson iteration was used to solve for the deflections corresponding to a given temperature distribution, and continuous stresses were computed using interpolation functions consistent with the element displacement functions. Thermal postbuckling deflections and stresses were found to compare very well with a previous 25-mode plate solution for both uniform and nonuniform temperature distributions. However, a relatively high number of elements were necessary to accurately determine the membrane stresses at the plate edge.

For a given postbuckled equilibrium configuration with inplane forces $\{N_o\}$, moments $\{M_o\}$ and deflection w_o, the linear stiffness matrices were computed. With the linear stiffness matrices, the mass matrix and neglecting inplane inertia, the linear mode shapes and frequencies were computed for the thermally buckled structure. Using a coordinate transformation and expressing the nodal displacements in terms of the linear mode shapes, the equations of motion were transformed to a system of coupled nonlinear modal equations. The method of equivalent linearization was then used to reduce these equations to a system of nonlinear algebraic equations. Solutions to these equations were found using an iterative method in conjunction with an underrelaxation approach. Following the same type of approach as used for the thermal postbuckling formulation, continuous root-mean-square strains were computed.

Four-mode random vibration solutions were found to compare very closely with 100-mode EL classical solutions for both flat, stress free beams and beams buckled by a uniform temperature distribution. Results indicate that at low sound spectrum levels, the maximum root-mean-square strain occurs at or near the critical buckling temperature; whereas, for high sound spectrum levels the maximum strain occurs at temperatures above the buckling temperature. The stability of a given configuration was evaluated by considering the incremental equations of motion, and predicted snap-through sound spectrum levels were found to be within the boundaries of a three-mode classical solution. Such results, although not conclusive, suggest that a reasonable prediction of the snap-through boundary can be made based on an approximate solution such as the EL method.

The most significant contributions of the present study are considered to be the formulation and solution, including snap-through, of the nonlinear modal equations used to describe the large deflection random response. These general modal equations are applicable not only to the present research, but also to other problems involving nonlinear dynamic response, and the present methodology can be extended to built-up structures with complex boundary conditions. For the formulation of the nonlinear modal equations, the linear mode shapes of the thermally buckled structure were used. Previous classical solutions have only considered the mode shapes of the initially flat structure. Therefore, the present formulation should more accurately reflect the dynamic behavior of the thermally buckled structure. Furthermore, the snap-through criteria presented herein is based on results obtained using the EL method which, according to Refs. [34] and [49], requires significantly less computer time than numerical simulation techniques.

Seide et al. [67] noted a reasonable agreement between numerical simulation and EL results. However, differences were also noted. In particular, at high levels of excitation, differences between the two solutions were reported to be possibly due to either using the EL method outside of its range of applicability or using too large of a time step for the numerical simulation technique. To resolve these differences and obtain better results, future research should consider improved EL and numerical simulation methods. Further extensions of the present study should include such things as temperature dependent material properties, time dependent thermal loads and alternative methods for predicting the snap-through boundary. For a more accurate determination of stresses/strains, higher order inplane element displacement functions

are recommended. In addition, thick plates, built-up structures, curved panels and composite materials should be considered. To validate present and future analytical results detailed, accurate experimental studies should also be undertaken to evaluate the random deflection and strain response of thermally stressed or buckled structures.

REFERENCES

1. Mixson, J. S. and Roussos, L. A., "Acoustic Fatigue: Overview of Activities at NASA Langley," for presentation at AIAA Dynamics Specialists Conference, April 9-10, 1987, Monterey, CA.

2. Gossard, M. L., Seide, P. and Roberts, W., "Thermal Buckling of Plates," NACA TN 2771, August 1952.

3. Heldenfels, R. R. and Roberts, W. M., "Experimental and Theoretical Determination of Thermal Stresses in Flat Plates," NACA TN 2769, August 1952.

4. Nolte, L. J., "Large Deflection of Clamped Rectangular Plates," Hughes Aircraft Special Research Study No. SRSM7-168, September 1957.

5. Bisplinghoff, R. L. and Pian, T. H. H., "On the Vibration of Thermally Buckled Bars and Plates," Proceedings of the 9th International Congress for Applied Mechanics, Vol. 7, 1957, pp. 307-318.

6. Schneider, C. W., "Acoustic Fatigue of Aircraft Structures at Elevated Temperatures," Wright-Patterson Air Force Base, Ohio, AFFDL-TR-73-155, Part I, March 1974.

7. Ng, C. F. and White, R. G., "Dynamic Behavior of Postbuckled Composite Plates Under Acoustic Excitation," Proceedings of AIAA/ASME/ASCE/AHS 27th SDM Conference, pp. 435-444, San Antonio, TX, May 1986. Also Ph.D. Dissertation, C. F. Ng, University of Southampton, 1986.

8. Holehouse, I., "Sonic Fatigue Design Techniques for Advanced Composite Aircraft Structures," Wright-Patterson Air Force Base, Ohio, AFWAL-TR-80-3019, April 1980. Also Ph.D. Dissertation, University of Southampton, 1984.

9. Jacobs, L. D. and Lagerquist, D. R., "Finite Element Analysis of Complex Panel to Random Loads," Wright-Patterson Air Force Base, Ohio, AFFDL-TR-68-44, October 1968.

10. Soovere, J., "The Effect of Acoustic-Thermal Environment on Advanced Composite Fuselage Panels," AIAA/ASME/ASCE/AHS 24th Structures, Structural Dynamics and Materials Conference, Lake Tahoe, NV, May 1983, pp. 466-472.

11. Wolfe, H. F. and Wentz, K. R., "Acoustic Fatigue Test Evaluation of Adhesively Bonded Aluminum Fuselage Panels Using FM73/BR126 Adhesive/Primer System," 24th Structures, Structural Dynamics and Materials Conference, Lake Tahoe, NV, May 1983, pp. 626-631.

12. Soovere, J., "Sonic Fatigue Testing an Advanced Composite Aileron," Journal of Aircraft, Vol. 19, April 1982, pp. 304-310.

13. Mei, C. and Wentz, K. R., "Analytical and Experimental Nonlinear Response of Rectangular Panels to Acoustic Excitation," AIAA/ASME/ASCE/AHS 23rd Structures, Structural Dynamics and Materials Conference, New Orleans, LA, May 1982, pp. 514-520.

14. White, R. G., "Comparison of the Statistical Properties of the Aluminum Alloy and CFRP Plates to Acoustic Excitation," Composites, October 1978, pp. 251-258.

15. Jacobson, M. J., "Sonic Fatigue Design Data for Bonded Aluminum Aircraft Structures," Wright-Patterson Air Force Base, Ohio, AFFDL-TR-77-45, June 1977.

16. Van de Heyde, R. C. W. and Wolf, N. D., "Comparison of the Sonic Fatigue Characteristics of Four Structural Designs," Wright-Patterson Air Force Base, Ohio, AFFDL-TR-76-66, September 1976.

17. Van der Heyde, R. C. W. and Smith, D. L., "Sonic Fatigue Resistance of Skin-Stringer Panels," Wright-Patterson Air Force Base, Ohio, AFFDL-TM-73-149-FYA, April 1974.

18. Jacobson, M. L., "Advanced Composite Joints: Design and Acoustic Fatigue Characteristics," Wright-Patterson Air Force Base, Ohio, AFFDL-TR-71-126, April 1972.

19. Rudder, F. F., Jr. and Plumblee, H. E., Jr., "Sonic Fatigue Design Guide for Military Aircraft," Wright-Patterson Air Force Base, Ohio, AFFDL-TR-74-112, May 1975.

20. Thomson, A. G. R. and Lambert, R. F., "Acoustic Fatigue Design Data," NATO Advisory Group for Aeronautics Research and Development, AGARD-AG-162, Part I and II, 1972.

21. Schneider, C. W., "Acoustic Fatigue Design Criteria for Elevated Temperatures," Wright-Patterson Air Force Base, Ohio, AFFDL-TR-73-155, Part II, March 1974.

22. Wilcox, M. W. and Clemmer, L. E., "Large Deflection Analysis of Heated Plates," ASCE Journal of Engineering Mechanics, Vol. 90, 1964, pp. 165-189.

23. Levy, S., "Bending of Rectangular Plates with Large Deflections," NACA Report 737, 1942.

24. Paul, D. B., "Large Deflections of Clamped Rectangular Plates with Arbitrary Temperature Distributions," Wright-Patterson Air Force Base, Ohio, AFFDL-TR-81-3003, Vol. I, February 1982.

25. Yang, T. Y., "A Finite Element Procedure for Postbuckling Analysis of Initially Curved Plates," AIAA Paper 71-357, April 1971.

26. Yang, Y. T. and Han, A. D., "Buckled Plate Vibrations and Large Amplitude Vibrations Using Higher-Order Triangular Elements," AIAA Journal, Vol. 21, No. 5, May 1983.

27. Rao, G. V. and Raju, K. K., "Post-buckling Behavior of Elastic Circular Plates Using a Simple Finite Element Formulation," Computers and Structures, Vol. 10, 1979, pp. 911-913.

28. Rao, G. V. and Raju, K. K., "A Reinvestigation of Post-buckling Behavior of Elastic Circular Plates Using a Simple Finite Element Formulation," Computers and Structures, Vol. 17, No. 2, 1983, pp. 233-235.

29. Raju, K. K. and Rao, G. V., "Thermal Post-Buckling of Circular Plates," Computers and Structures, Vol. 18, No. 6, 1984, pp. 1179-1182.

30. Rao, G. V. and Raju, K. K., "Thermal Postbuckling of Columns," AIAA Journal, Vol. 22, No. 6, June 1984, pp. 850-851.

31. Wellford, L. C., Jr. and Dib, G. M., "Finite Element Methods for Nonlinear Eigenvalue Problems and the Postbuckling Behavior of Elastic Plates," Computers and Structures, Vol. 6, 1976, pp. 413-418.

32. Coan, J. M., "Large Deflection Theory for Plates with Small Initial Curvature Loaded in Edge Compression," ASME Journal of Applied Mechanics, Vol. 18, June 1951, pp. 143-151.

33. Yamaki, N., "Postbuckling Behavior of Rectangular Plates with Small Initial Curvature Loaded in Edge Compression," ASME Journal of Applied Mechanics, Vol. 26, Sept. 1959, pp. 407-414, (continued) Vol. 27, June 1960, pp. 335-342.

34. To, C. W. S., "Random Vibration of Nonlinear Systems," The Shock and Vibration Digest, Vol. 19, March 1987.

35. Bolotin, V. V., Random Vibrations of Elastic Systems, Martinus Nijhoff Publishers, 1984, pp. 290-292, 314-316.

36. Caughey, T. K. and Ma, F., "The Exact Steady-State Solution of a Class of Nonlinear Stochastic Systems," International Journal of Nonlinear Mechanics, Vol. 17, No. 3, 1982, pp. 137-142.

37. Roberts, J. B., "Response of Nonlinear Mechanical Systems to Random Excitation, Part I: Markov Methods," The Shock and Vibration Digest, Vol. 13, No. 4, April 1981, pp. 17-28.

38. Herbert, R. E., "Random Vibrations of Plates with Large Amplitude," ASME Journal of Applied Mechanics, Vol. 32, September 1965, pp. 547-552.

39. Prasad, C. B. and Mei, C., "Multiple Mode Large Deflection Random Response of Beams with Nonlinear Damping Subjected to Acoustic Excitation," AIAA 11th Aeroacoustics Conference, Paper No. 87-2712-CP, October 19-21, 1987, Sunneyvale, CA.

40. Prasad, C. B., "The Effect of Nonlinear Damping on the Large Deflection Response of Structures Subjected to Random Excitation," Ph.D. Dissertation, Old Dominion University, Norfolk, VA, 1987.

41. Mei, C. and Prasad, C. B., "Effect of Large Deflection and Transverse Shear on Response of Rectangular Symmetric Composite Laminates Subjected to Acoustic Excitation," AIAA Dynamics Specialist Conference, Monterey, CA, April 1987, pp. 809-826.

42. Mei, C. and Wolfe, H. F., "On Large Deflection Analysis in Acoustic Fatigue Design," in Random Vibration-Status and Recent Developments, The Stephen Harry Crandall Festschrift, edited by I. Elishafkoff and R. H. Lyon, Elsevier Science, 1986, pp. 279-302.

43. Gray, C. E., Jr., Decha-Umphai, K. and Mei, C., "Large Deflection, Large Amplitude Vibrations and Random Response of Symmetrically Laminated Rectangular Plates," Journal of Aircraft, Vol. 22, November 1985, pp. 929-930.

44. Mei, C., "Large Deflection Multimode Response of Clamped Rectangular Panels to Acoustic Excitation," Wright Patterson Air Force Base, Ohio, AFWAL-TR-83-3121, Vol. I, December 1983.

45. Seide, P., "Nonlinear Stresses and Deflections of Beams Subjected to Random Time Dependent Uniform Pressure," ASME Journal of Engineering for Industry, Vol. 98, No. 3, August 1976, pp. 1014-1020.

46. Hwang, C. and Pi, W. S., "Nonlinear Acoustic Response Analysis of Plates Using the Finite Element Method," AIAA Journal, Vol. 10, 1972, pp. 276-281.

47. Busby, H. R. and Weingarten, V. I., "Response of Nonlinear Beam to Random Excitation," ASCE Journal of Engineering Mechanics, 1973, pp. 55-68.

48. Chiang, C. K. and Mei, C., "A Finite Element Large Deflection Multiple-Mode Random Response Analysis of Beams Subjected to Acoustic Loading," Third International Conference on Recent Advances in Structural Dynamics, July 18-22, 1988, Southampton, England.

49. Chen, C. T. and Yang, Y. T., "Random Vibrations of Geometrically Nonlinear Finite Element Structures," Proceedings of 5th ASCE Specialty Conference, Virginia Tech, May 1988, pp. 281-284.

50. Dokmeci, M. C. and Boley, B. A., "Vibration Analysis of a Rectangular Plate," Journal of The Franklin Institute, Vol. 296, No. 5, November 1973.

51. Yamaki, N. and Mori, A., "Non-Linear Vibrations of a Clamped Beam with Initial Deflection and Initial Axial Displacement, Part I: Theory," Journal of Sound and Vibration, Vol. 71, No. 3, 1980, pp. 333-346.

52. Yamaki, N. and Mori, A., "Non-Linear Vibrations of a Clamped Beam with Initial Deflection and Initial Axial Displacement, Part II: Experiment," Journal of Sound and Vibration, Vol. 71, No. 3, 1980.

53. Yamaki, N., Otomo, K. and Chiba, M., "Non-Linear Vibrations of a Clamped Circular Plate with Initial Deflection and Initial Edge Displacement, Part I: Theory," Journal of Sound and Vibration, Vol. 79, No. 1, 1981, pp. 23-42.

54. Yamaki, N., Otomo, K. and Chiba, M., "Non-Linear Vibrations of a Clamped Circular Plate with Initial Deflection and Initial Edge Displacement, Part II: Experiment," Journal of Sound and Vibration, Vol. 79, No. 1, 1981, pp. 43-59.

55. Tseng, W. Y. and Dugundji, J., "Nonlinear Vibrations of a Buckled Beam Under Harmonic Excitation," ASME Journal of Applied Mechanics, 1971, pp. 467-476.

56. Min, G. B. and Eisley, J. G., "Nonlinear Vibration of Buckled Beams," ASME Journal of Engineering for Industry, 1972, pp. 637-646.

57. Eisley, J. G., "Large Amplitude Vibration of Buckled Beams and Rectangular Plates," AIAA Journal, Vol. 2, No. 12, December 1964, pp. 2207-2209.

58. Seide, P., "Dynamic Stability of Laterally Loaded Buckled Beams," Journal of Engineering Mechanics, Vol. 110, October 1984, pp. 1556-1569.

59. Humphreys, J. S., "On the Adequacy of Energy Criteria for Dynamic Buckling of Arches," AIAA Journal, Vol. 4, No. 5, May 1966, pp. 921-923.

60. Humphreys, J. S., "On the Dynamic Snap Buckling of Shallow Arches," AIAA Journal, Vol. 4, No. 5, May 1966, pp. 878-886.

61. Huang, N. C., "Dynamic Buckling of Some Elastic Shallow Structures Subject to Periodic Loading with High Frequency," International Journal of Solids and Structures, Vol. 8, 1972, pp. 315-326.

62. Simitses, G. J., "On the Dynamic Buckling of Shallow Spherical Shells," ASME Journal of Applied Mechanics, March 1974, pp. 299-300.

63. Huang, N. C., " Axisymmetric Dynamic Snap-Through of Elastic Clamped Shallow Spherical Shells," AIAA Journal, Vol 7, No. 2, February 1969, pp. 215-220.

64. Dumir, P. C. and Khatri, K. N., "Axisymmetric Static and Dynamic Buckling of Orthotropic Shallow Conical Caps," AIAA Journal, Vol. 23, November 1985, pp. 1762-1767.

65. Akkas, N. and Bauld, N. R., Jr., "Static and Dynamic Buckling Behaviors of Clamped Shallow Conical Shells," International Journal of Mechanical Sciences, Vol. 13, August 1971, pp. 689-706.

66. Barton, F. W. and Fulton, R. E., "Dynamic Buckling of Shallow Arches," ASCE Journal of Engineering Mechanics, Vol. 97, pp. 865-877.

67. Seide, P. and Adami, C., "Dynamic Stability of Beams in a Combined Thermal-Acoustic Environment," Wright-Patterson Air Force Base, Ohio, AFWAL-TR-83-3072, October 1983.

68. Seide, P., "RMS Response of Initially Buckled Beams Subjected to Random Time Dependent Uniform Pressure," 23rd Structures, Structural Dynamics and Materials Conference, New Orleans, LA, May 10-12, 1982, Part 1, pp. 506-510.

69. Seide, P., "Snap-Through of Initially Buckled Beams Under Uniform Random Pressure," 2nd International Conference of Recent Advances in Structural Dynamics, Southampton, England, April 9-13, 1984, Vol. 1, pp. 329-340.

70. Pi, H. N., Ariaratnam, S. T. and Lennox, W. C., "First-Passage Time for the Snap-Through of a Shell-Type Structure," Journal of Sound and Vibration, Vol.14, No. 3, 1971, pp. 375-384.

71. Wood, R. D. and Schrefler, B., "Geometrically Non-Linear Analysis - A Correlation of Finite Element Notations," International Journal for Numerical Methods in Engineering, Vol. 12, 1978, pp. 635-642.

72. Rajasekaran, S. and Murray, D. W. "On Incremental Finite Element Matrices," ASCE Journal of the Structural Division, Vol. 99, 1973, pp. 2423-2438.

73. Takeuti, Y., Komori, S., Noda, N. and Nyuko, H., "Thermal-Stress Problems in Industry, 3: Temperature Dependency of Elastic Moduli for Several Metals at Temperatures from - 196 to 1000°C," Journal of Thermal Stresses, Vol. 2, 1979, pp. 233-250.

74. Bogner, F. K., Fox, R. L. and Schmit, L. A., "The Generation of Inter-element Compatible Stiffness and Mass Matrices by the Use of Interpolation Formulas," AFDL-TR-66-80, Wright-Patterson AFB, OH, November 1966, pp. 396-443.

75. Bush, D. O. and Almroth, B. O., Buckling of Bars, Plates, and Shells, McGraw-Hill Book Company, 1975.

76. Cook, R. D., Concepts and Applications of Finite Element Analysis, John Wiley and Sons, Inc., 1981.

77. Zienkiewicz, O. C., The Finite Element Method, Third Edition, McGraw-Hill, 1982.

78. Atalik, T. S. and Utku, S., "Stochastic Linearization of Multi-Degree-of-Freedom Nonlinear Systems," Earthquake Engineering and Structural Dynamics, Vol. 4, 1976, pp. 411-420.

79. Yang, C. Y., Random Vibration of Structures, John Wiley and Sons, Inc., 1986.

80. Oden, J. T. and Brauchli, H. J., "On the Calculation of Consistent Stress Distributions in Finite Element Approximations," International Journal for Numerical Methods in Engineering, Vol. 3, 1971, pp. 317-325.

81. Bergan, P. G. and Clough, R. W., "Convergence Criteria for Iterative Processes," AIAA Journal, Vol. 10, 1972, pp. 1107-1108.

APPENDICES

APPENDIX A

ELEMENT MATRICES

The inverse of matrix $[T_b]$ in Eq. (2.9) is expressed as

$$[T_b]^{-1} = \begin{array}{c} \\ 1 \\ 2 \\ 3 \\ 4 \\ 5 \\ 6 \\ 7 \\ 8 \\ 9 \\ 10 \\ 11 \\ 12 \\ 13 \\ 14 \\ 15 \\ 16 \end{array} \begin{array}{c} \alpha_1 \\ \left[\begin{array}{cccccccc} 1 & 0 & 0 & 0 & 0 & 0 & 0 & 0 \\ 1 & \bar{a} & 0 & \bar{a}^2 & 0 & 0 & \bar{a}^3 & 0 \\ 1 & \bar{a} & \bar{b} & \bar{a}^2 & \bar{a}\bar{b} & \bar{b}^2 & \bar{a}^3 & \bar{a}^2\bar{b} \\ 1 & 0 & \bar{b} & 0 & 0 & \bar{b}^2 & 0 & 0 \\ 0 & 1 & 0 & 0 & 0 & 0 & 0 & 0 \\ 0 & 1 & 0 & 2\bar{a} & 0 & 0 & 3\bar{a}^2 & 0 \\ 0 & 1 & 0 & 2\bar{a} & \bar{b} & 0 & 3\bar{a}^2 & 2\bar{a}\bar{b} \\ 0 & 1 & 0 & 0 & \bar{b} & 0 & 0 & 0 \\ 0 & 0 & 1 & 0 & 0 & 0 & 0 & 0 \\ 0 & 0 & 1 & 0 & \bar{a} & 0 & 0 & \bar{a}^2 \\ 0 & 0 & 1 & 0 & \bar{a} & 2\bar{b} & 0 & \bar{a}^2 \\ 0 & 0 & 1 & 0 & 0 & 2\bar{b} & 0 & 0 \\ 0 & 0 & 0 & 0 & 1 & 0 & 0 & 0 \\ 0 & 0 & 0 & 0 & 1 & 0 & 0 & 2\bar{a} \\ 0 & 0 & 0 & 0 & 1 & 0 & 0 & 2\bar{a} \\ 0 & 0 & 0 & 0 & 1 & 0 & 0 & 0 \end{array}\right] \\ \\ \alpha_4 \\ \\ \\ \\ \\ \\ \\ \\ \\ \\ \\ \\ \\ \\ \\ \alpha_8 \end{array}$$

$$
\begin{array}{cccccccc}
\alpha_9 & & & \alpha_{12} & & & & \alpha_{16} \\
0 & 0 & 0 & 0 & 0 & 0 & 0 & 0 \\
0 & 0 & 0 & 0 & 0 & 0 & 0 & 0 \\
\bar{a}\bar{b}^2 & \bar{b}^3 & \bar{a}^3\bar{b} & \bar{a}^2\bar{b}^2 & \bar{a}\bar{b}^3 & \bar{a}^3\bar{b}^2 & \bar{a}^2\bar{b}^3 & \bar{a}^3\bar{b}^3 \\
0 & \bar{b}^3 & 0 & 0 & 0 & 0 & 0 & 0 \\
0 & 0 & 0 & 0 & 0 & 0 & 0 & 0 \\
0 & 0 & 0 & 0 & 0 & 0 & 0 & 0 \\
\bar{b}^2 & 0 & 3\bar{a}^2\bar{b} & 2\bar{a}\bar{b}^2 & \bar{b}^3 & 3\bar{a}^2\bar{b}^2 & 2\bar{a}\bar{b}^3 & 3\bar{a}^2\bar{b}^3 \\
\bar{b}^2 & 0 & 0 & 0 & \bar{b}^3 & 0 & 0 & 0 \\
0 & 0 & 0 & 0 & 0 & 0 & 0 & 0 \\
0 & 0 & \bar{a}^3 & 0 & 0 & 0 & 0 & 0 \\
2\bar{a}\bar{b} & 3\bar{b}^2 & \bar{a}^3 & 2\bar{a}^2\bar{b} & 3\bar{a}\bar{b}^2 & 2\bar{a}^3\bar{b} & 3\bar{a}^2\bar{b}^2 & 3\bar{a}^3\bar{b}^2 \\
0 & 3\bar{b}^2 & 0 & 0 & 0 & 0 & 0 & 0 \\
0 & 0 & 0 & 0 & 0 & 0 & 0 & 0 \\
0 & 0 & 3\bar{a}^2 & 0 & 0 & 0 & 0 & 0 \\
2\bar{b} & 0 & 3\bar{a}^2 & 4\bar{a}\bar{b} & 3\bar{b}^2 & 6\bar{a}^2\bar{b} & 6\bar{a}\bar{b}^2 & 9\bar{a}^2\bar{b}^2 \\
2\bar{b} & 0 & 0 & 0 & 3\bar{b}^2 & 0 & 0 & 0
\end{array}
\qquad \text{(A1)}
$$

where $\bar{a}$ and $\bar{b}$ are the length and width of the rectangular plate element.

Matrix $[T_m]$ in Eq. (2.10) is expressed as

$$[T_m] = \begin{array}{c} \begin{matrix} U_1 & & & U_4 & V_1 & & & V_4 \end{matrix} \\ \begin{bmatrix} 1 & 0 & 0 & 0 & & & & \\ -a^* & a^* & 0 & 0 & & 0 & & \\ -b^* & 0 & 0 & b^* & & & & \\ a^*b^* & -a^*b^* & a^*b^* & -a^*b^* & & & & \\ & & & & & & & \\ & & & & & & & \\ & 0 & & & 1 & 0 & 0 & 0 \\ & & & & -a^* & a^* & 0 & 0 \\ & & & & -b^* & 0 & 0 & b^* \\ & & & & a^*b^* & -a^*b^* & a^*b^* & -a^*b^* \end{bmatrix} \end{array} \qquad \text{(A2)}$$

where $a^* = 1/\bar{a}$ and $b^* = 1/\bar{b}$.

Matrix $[B_m]$ in Eq. (2.22) is expressed as

$$[B_m] = \begin{array}{c} \begin{matrix} \beta_1 & & & \beta_4 & & & & \beta_8 \end{matrix} \\ \begin{bmatrix} 0 & 1 & 0 & y & 0 & 0 & 0 & 0 \\ 0 & 0 & 0 & 0 & 0 & 0 & 1 & x \\ 0 & 0 & 1 & x & 0 & 1 & 0 & y \end{bmatrix} \end{array} \qquad \text{(A3)}$$

Matrix $[B_\theta]$ in Eq. (2.24) is expressed as

$$[B_\theta] = \begin{bmatrix} \alpha_1 & & & \alpha_4 & & & & \alpha_8 \\ 0 & 1 & 0 & 2x & y & 0 & 3x^2 & 2xy \\ 0 & 0 & 1 & 0 & x & 2y & 0 & x^2 \end{bmatrix}$$

$$\begin{matrix} \alpha_9 & & & \alpha_{12} & & & & \alpha_{16} \end{matrix}$$

$$\begin{bmatrix} y^2 & 0 & 3x^2y & 2xy^2 & y^3 & 3x^2y^2 & 2xy^3 & 3x^2y^3 \\ 2xy & 3y^2 & x^3 & 2x^2y & 3xy^2 & 2x^3y & 3x^2y^2 & 3x^3y^2 \end{bmatrix} \quad \text{(A4)}$$

Matrix $[B_b]$ in Eq. (2.28) is expressed as

$$[B_b] = -\begin{bmatrix} \alpha_1 & & & \alpha_4 & & & & \alpha_8 \\ 0 & 0 & 0 & 2 & 0 & 0 & 6x & 2y \\ 0 & 0 & 0 & 0 & 0 & 2 & 0 & 0 \\ 0 & 0 & 0 & 0 & 2 & 0 & 0 & 4x \end{bmatrix}$$

$$\begin{matrix} \alpha_9 & & & \alpha_{12} & & & & \alpha_{16} \end{matrix}$$

$$\begin{bmatrix} 0 & 0 & 6xy & 2y^2 & 0 & 6xy^2 & 2y^3 & 6xy^3 \\ 2x & 6y & 0 & 2x^2 & 6xy & 2x^3 & 6x^2y & 6x^3y \\ 4y & 0 & 6x^2 & 8xy & 6y^2 & 12x^2y & 12xy^2 & 18x^2y^2 \end{bmatrix} \quad \text{(A5)}$$

APPENDIX B

CONVERGENCE CRITERIA

The displacement convergence criteria (norms) used for the present study are due to Bergan and Clough [81]. For the thermal postbuckling formulation, two norms are considered: the modified absolute norm and the modified Euclidean norm. These two norms, respectively, are defined as

$$||\varepsilon||_A = \frac{1}{N} \sum_{j=1}^{N} \left| \frac{\Delta v_j}{v_{j,ref}} \right| \tag{B1}$$

$$||\varepsilon||_E = \left(\frac{1}{N} \sum_{j=1}^{N} \left| \frac{\Delta v_j}{v_{j,ref}} \right|^2 \right)^{1/2} \tag{B2}$$

where N is the number of system degrees-of-freedom. Convergence is considered to be achieved when either of these two norms satisfy the postbuckling convergence criteria. The quantity Δv_j is the change in the jth displacement component for a given iterative cycle, and $V_{j,ref}$ is the largest displacement component of the proper "type". For example, if j corresponds to a rotation θ_x or θ_y then $v_{j,ref}$ is the largest rotation; whereas, if j corresponds to an inplane displacement u or v then $v_{j,ref}$ is the largest inplane displacement.

For the random vibration formulation the norm used is based on the maximum norm and is defined as

$$||\varepsilon|| = \left| \frac{\Delta v}{v} \right| \quad , \tag{B3}$$

and convergence is considered to be achieved when this norm satisfies the random vibration convergence criteria. For this expression v and Δv correspond to the root-mean-square center deflection.

BIOGRAPHY

James Eugene Locke was born in Ardmore, Oklahoma, on November 20, 1958. He received Bachelor of Science and Master of Science degrees in Civil Engineering from Oklahoma State University in 1981 and 1983, respectively. From 1983 until 1986, he was employed as a structural engineer for LTV Aerospace and Defense Company in Dallas, Texas, during which time he also taught courses and pursued further graduate studies at The University of Texas at Arlington. In August 1986, he was awarded a Doctoral Fellowship at Old Dominion University in Norfolk, Virginia, and began studies toward the Doctor of Philosophy degree in Engineering Mechanics. During his graduate studies at Old Dominion University, he has worked as a research assistant at the Structural Acoustics Branch of NASA Langley Research Center in Hampton, Virginia, where he is presently employed.